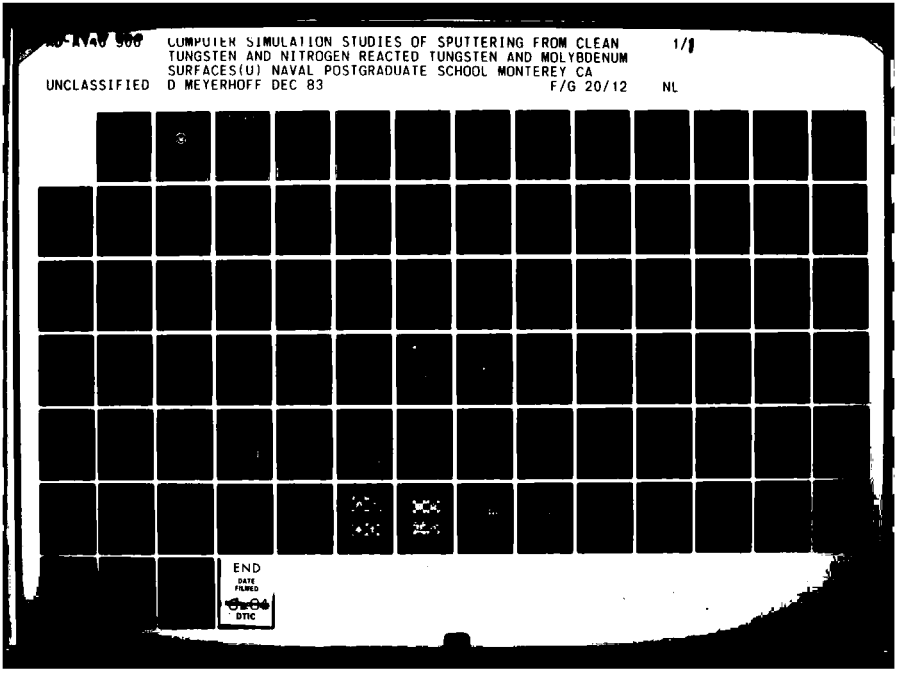
COMPUTER SIMULATION STUDIES OF SPUTTERING FROM CLEAN TUNGSTEN AND NITROGEN REACTED TUNGSTEN AND MOLYBDENUM SURFACES(U) NAVAL POSTGRADUATE SCHOOL MONTEREY CA
1/1
UNCLASSIFIED
D MEYERHOFF DEC 83
F/G 20/12
NL
END
DATE FILMED
DTIC

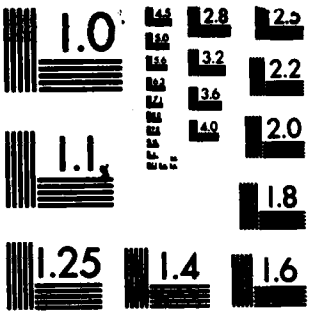

# NAVAL POSTGRADUATE SCHOOL
## Monterey, California

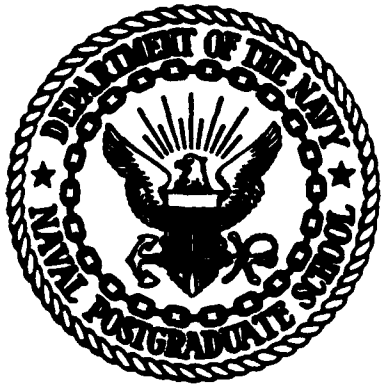




# THESIS

COMPUTER SIMULATION STUDIES OF SPUTTERING FROM CLEAN TUNGSTEN AND NITROGEN REACTED TUNGSTEN AND MOLYBDENUM SURFACES

by

Dirk Meyerhoff

December 1983

Thesis Advisor: Don E. Harrison, Jr.



Approved for public release; distribution unlimited

UNCLASSIFIED

SECURITY CLASSIFICATION OF THIS PAGE (When Data Entered)

| REPORT DOCUMENTATION PAGE | READ INSTRUCTIONS BEFORE COMPLETING FORM |
|---|---|
| 1. REPORT NUMBER | 2. GOVT ACCESSION NO. A140 900 / 3. RECIPIENT'S CATALOG NUMBER |
| 4. TITLE (and Subtitle) Computer Simulation Studies of Sputtering from Clean Tungsten and Nitrogen Reacted Tungsten and Molybdenum Surfaces | 5. TYPE OF REPORT & PERIOD COVERED Masters Thesis December 1983 |
| | 6. PERFORMING ORG. REPORT NUMBER |
| 7. AUTHOR(s) Dirk Meyerhoff | 8. CONTRACT OR GRANT NUMBER(s) |
| 9. PERFORMING ORGANIZATION NAME AND ADDRESS Naval Postgraduate School Monterey, CA. 93943 | 10. PROGRAM ELEMENT, PROJECT, TASK AREA & WORK UNIT NUMBERS |
| 11. CONTROLLING OFFICE NAME AND ADDRESS Naval Postgraduate School Monterey, CA. 93943 | 12. REPORT DATE December 1983 |
| | 13. NUMBER OF PAGES 84 |
| 14. MONITORING AGENCY NAME & ADDRESS(if different from Controlling Office) | 15. SECURITY CLASS. (of this report) UNCLASSIFIED |
| | 15a. DECLASSIFICATION/DOWNGRADING SCHEDULE |

16. DISTRIBUTION STATEMENT (of this Report)

Approved for public release; distribution unlimited

17. DISTRIBUTION STATEMENT (of the abstract entered in Block 20, if different from Report)

18. SUPPLEMENTARY NOTES

19. KEY WORDS (Continue on reverse side if necessary and identify by block number)

Supttering
Computer Simulation
Chemically Reacted Surfaces

20. ABSTRACT (Continue on reverse side if necessary and identify by block number)

The Naval Postgraduate School computer simulation model QRAD was used to study sputtering from clean and nitrogen reacted tungsten, and from nitrogen reacted molybdenum, for (001) surfaces bombarded by normal incidence argon ions in the energy range from 0.5 keV to 3.0 keV. The simulation results are compared to experimental data obtained by Winters, who concludes, that the difference in the cross sections for the sputtering of nitrogen from W(001) and Mo(001) is dominated by the

DD FORM 1 JAN 73 1473 EDITION OF 1 NOV 65 IS OBSOLETE S/N 0102-LF-014-6601

UNCLASSIFIED

SECURITY CLASSIFICATION OF THIS PAGE (When Data Entered)

adsorbate-substrate mass difference since the other important parameters are similar. The simulation however shows little dependence on the substrate mass, but a strong dependence of the sputtering cross sections on the distance of the adatoms above the substrate. The nitrogen position is required to be higher on tungsten than on molybdenum.

Approved for public release, distribution unlimited

# Computer Simulation Studies of Sputtering from Clean Tungsten and Nitrogen Reacted Tungsten and Molybdenum Surfaces

by
Dirk Meyerhoff
Kapitänleutnant, Federal German Navy

Submitted in partial fulfillment of the
requirements for the degree of

MASTER OF SCIENCE IN PHYSICS

from the

NAVAL POSTGRADUATE SCHOOL
December 1983

Author: _____

Approved by: _____
Thesis Advisor

_____
Second Reader

_____
Chairman, Department of Physics

_____
Dean of Science and Engineering

## ABSTRACT

The Naval Postgraduate School computer simulation model QRAD was used to study sputtering from clean and nitrogen reacted tungsten, and from nitrogen reacted molybdenum, for (001) surfaces bombarded by normal incidence argon ions in the energy range from 0.5 keV to 3.0 keV. The simulation results are compared to experimental data obtained by Winters, who concludes, that the difference in the cross sections for the sputtering of nitrogen from W(001) and Mo(001) is dominated by the adsorbate-substrate mass difference since the other important parameters are similar. The simulation however shows little dependence on the substrate mass, but a strong dependence of the sputtering cross sections on the distance of the adatoms above the substrate. The nitrogen position is required to be higher on tungsten than on molybdenum.

TABLE OF CONTENTS


I. INTRODUCTION ---- 6

A. OVERVIEW ---- 6

B. PHYSICAL MEANING ---- 7

C. LATER WORK ---- 8

D. APPLICATIONS OF SPUTTERING ---- 10

E. COMPUTER SIMULATIONS ---- 11

II. OBJECTIVES ---- 12

III. THE SIMULATION ---- 13

A. THE TARGET ---- 13

B. POTENTIAL FUNCTIONS ---- 16

C. THE IMPACT AREA ---- 19

IV. DISSCUSSION AND RESULTS ---- 19

A. GRAPHICAL ANALYSIS ---- 19

B. NUMERICAL ANALYSIS ---- 22

V. SUMMARY AND RECOMMENDATIONS ---- 29

LIST OF REFERENCES ---- 30

FIGURES ---- 32

INITIAL DISTRIBUTION LIST ---- 84

# I. INTRODUCTION

## A. OVERVIEW

Sputtering is the removal of surface atoms due to energetic particle bombardment. It is caused by collisions between incoming particles and atoms in the selvage, i.e., the near surface of solid material. First discovered by Grove [1] in 1853 and Faraday in 1854, it took about 50 years until the physical process involved was recognized and another 50 years until a quantitative theory began to develop. Grove [1] noticed the disintegration of cathodes in glow-discharge tubes and observed, that the cathode material was deposited on the surrounding glass walls. He called this process "cathode sputtering". 50 years later, Goldstein [2] presented evidence that the sputtering effect was caused by positive ions of the discharge hitting the cathode.

Stark [3,4] introduced a so-called 'hot-spot' model of sputtering (now known as 'evaporation theory') and later a collision theory, which viewed sputtering as a sequence of binary collisions initiated by the bombarding ion. Stark found that at low energies the yield, Y, increases with increasing ion energy, and interpreted this result on the assumption that an increasing amount of energy is transferred to the target atoms near the surface. At higher energies, increasing penetration depth of the ion causes a relatively smaller sputtering yield and thus a plateau in the yield curve. The reason for this is a decrease in the "size" of the ion as its energy increases. Stark considered his hot-spot model, the evaporation of target material from

a microscopically small region with high local temperature, and his collision theory as two different views of the same process. Von Hippel and Blechschmidt [5], who developed a quantitative form of Stark's hot spot model, made the first attempt to formulate a sputtering theory on the basis of local heat. Subsequent investigators found that this model is inadquate. Wehner [6] showed that local evaporation alone couldn't explain sputtering phenomena from single crystals. In 1934 Lamar and Compton [7] suggested that binary collision processes dominate in light-ion sputtering and local evaporation is dominant in heavy-ion sputtering. Their ideas led to the 'thermal spike' concept, in which a long lived high temperature volume presists in the target after the collision cascade is complete. Wehner's observations revived the interest in the collision theory. Keywell [8] applied neutron transport theory to Stark's collision model. Due to his and subsequent calculations by Harrison [9], probability concepts and collision cross sections were introduced as important parts of the sputtering theory.

## B. PHYSICAL MEANING

Sputtering mechanisms operate in the near surface region of the target, and are caused by a collision cascade. The processes involved are simular to those causing radiation damage in the bulk material of a solid. Sputtering happens far from thermal equilibrium, which means that it isn't to be confused with evaporation. Generally an incident particle collides with atoms of the bulk material and transfers energy. If the transffered energy is larger than the cohesive energy at the

lattice site a primary recoil atom is created. This recoil atom collides with other target atoms and distributes the energy into a collision cascade. The condition for an atom to be ejected is that the kinetic energy associated with the normal component of its velocity is larger than the potential energy binding it to the surface. The sputtering yield is defined as the average number of target atoms ejected per incident particle.

## C. LATER WORK

Although considerable discrepancies exist in the experimental results produced by various scientific groups, standards have developed which define the basic requirements for reproducible and reliable experiments. This development is shown in reviews of Behrisch [10], Kaminsky [11], Carter and Colligen [12], and Pleshivtsev [13]. Over the last 30 years theoretical efforts have been increasingly successful in explaining the main features of sputtering.

The analytic theoretical work in this area was done by Sigmund [14]. He presented a systematic theory of sputtering on the basis of a minimum of assumptions. Basic assumptions concern the characteristics of a single collision (differential cross section, inelastic stopping), the structure of the medium (random or crystalline), the structure and binding forces of the surface, and some factors that depend on specific experimental arrangements like beam-target geometry, high or low ion energy, etc. The yield calculation consists of the following steps:

1) to determine the amount of energy deposited by energetic particles (ion and recoil atoms) near the surface;

2) to convert this energy into a number of low-energy recoil atoms;

3) to determine how many of these atoms come to the surface;

4) to select those atoms that have enough energy to overcome the surface binding forces.

Considering, for example, the backsputtering yield from a plane surface, the outward current of the target atoms through the surface plane at $x = 0$ is found to be:

$$J(E_o,\Omega_o)dE_o d^2\Omega_o = \Psi F_D(E, \theta, 0) \frac{\Gamma_m dE_o}{E_o |dE_o/dx|} |\cos \theta_o| \frac{d^2\Omega_o}{4\pi}$$

where E is the energy of the ion impinging at an angle $\theta$ onto a plane surface, $F_D$ is the deposited energy density, $\Psi$ is the number of projectiles per unit time, $\Omega_o$ is the unit solid angle, and $\Gamma_m$ is a parameter which depends on $\Psi$ and the scattering cross section. The sputtering yield is found by integrating this equation over $E_o$ and $\theta_o$ and dividing the sputtered current by the incident current $\Psi$. This leads to

$$\boxed{Y = \Lambda F_d(E, \theta, 0)}$$

with

$$\Lambda = \frac{\Gamma_m}{2} \int \frac{dE_o}{E_o |dE_o/dx|} \int d(\cos \theta_o) |\cos \theta_o| P(E_o, \theta_o)$$

where $P(E_o, \theta_o)$ is the probability that an atom will escape from the surface. The simplest model for the surface binding of a metal is based on a planar surface barrier $U_o$. In this case,

$$P(E_o,\theta_o) = \begin{cases} 1 \text{ for } E_o \cos^2\theta_o > U_o \\ 0 \text{ for } E_o \cos^2\theta_o < U_o \end{cases}$$

which leads to a simple form:

$$A = \frac{3}{4\Pi^2} \frac{1}{N C_o U_o},$$

with

$$C_o = \frac{\Pi}{2} \lambda_o a^2_{BM},$$

where $\lambda_o \cong 24$ and $a_{BM} = 0.219$ A.

## D. APPLICATIONS OF SPUTTERING

For a long time sputtering was regarded as an undesired effect which destroyes the cathodes and grids in discharge tubes. In fusion research, plasma contamination by metal atoms is still one of the major problems. Sputtering also may cause the distruction of diaphragms and targets in accelerators and high-voltage electron microscopes.

On the other hand, sputtering has become an indispensible process in modern technology. It allows the removal of very tightly bound surface layers on a nearly atomic scale. Sputtering is used in sputter-ion sources, for obtaining reproducibly clean surfaces and, for example, in micro-machining and depth profiling of thin films.

Sputtering also can be used to obtain information about processes occuring on a atomic scale. Many scientists, including Kingdon and Langmuir (15), Winters (16), and Taglauer and Heiland (17), studied the sputtering of chemisorbed gas to investigate mechanisms which lead to the emission of multi-component materials. This thesis uses a computer simulation to varify one assumption made by Winters.

## E. COMPUTER SIMULATIONS

Due to their high operating speed, computers are attractive for calculations concerning sputtering events. A computer simulation can never replace an experiment, but by matching the results, a simulation can help to understand and identify sputtering mechanisms, and to interpret experimental results. A computer simulation is not a theory, it is a mathematical tool used to test the fundamentals of a theory [19].

Computer simulations can be divided in two categories: time-step and event-store models. Event-store programs move from event to event skipping the intervening time. For sputtering, they are based on binary collision theory. These fast, complex programs are useful when the physical model is well understood. The program used at the Naval Postgraduate School is a time-step model based on simultaneous multiple interactions (MI). MI simulations of physical systems usually require the calculation of about 100 individual ion trajectories (cascades), while binary collision simulations use several thousands. This, and the fact that in MI simulations mechanisms are easy to trace, makes the time-step model attractive.

This thesis is based on QRADS, a refined version of QRAD, the standard program in use at the Naval Postgraduate School for some time, which is a full-lattice simulation computer program, designed to model the dissipation of an incident ion's momentum in a single crystal target, using classical mechanics. The program has the ability to generate different surfaces of several crystal structures. To obtain reacted surfaces, a special subroutine places adatoms on the surface.

After the lattice is build, the potential functions are calculated. The impotant mathematical manipulations, concerning the trajectory, are done by the subroutine INTEG (integrator). This subroutine also tests for the termination of the trajectory. Finally, subroutine LEGIT determines which atoms were actually ejected.

## II. OBJECTIVES

Some experimental results exist for sputtering from polycrystalline BCC structures [19] but only a few for clean single crystal surfaces or chemically reacted single crystal surfaces [19]. Winters [18] investigated the sputtering cross sections of tungsten and molybdenum bombarded by argon and xenon ions in the energy range from 0.3 keV up to 5.0 keV. Figure 1 shows the cross sections as a function of incident ion energy. Winters' experiments show that the sputtering yield of nitrogen tends to increase as the atomic weight of the surrounding atoms increases. He furthermore concludes, that the difference in the cross sections for the sputtering on nitrogen from W(001) and Mo(001) is dominated by the absorbate-substrate mass difference since the other important parameters are similar.

The primary objective of this thesis is to study sputtering from nitrogen reacted (001) tungsten and molybdenum surfaces using a

computer simulation model and to compare the results with the experimental data obtained by Winters.

The incident ion will be $Ar^+$ in the energy-range from 0.5 keV to 3.0 keV.

The simulation includes:

1) Bombardment of a clean (001) tungsten surface (used for comparison).
2) Bombardment of a nitrogen reacted (001) tungsten surface.
3) Bombardment of a nitrogen reacted (001) tungsten surface where the atomic mass of tungsten is replaced by the atomic mass of molybdenum.
4) Bombardment of a nitrogen reacted (001) molybdenum surface, where the nitrogen is closer to the target surface plane than in the cases listed above. (The nitrogen is assumed to be in a 4-fold symmetry position for all reacted surfaces.)

## III. THE SIMULATION

### A. THE TARGET

#### 1. Properties of Materials

a) Tungsten (W, Wolfram): atomic mass 183.85, lattice parameter 3.165 Å, crystal structure BCC, nearest-neighbor distance 2.74 Å, cohesive energy 8.9 eV,

b) Nitrogen (N): atomic mass 14.0, binding energy to the tungsten substrate 6.5 eV,

c) Molybdemun (Mo): atomic mass 94.94, lattice parameter 3.147 Å, crystal structure BCC, nearest-neighbour distance 2.73 Å, cohensive energy 6.82 eV.

2. Location of the Adatoms

The location of nitrogen atoms on a tungsten or molybdenum surface is not known. Clavenna [21] and Adams [22] suggest that the nitrogen is single-bounded in a 4-fold position above an atom in the second layer of the tungsten substrate. (The 4-fold position is also assumed by Winters.) Figures 2a,b show side and top view of the reacted surface where the radius of the nitrogen is assumed to be 0.59 Å [22]. (The smaller circles are the nitrogen atoms.) Criffiths et. al. [23], agree with this position at a fractional coverage ($\theta_f$) of 0.5 but mention, that at this coverage the nitrogen is unstable. They recommend study at the most stable coverage of $\theta_f = 0.4$. This requires formation of islands of nitrogen atoms on the surface, (see Figs. 3a,b). Harrison et. al. [24], propose that the nitrogen might be below the first layer of the substrate in an interstitial site. In this case some second layer atoms would be pushed down into the substrate to set equal distances to all nearest-neighbors. For this simulation the nitrogen is assumed to be in the 4-fold position for both substrate materials. For the nitrogen reacted tungsten surface the location above the substrate is chosen so that the distance to all five nearest-neighbors is equal. The distance above the surface is 0.504 LU (where 1.0 LU = 1.58 Å = 0.5 lattice parameters, see Fig. 4).

(Lattice units were introduced in the program so that rescaling to a new target material can be done without major reprogramming and so that results from different substrates can be compared directly.) Runs also were made with the tungsten mass replaced by the molybdenum mass to examine the mass effect proposed by Winters [18], discussed in chapter 2. On the nitrogen reacted molybdenum surface the nitrogen is placed closer to the surface layer (see Fig. 4). The distance above the surface is 0.243 LU (where 1.0 LU = 1.57 Å = 0.5 lattice parametrs).

3. The Target Size

The inability of the lattice of target atoms to contain the entire cascade generated by the incident ion is called ' a failure in containment'. The size of the target determines the containment of the trajectory. If an increase in target size doesn't change the results of the computations, the trajectory is effectively contained for the purposes of the computations. (Unnecessarily large targets waste computer resources.)

The minimum target size for the ion energy of 0.5 keV was found to be 19x8x19, where the numbers represent the numbers of planes in the x,y and z directions. 40 nitrogen atoms (equivalent to a fractional coverage of $\theta_f = 0.4$) are placed as described above (see Fig. 5; solid lines mark the smaller target). The minimum target size for ion energies between 1.0 keV and 3.0 keV was found to be 23x8x23 with a fractional coverage of $\theta_f = 0.416$, equivalent to 60 adatoms. The difference in coverage does not significantly affect the result. Winters [18], determined the coverage in his experiments by Auger spectroscopy, and found that the Auger intensity is a nonlinear

function of coverage above $\Theta = 6 \times 10^{14}$ atoms per $cm^2$. Thus all his measurements were taken below this value.

The coverage chosen for the simulation is equivalent to $4.9 \times 10^{14}$ atoms per $cm^2$.

## B. POTENTIAL FUNCTIONS

### 1. In General

A primary uncertainty in sputtering models and theory is the form of the interatomic potential functions. No single potential function has yet been deduced which fits every sputtering experiment. The functions used for this simulation are Morse, and Moliere [25] joined with a cubic spline [24]. The Morse potential function is of the form:

$$V(r) = D_e \exp[-2\alpha(r-r_o)] - 2D_e \exp[-\alpha(r-r_o)]$$

where $D_e$ is the well depth, $\alpha$ is a scale factor of the potential function, and $r_o$ is the equilibrium separation. For $r > r_o$ the Morse potential is attractive and for $r < r_o$ repulsive.

The Moliere potential function is of the form:

$$V(r) = (Z_1 Z_2 e^2/r)(0.35 \exp[-0.3r/a] + 0.55 \exp[-1.2r/a] + 0.10 \exp[-6.0r/a])$$

where 'a' is the Firsov screening length. The Moliere function is a pure repulsive potential function.

The cubic spline is of the form:

$$V(r) = C_o + C_1 r + C_2 r^2 + C_3 r^3$$

where the coefficients are determined by the program. The cubic spline is necessary to combine Morse and Moliere functions into a single

composite potential. For hard collisions, at close approach in the keV-range, the Morse potential bends towards the Y-axis and thus cannot be physically correct, because all potential functions must approach ∞ as $r \to 0$ like $1/r$. The cubic spline is inserted where the Morse and the Moliere functions overlap, thus the combined function is a Moliere to the left and a Morse to the right of the spline. In general the spline shouldn't be longer than 0.05 LU to get smooth potential and force curves.

2. Crystal Potential Functions

The composite potential functions are used for the bulk materials as well as for the reacted surfaces. The Moliere function is a standard Moliere in each case. The Morse parameters have physical meaning: $\alpha$, used as an adjustable parameter, is chosen so that the slope of the Morse matches that of the Moliere function. For the substrate materials $D_e$ is chosen to generate individual atom energies in the center of the target equal to the cohesive energy, i.e., 8.9 eV for tungsten and 6.82 eV for molybdenum. For the reacted surfaces $D_e$ has to match the binding energies between the nitrogen and the substate i.e., 6.5 eV in each case. Because the potential function is truncated after one nearest-neighbor distance, $r_o$ is greater than the separation between atoms in the substrate materials. For the reacted surfaces, $r_o$ is the nearest-neighbor distance.

The cubic spline is bounded by the values $R_A$ and $R_B$. The table below shows the parameters for the crystals and adatoms.

Table 1: Parameters for Crystal Potential Function.

| | $\alpha(A^{-1})$ | $r_e(A)$ | $D_e(eV)$ | $R_A(A)$ | $R_B(A)$ | see Figs. |
|---|---|---|---|---|---|---|
| W -W | 1.20 | 2.849 | 1.335 | 1.83 | 1.90 | 6,10 |
| W -N | 1.65 | 2.380 | 1.300 | 1.14 | 1.14 | 7,10 |
| Mo-Mo | 1.50 | 2.800 | 0.997 | 1.24 | 1.30 | 8,10 |
| Mo-N | 2.20 | 1.950 | 1.612 | 0.91 | 0.97 | 9.10 |

Figures 6, 7, 8, 9 show the Morse and Moliere functions and Figure 10 shows the combined functions generated by the program.

3. Gas Phase Substrate Atom Potential Functions

The gas phase potential functions are pure Morse functions because no hard collisions are expected. The parameters are listed below:

Table 2: Parameters for Gas Phase Substrate Atom Potential Functions.

| | $\alpha(A^{-1})$ | $r_e(A)$ | $D_e(eV)$ | see Figs. |
|---|---|---|---|---|
| W -W | 1.20 | 2.74 | 8.900 | 11 |
| W -N | 1.65 | 1.96 | 6.721 | 11 |
| Mo-Mo | 1.50 | 2.73 | 6.820 | 12 |
| Mo-N | 2.20 | 1.96 | 5.100 | 12 |

4. Nitrogen-Nitrogen Potential Functions

The N-N potential function in the gas phase as well as in the crystal phase is a pure Morse functions with:

$\alpha = 2.7$ $A^{-1}$
$r_e = 1.098$ A
$D_e = 7.373$ eV (crystal phase)
$D_e = 9.834$ eV (gas phase)

see Figures 11, 12 for the gas phase potential functions.

5. Argon-Tungsten/Molybdenum and Argon-Nitrogen Potential Functions

Because it's not likely that argon ions react with nitrogen tungsten or molybdenum, these potential functions have the standard Moliere form, (see Fig. 13).

C. THE IMPACT AREA

The impact area for each simulation is a rectangle containing a grid of 104 impact points, (see Fig. 14), where the length of the sides is 3.165Å = 2.0 LU for tungsten and 3.147 Å = 2.0 LU for molybdenum. The origin of the rectangle is placed at the following locations:

Table 3: Origns of the Impact Area

| target size | | locations | |
|---|---|---|---|
| 23x8x23 | N-reacted | (10,10) (10,12) | Fig. 5 |
| 19x8x19 | N-reacted | (08,08) (08,06) | Fig. 5 |
| 23x8x23 | clean | (11,11) | Fig. 5 |
| 19x8x19 | clean | (09,09) | Fig. 5 |

On the Nitrogen-reacted surface, two impact point sets are necessary to assure complete converage.

## IV. DISCUSSION AND RESULTS

All output was analyzed by a separate analyzer program, AN83, which provides a numerical analysis, and by the program PLOTAN, providing a graphical analysis. The latter is discussed first.

### A. GRAPHICAL ANALYSIS

#### 1. Spot Pattern

The spot pattern plots show the polar and azimuthal angular distribution of the ejected atoms, (see Figs. 15, 16, 17). The distances of the crosses form the center is a measure of the polar angle of the ejected atoms, i.e., a cross far out corresponds to a large ejection angle measured from the surface normal. The spot

pattern obtained for the substrate materials (W, Mo, Mo-mass) show a four-fold symmetry, where 'Mo-mass' means, that in the program the tungsten mass was replaced by the molybdenum mass and all other parameters were unchanged.

The spots at 45°, 135°, 255° and 315° point in the direction of the nearest-neighbors. Figure 15 shows the spot pattern for molybdenum atoms ejected from the substrate after bombarding a nitrogen-reacted molybdenum surface by 2.0 keV argon ions. This figure is typical of all spot pattern obtained from substrate materials.

The spot pattern obtained from the adatoms show no symmetry. Figures 16, 17 are representative for ejected nitrogen atoms. Figure 16, the case where the nitrogen is placed further above the surface, shows a heavier concentration of ejected atoms at low angles than Figure 17.

2. Energy Distribution

Figure 18 shows typical energy distributions for atoms sputtered from the substrate in the ion energy range from 0.5 keV to 3.0 keV. The envelopes peak near 7.0 eV.

The energy distribution of the sputtered nitrogen atoms depends on the location of the adatom. If the nitrogen is close to the surface layer, the distribution peaks at about 2.5 eV/atom, (see Fig. 19). If the nitrogen is further away, as in the case of the tungsten or molybdenum-mass substrate, the distribution is much broader, and the maximum is roughly 15 eV/atom, (see Fig. 20).

3. Energy Distribution >100 Fsec

The energy distribution for particles ejected from the substrate after 100 fsec (1.0 fsec = $10^{-15}$ sec) is similar for all materials, but with the difference that the fraction for molybdenum or molybdenum-mass is less than for tungsten, (see Figs. 21, 22, 23). More low energy atoms are ejected after 100 fsec in the case of the heavier substrate material. This could indicate a mass effect.

Energy distributions for the ejected nitrogen atoms are shown in Figures 24 and 25. If the nitrogen is in the lower position there were no atoms ejected with energy greater than 7.0 eV. This behavior, is seen throughout the whole energy range, (0.5 keV to 3.0 keV). Although the total number of atoms is low, (see Fig. 25), and therefore the statistics are poor, the difference between Fig. 24 and Fig. 25 may be indicating a distance effect.

4. Energy Versus Time.

Figures 26, 27, 28 and 29 show that no high energy particles are ejected later than 100 fsec. The spectrum for substrate materials (Fig. 26) is wider than that for the ejected nitrogen atoms.

Figure 28 shows that hardly any nitrogen atoms are ejected after 100 fsec. The difference between Fig. 27 and 29 and Fig. 28 on the other hand shows again, that there may be a distance effect.

5. Ejection Time Distribution

The ejection time distribution is essentially the same for all substrate materials. For high energies the distribution is lower and broader, (see Figs. 30 and31). The distribution peaks at about 80 fsec.

6. Atoms per Single Ion

The atoms per single ion diagrams are similar throughout all runs. The spectrum broadens with increasing energy, (see Figs. 38, 39, 40 and 41).

7. Yield per Single Impact Point

The yield per single impact point diagrams are also similar for all runs, (see Figs. 42 and 43), where the open circles represent no yield. The diagrams are combined for the locations (10, 10) and (10, 12), i.e., the upper left corner of each rectangular box represents the location (10, 10). Comparison of the centers of the combined squares shows, that whenever the ions hit a substrate atom the yields are larger. The center of each right square is occupied by a nitrogen atom. The nitrogen acts like a 'buffer'. The open circles are caused by channeling. Figures 42 and 43 show that with decreasing ion energy the areas where channeling occurs decrease. The reason for this is that for decreasing energies the cross sections increase because the impact energy appears in the denominator.

8. Yield per Surface Atom

Figures 44, 45 show the yield obtained from the surface layers for both target sizes. Almost no atoms are ejected from the edges of the crystal. This indicates that the crystals are large enough to contain the trajectories.

## B. NUMERICAL ANALYSIS

The numerical analysis done by the analyzer program AN 83 provides the following nitrogen yields, (see also Fig. 46):

Table 4: Nitrogen Yields from Simulations.

| substrate: energy in keV | W(001) yields | Mo-mass(001) yields | Mo(001) yields |
|---|---|---|---|
| 0.5 | 2.36 | 2.04 | 0.60 |
| 1.0 | 2.25 | 2.29 | 0.68 |
| 2.0 | 1.80 | 2.19 | 0.51 |
| 3.0 | 1.37 | 1.87 | 0.51 |

Experimental yields in the ion energy range from 0.5 keV to 3.0 keV are known only for polycrystalline tungsten and molybdenum surfaces [26]. Figure 47 shows the experimental metal yields obtained from polycrystalline tungsten and molybdenum as well as the yield from clean W(001) obtained from the simulation. The yields are listed below:

Table 5: Yields from Clean Metal Surfaces.

| | Experiment | | Simulation |
|---|---|---|---|
| energy in keV | W(poly) | Mo(poly) | W(001) |
| 0.5 | 0.58 | 0.57 | 2.31 |
| 1.0 | 0.88 | 0.80 | 2.94 |
| 2.0 | 1.30 | 1.10 | 2.40 |
| 3.0 | 1.50 | 1.30 | 2.18 |

Some data are known for 5.0 keV $Ar^+$ bombardment of molybdenum [20] at normal incidence onto the (001) planes and onto polycrystalline molybdenum. The yield from polycrystalline Mo is found to be larger than from Mo(001). Thus Roosendaal [20] concludes that for a BCC crystal the same result is found as for FCC structures: the sputtering yield for less closed packed planes is less than the yield from polycrystalline targets, i.e., Y(Poly) > Y(001). The results of this simulation show a yield of about twice the yield from polycrystalline tungsten. Winters [16] and Wehner [27] who bombarded W(001) surfaces in the low energy range with various ion types obtained the results

shown below:

Table 6: Experimental Yields from Clean Metal Surface for Ion Energy of 0.5 keV.

| | Neon | Argon | Krypton | Xenon |
|---|---|---|---|---|
| Winters: | 0.25 | ---- | 0.91 | 1.21 |
| Wehner: | 0.27 | ---- | 0.92 | 1.02 |

The yield is increasing with increasing ion mass and should be about 0.6 for 0.5 keV $Ar^+$ ions. The result of this simulation is higher than this value by a factor of about 4. This shows that the (Ar-W) potential (a standard Moliere) is too hard in this energy range.

Winters [18] shows his results as cross section versus ion energy, (see Fig. 1). The nitrogen cross sections are:

Table 7: Experimental Nitrogen Cross Sections.

| | | cross sections x $10^{-15}$, ($cm^2$) | |
|---|---|---|---|
| energy in kev | substrate | W(001) | Mo(001) |
| 0.5 | | 0.91 | 0.65 |
| 1.0 | | 0.98 | 0.72 |
| 2.0 | | 1.00 | 0.75 |
| 3.0 | | 0.94 | 0.73 |

Winters assumes that the nitrogen sputtering rate is given by

$$-R_N = d\theta_N/dt = \sigma_N \theta_N \nu^+,$$

where $\theta_N$ is the nitrogen atom concentration (atoms/$cm^2$), $\sigma_N$ is the sputtering cross section ($cm^2$), $\nu^+$ the ion flux (ions/$cm^2$-s), and t the time in seconds. The product $t\nu^+$ is the ion dose (fluence) while the product $\sigma_N\theta_N$ gives the sputtering yield in nitrogen atoms/ion.

Using this relation ($Y = \Theta_N \sigma_N$) the cross section obtained from the simulation are:

Table 8: Simulation Nitrogen Cross Sections.

cross sections x $10^{-15}$, ($cm^2$)

| energy in keV | substrate: W(001) | Mo-mass(001) | Mo(001) |
|---|---|---|---|
| 0.5 | 4.77 | 4.12 | 1.20 |
| 1.0 | 4.55 | [illegible] | 1.36 |
| 2.0 | 3.64 | 3.42 | 1.02 |
| 3.0 | 2.77 | 3.78 | 1.02 |

Figures 48 and 49 show Winters cross sections in comparison to the cross sections obtained from the simulation. In the case where the nitrogen is in the lower position (Mo) (Fig. 48), the simulation cross sections are in a better agreement with the experimental results. But even in this case the simulated cross sections are still too large. This suggests that the (Ar-N) potential (also a standard Moliere) is too hard. Winters' experiments showed that the sputtering yield of nitrogen tends to increases as the atomic weight of the substrate increases. He suggests that the difference in the cross section for the sputtering of nitrogen from W(001) and Mo(001) is dominated by the adsorbate-substrate mass difference since the other important parameters are similar. The simulation shows that the distance between the nitrogen and the substrate is more important than the mass difference.

Winters furthermore states that the shape of the yield curves for the chemisorbed gas and the substrate material is different because the ratio $\sigma$(gas)/$\sigma$(substrate) decreases with increasing ion energy. Winters used $\sigma$(substrate) cross sections obtained from polycrystalline W and Mo assuming a surface coverage of $\Theta = 10^{+15}$ atoms/$cm^2$. The following ratios were calculated from the simulation: $\sigma N(W)/\sigma W(clean)$,

$\sigma$(Mo-mass)/$\sigma$W(clean), $\sigma$N(Mo)/$\sigma$W(clean). Using $\sigma$W(clean) in the latter case seems reasonable, because comparision of yields from polycrystal- line W and Mo as well as the yields obtained from the substrates are not too different, i.e., the yields from Mo(clean) shouldn't diviate much from W(clean). $\Theta$ for W(001) is $9.98 \times 10^{+15}$ atoms/$cm^2$. The ratios are shown below (see also Fig. 49).

Table 9: Cross Section Ratios.

| | Experiment | | Simulation | | |
|---|---|---|---|---|---|
| energy in keV | $\frac{\sigma N(W)}{\sigma W(poly)}$ | $\frac{\sigma N(Mo)}{\sigma Mo(poly)}$ | $\frac{\sigma N(W)}{\sigma W(clean)}$ | $\frac{\sigma N(Mo\text{-}mass)}{\sigma W(clean)}$ | $\frac{\sigma N(Mo)}{\sigma W(clean)}$ |
| 0.5 | 1.57 | 1.14 | 2.06 | 1.78 | 0.52 |
| 1.0 | 1.11 | 0.90 | 1.54 | 1.57 | 0.46 |
| 2.0 | 0.77 | 0.68 | 1.52 | 1.84 | 0.43 |
| 3.0 | 0.63 | 0.56 | 1.27 | 1.73 | 0.47 |

In comparison to Winters' results, Figure 50 shows the ratios for nitrogen in the lower position and Figure 51 for nitrogen in the higher position. (Mo-mass not shown.) The values obtained from the simulation show the general trend observed by Winters for the W and Mo substrate, but indicate that the location of the high nitrogen is perferable for the tungsten substrate and low for the molybdenum substrate. Even with these choices, the difference between the nitrogen locations is too large. This is also seen by comparing $\sigma$N(W)/$\sigma$N(Mo) between Winters data and the data obtained from the simulation. The ratios are shown below, (see also Fig. 52):

Table 10: Cross Section Ratios.

| energy | Experiment | Simulation | |
|---|---|---|---|
| in keV | $\sigma N(W)/\sigma N(Mo)$ | $\sigma N(W)/\sigma N(Mo\text{-}mass)$ | $\sigma N(W)/\sigma N(Mo)$ |
| 0.5 | 1.40 | 1.16 | 3.98 |
| 1.0 | 1.36 | 0.98 | 3.35 |
| 2.0 | 1.33 | 0.82 | 3.57 |
| 3.0 | 1.29 | 0.73 | 2.72 |

As mentioned in section A7, with decreasing ion energy the cross sections increase and the areas where channeling occur decrease. This is also seen comparing the reflected argon yields, listed below:

Table 11: Simulation Argon Yields.

| | clean | | nitrogen reacted | |
|---|---|---|---|---|
| energy in keV | substrate W(001) | Mo-mass(001) | W(001) | Mo(001) |
| 0.5 | 0.40 | 0.30 | 0.43 | 0.24 |
| 1.0 | 0.27 | 0.11 | 0.22 | 0.13 |
| 2.0 | 0.12 | 0.07 | 0.09 | 0.05 |
| 3.0 | 0.07 | 0.07 | 0.05 | 0.03 |

Due to the increase in cross sections, more ions are reflected at low energies. Harrison (19) says that about 85% of the ejected atoms (bulk material) from clean targets come from the first layer. This simulation shows that at least 80% of the ejected atoms come from the first layer. The yield from deeper layers varies between 19% and 5%, where the yield from below the second layer is almost neglible. The yields from below the first one are shown below:

Table 12: Yields from Second or Deeper Layers (Simulation).

| | clean | | nitrogen reacted | |
|---|---|---|---|---|
| energy in keV | substrate W(001) | Mo-mass(001) | W(001) | Mo(001) |
| 0.5 | 11% | 12% | 16% | 5% |
| 1.0 | 10% | 14% | 17% | 8% |
| 2.0 | 16% | 16% | 19% | 12% |
| 3.0 | 17% | 18% | 17% | 16% |

Some of the ejected atoms, which have similar energy, velocity and position, combine above the surface, forming multimers. Most of the multimers observed are dimers: (W-W, (W-N), Mo-Mo), (Mo-N). No (N-N) dimers were found. The numbers of dimers observed are listed below:

Table 13: Dimers from Clean Tungsten (Simultion).

| energy in keV | W - W |
|---|---|
| 0.5 | 40 |
| 1.0 | 53 |
| 2.0 | 18 |
| 3.0 | 22 |

Table 14: Dimers from Nitrogen Reacted Surfaces (Simulation).

| energy in keV | W - N | Mo - N | W - W | Mo - Mo |
|---|---|---|---|---|
| 0.5 | 50 | 9 | 18 | 18 |
| 1.0 | 65 | 12 | 23 | 31 |
| 2.0 | 27 | 15 | 24 | 15 |
| 3.0 | 14 | 8 | 19 | 10 |

The table below shows the number of linked atoms (taken from all multimers).

Table 15: Linked Atoms (Simulations).

| energy in keV | substrate | W | | Mo-mass | | Mo | |
|---|---|---|---|---|---|---|---|
| | | (WW) | (WN) | (MoMo) | (MoN) | (MoMo) | (MoN) |
| 0.5 | | 33 | 71 | 56 | 85 | 33 | 18 |
| 1.0 | | 41 | 82 | 74 | 92 | 54 | 29 |
| 2.0 | | 72 | 66 | 37 | 64 | 27 | 18 |
| 3.0 | | 42 | 37 | 42 | 65 | 29 | 19 |

In the case of the molybdenum substrate the number of Mo-N links exceeds the number of Mo-Mo links throughout the whole energy range. In the case of the tungsten substrate the number of linked W-W is higher for 3 keV and 2 keV.

## V. SUMMARY AND RECOMMENDATIONS

The results of the simulation show that the ion-substrate potential functions are chosen too hard. Further work should be done to reduce the yields for the substrate materials. The graphical analysis shows that there may be mass as well as distance effects, but the results of the simulation clearly show that the adsorbate-substrate distance is more important than the adsorbate-substrate mass difference, when the nitrogen sits in the higher position on the substrate with the higher atomic mass. After adjusting the substrate yields, futher work should be done to find the right distance between the adatoms and the substrate.

## LIST OF REFERENCES


1. W.R. Rove, Trans. Roy Soc. (Loden) 142, 87 (1852).
2. E. Goldstein, Verh. Dtsch. Phys. Ges., 4,228,237 (1902).
3. J. Stark, Kie Electizitaet in Gasen (Barth, Leibzig 1902).
4. J. Stark, Z. Elektrochem. 14, 752 (1908); 15, 509 (1909).
5. A. V. Hippel, E. Blechschmidt: Ann. Phys. (Leipzig) 80, 627 (1926); 81, 999, 1043, (1926); 86, 1006 (1928).
6. G. K. Wehner, Phys. Rev. 102, 690 (1956).
7. E. S. Lamar, K. T. Compton, Science 80, 541 (1934).
8. F. Keywell, Phys. Rev. 87, 160 (1952).
9. D. E. Harrison, Phys. Rev. 102, 1473 (1956); 105, 1202 (1957); J. Chem Phys. 32, 1336 (1960).
10. R. Behrisch, Ergeb. Exaktk. Naturw. 35, 295 (1964).
11. M. Kaminsky, Atomic and Ionic Impact Phenomena on Metal Surfaces (Springer Verlag, Berlin, 1965).
12. G. Carter and J. S. Colligan, Ion Bombardment of Solids (Elsevier Publishing Co., Inc., New York 1968).
13. N. V. Pleshivtsev, Cathode Sputtering, (Atomizdat, Moscow, 1968).
14. P. Sigmund, Phys. Rev. 184, 383 (1969).
15. K. H. Kingdon and I. Langmuir, Phys. Rev. 20,107 (1922); 21,210 (1923); 22, 148 (1923).
16. H. F. Winters, J. Appl. Phys., Vol. 45, No. 11 (1974).
17. E. Taglauer and W. Heiland, J. Nucl. Mater. 93, *23 (1980).
18. H. F. Winters, J. Vac Sci. Tehnol., 20(3), 493 (1982).
19. D. E. Harrison, Radiation Effects, 70, 1-64 (1983).
20. R. Behrisch, Sputtering by Particle Bombardment I, (Springer-Verlag 1981).
21. I. R. Clavenna, Surface Science , 22, 365 (1970).
22. D. L. Adams, Surface Science , 27, 21 (1971).
23. K. Criffiths, Phys. Rev. Letters, 461, 1584 (1981).

24. D. E. Harrison, Application of ion beams to metals, 427 (1973), (Plenum Press, New York).

25. I. M. Torrens, Interatomic Potentials (Academic Press 1972).

26. N. Matsunami, Energy dependence of sputtering yields of monatomic solids, Institut of Plasma Physics Nagoya University, Japan.

27. G. K. Wehner, J. Appl. Phys., 32, 365 (1961).

## FIGURES

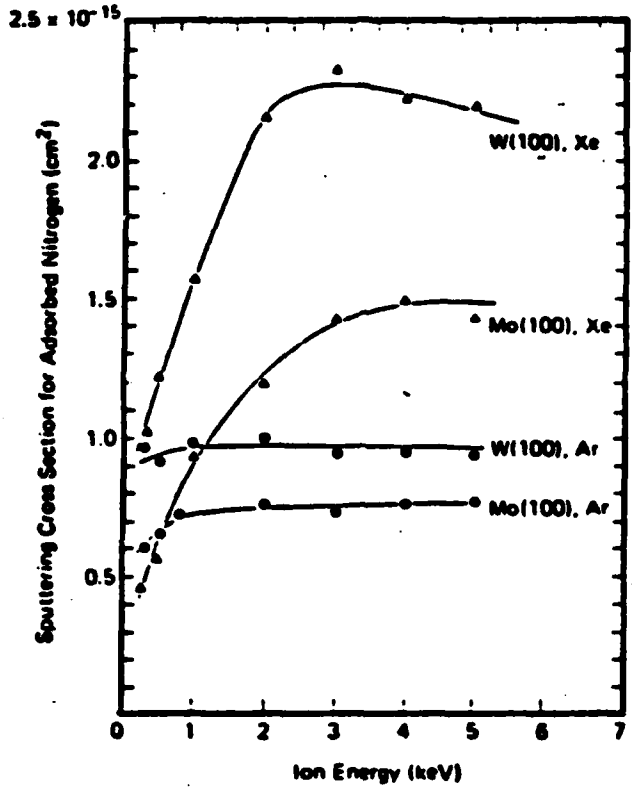


FIG. 1 Sputtering cross sections for nitrogen from W(100) and Mo(100) versus ion energy. The sputtering yield is the product of the cross section and the atomic density of adsorbed nitrogen.

Fig. 1. Sputtering Cross Sections.

a)

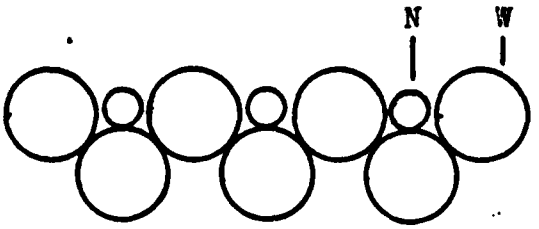


Sideview

b)

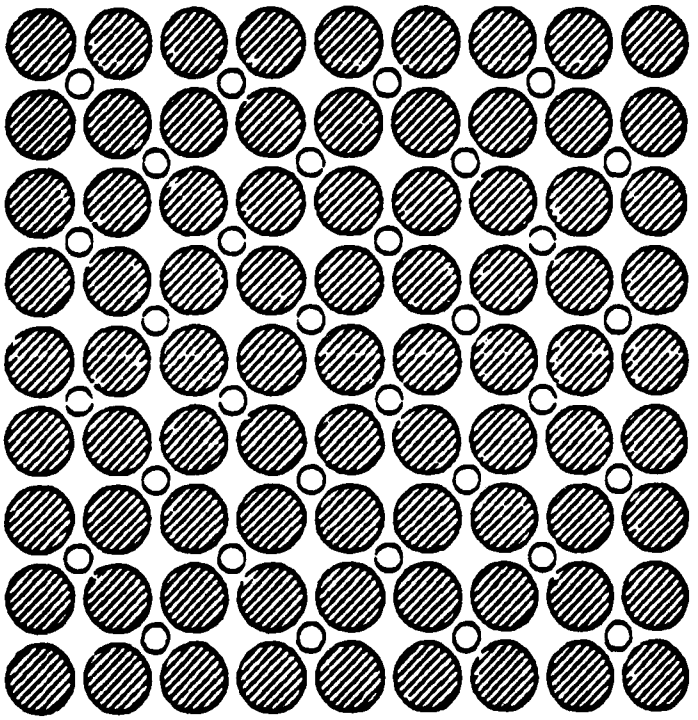

Topview

Fig. 2. Nitrogen reacted tungsten surface.
Small circles represent the N-atoms.

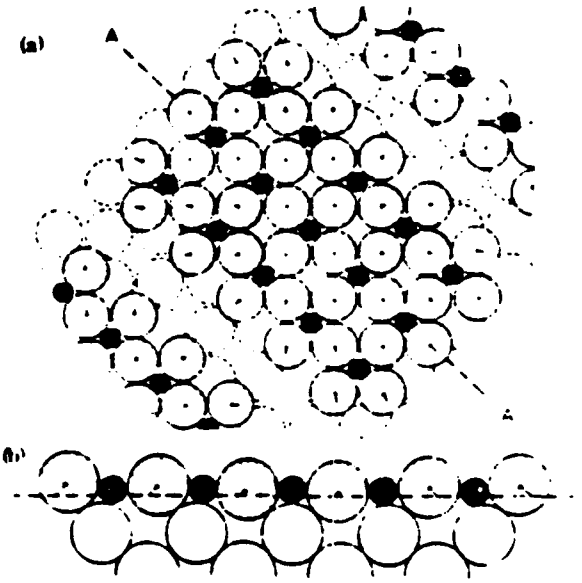


The proposed contracted-domain structure for the C(4 monolayer N on W(001) surface: Large hatched circles, top-layer W-atoms, small filled circles, N-atoms.
a) Plan view, illustrating domain and boundary structure.
b) Cross section through the domain along AA.

Fig. 3. Island formation of a nitrogen reacted tungsten surface.

a) Sideview

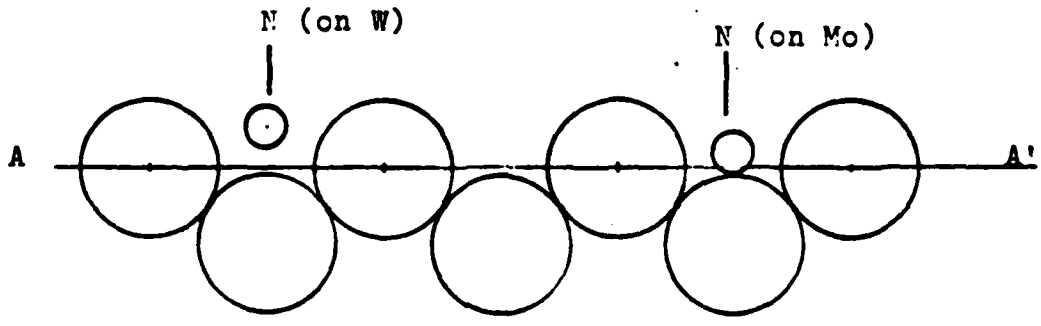


b) Topview

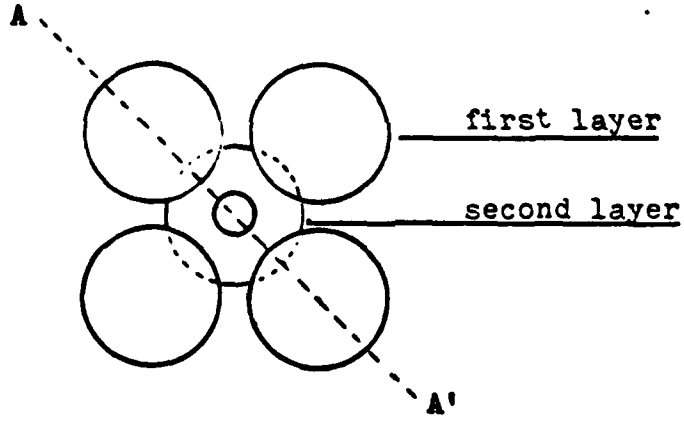


Small circles represent nitrogen atoms.

Fig. 4. Location of nitrogen atoms on tungsten and molybdenum substrates.

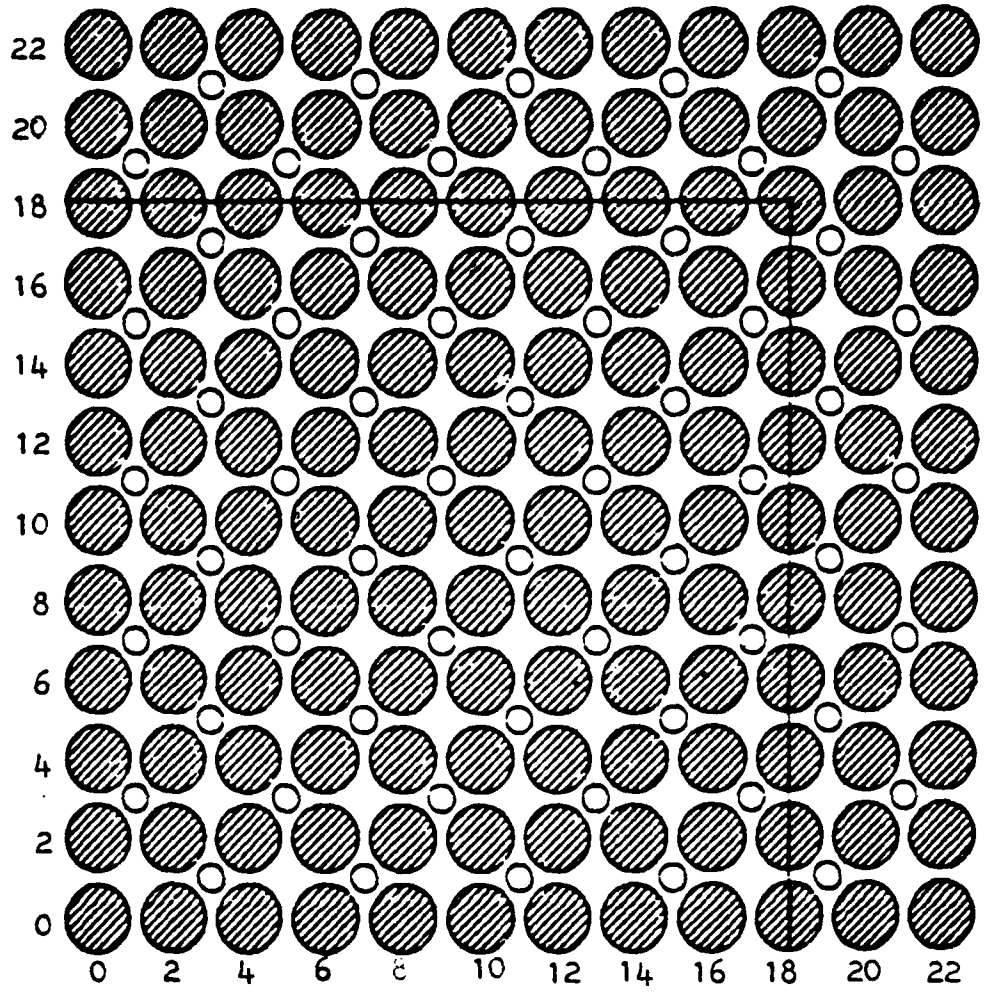


Small circles represent nitrogen atoms.
Solid lines mark smaller target.
Numbers represent layers.

Fig. 5. Topview of reacted surface.

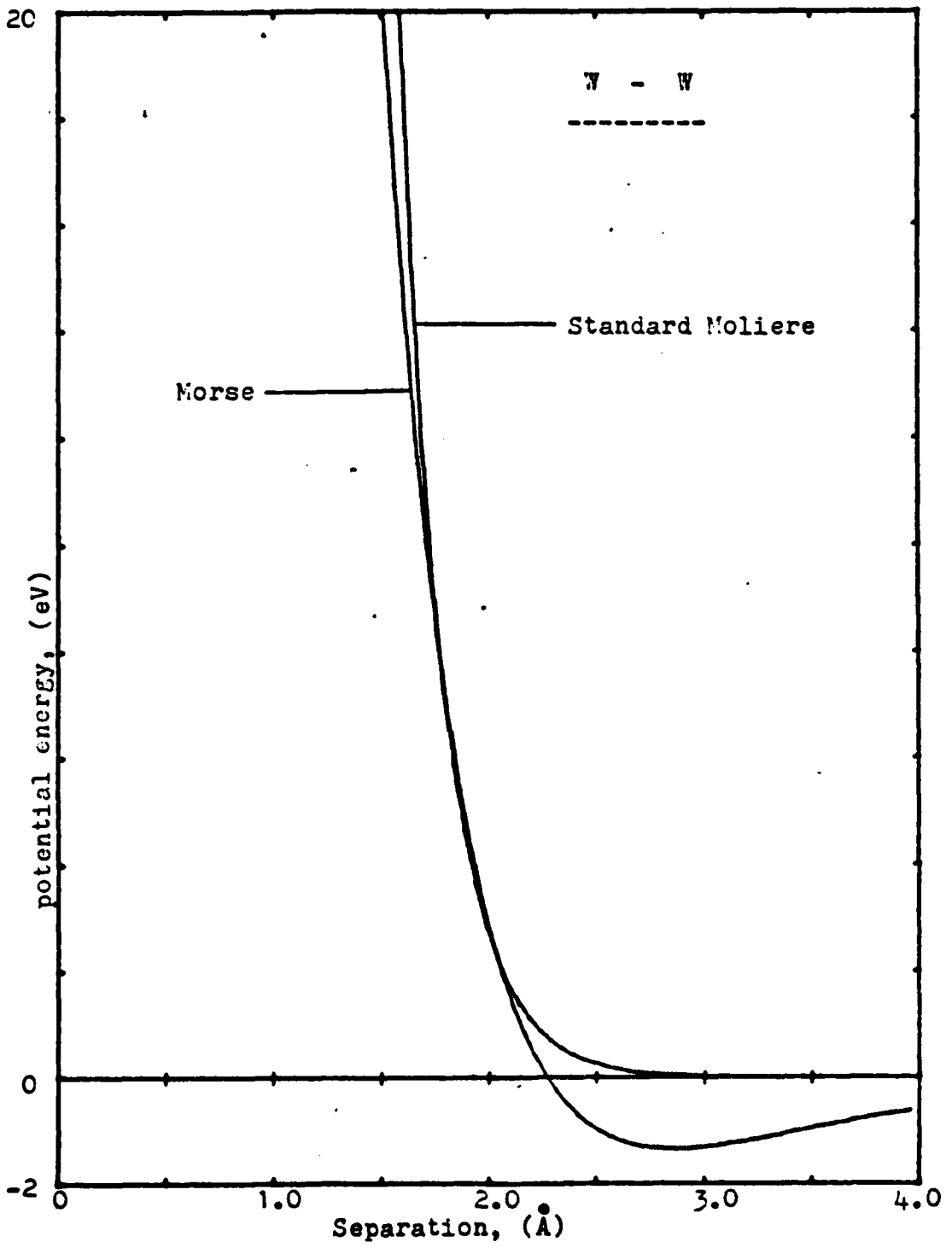


Fig. 6. Interatomic potential functions.

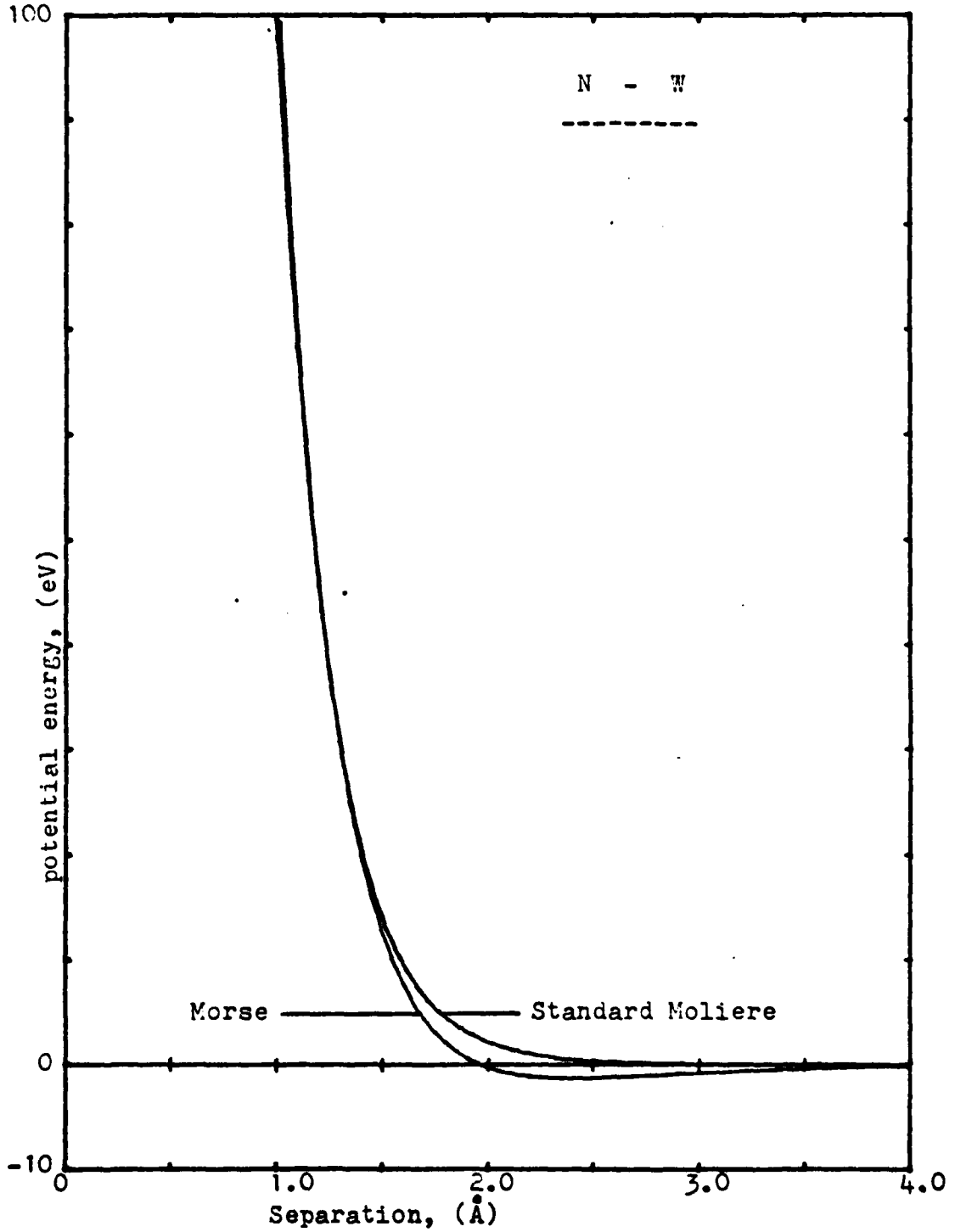


Fig. 7. Interatomic potential functions.

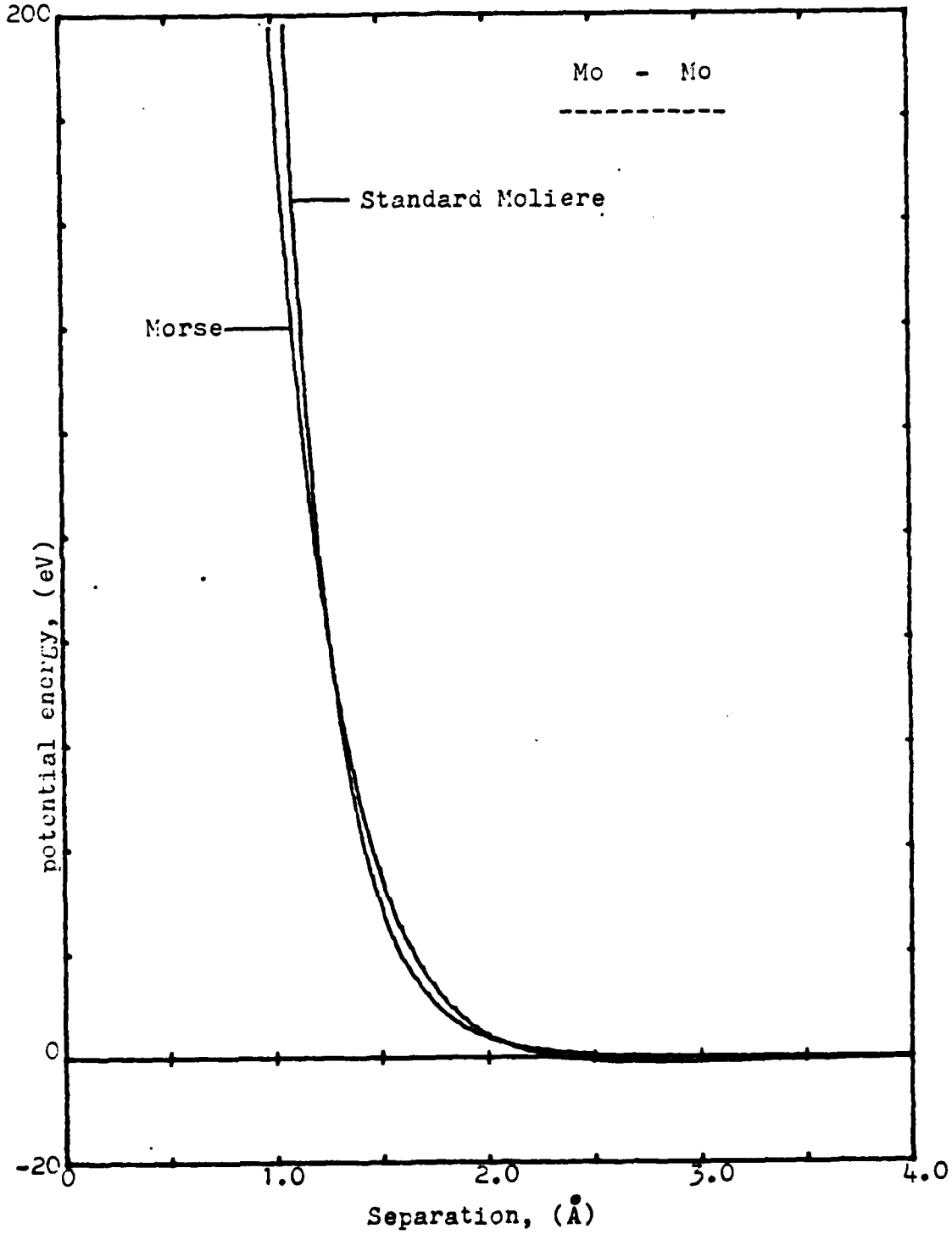


Fig. 8. Interatomic potential functions.

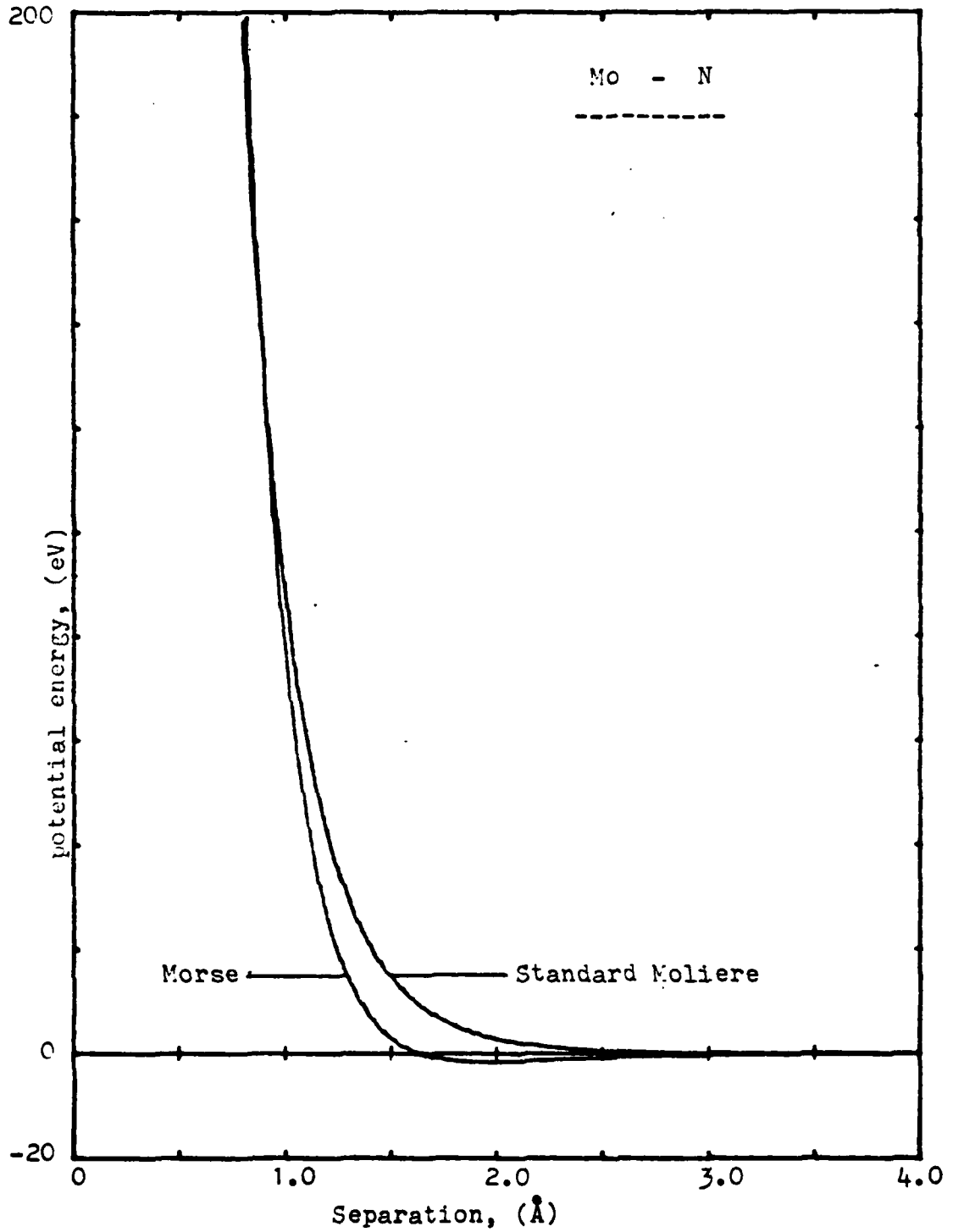


Fig. 9. Interatomic potential functions.

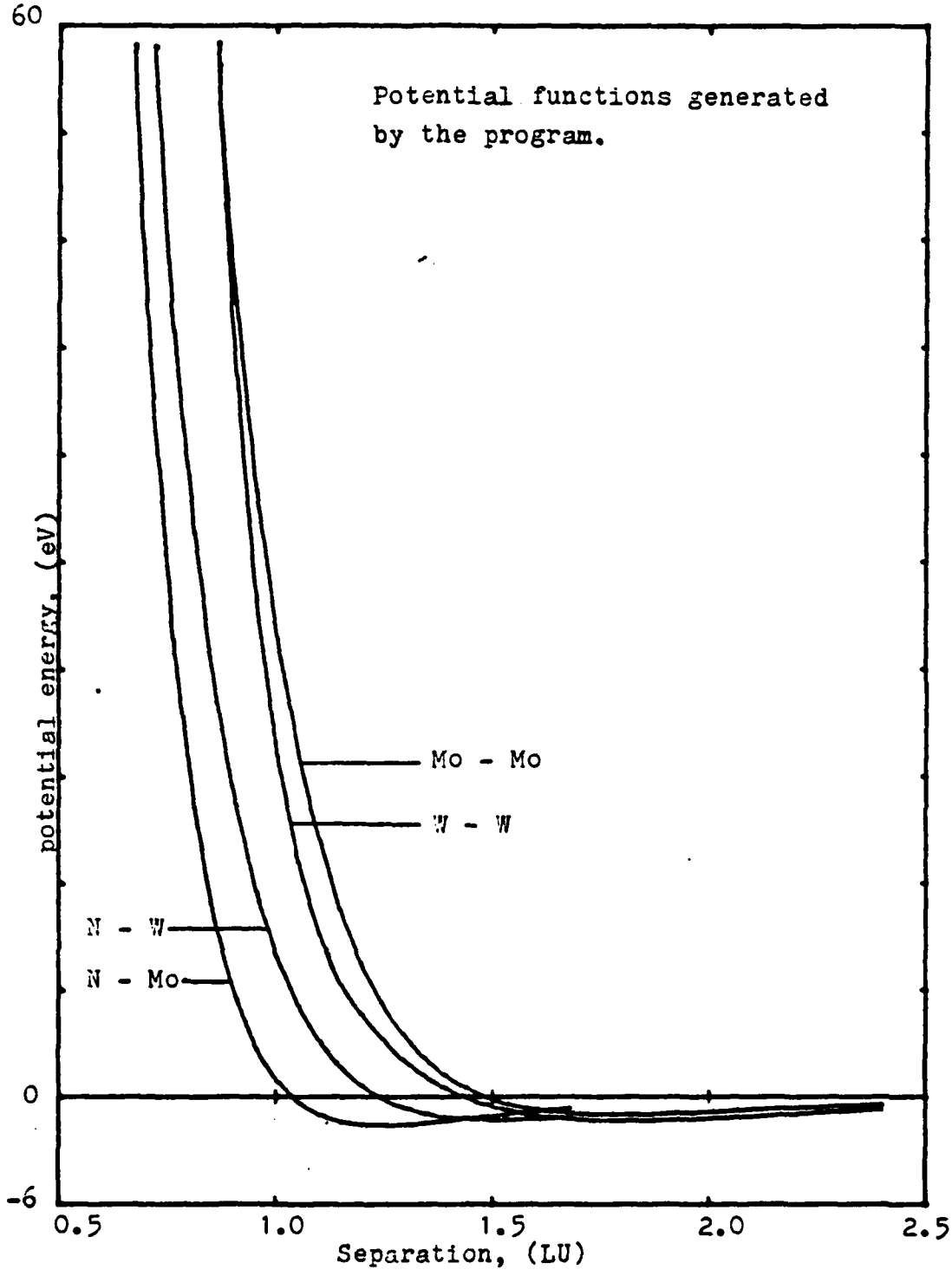


Fig. 10. Interatomic potential functions.

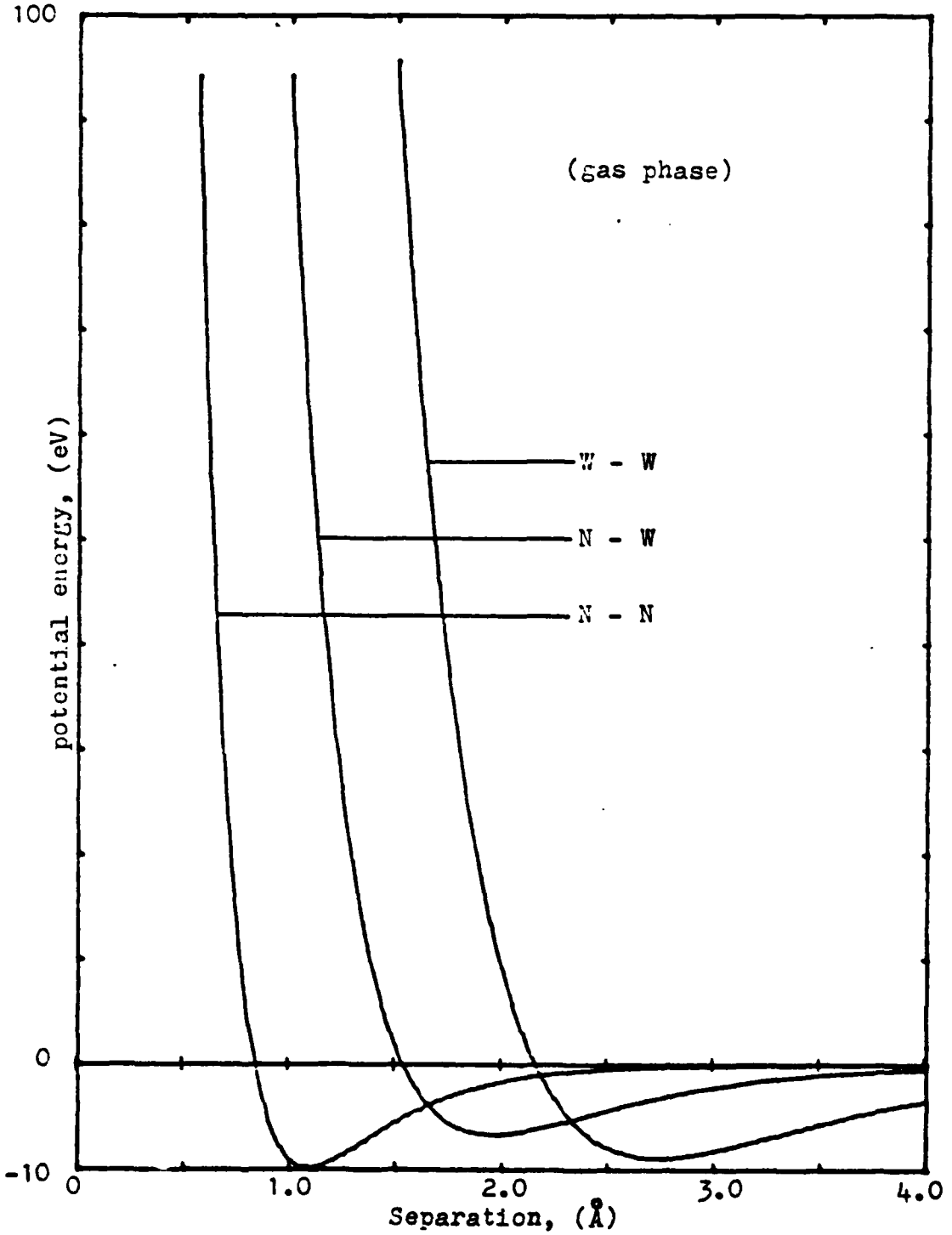


Fig. 11. Interatomic potential functions.

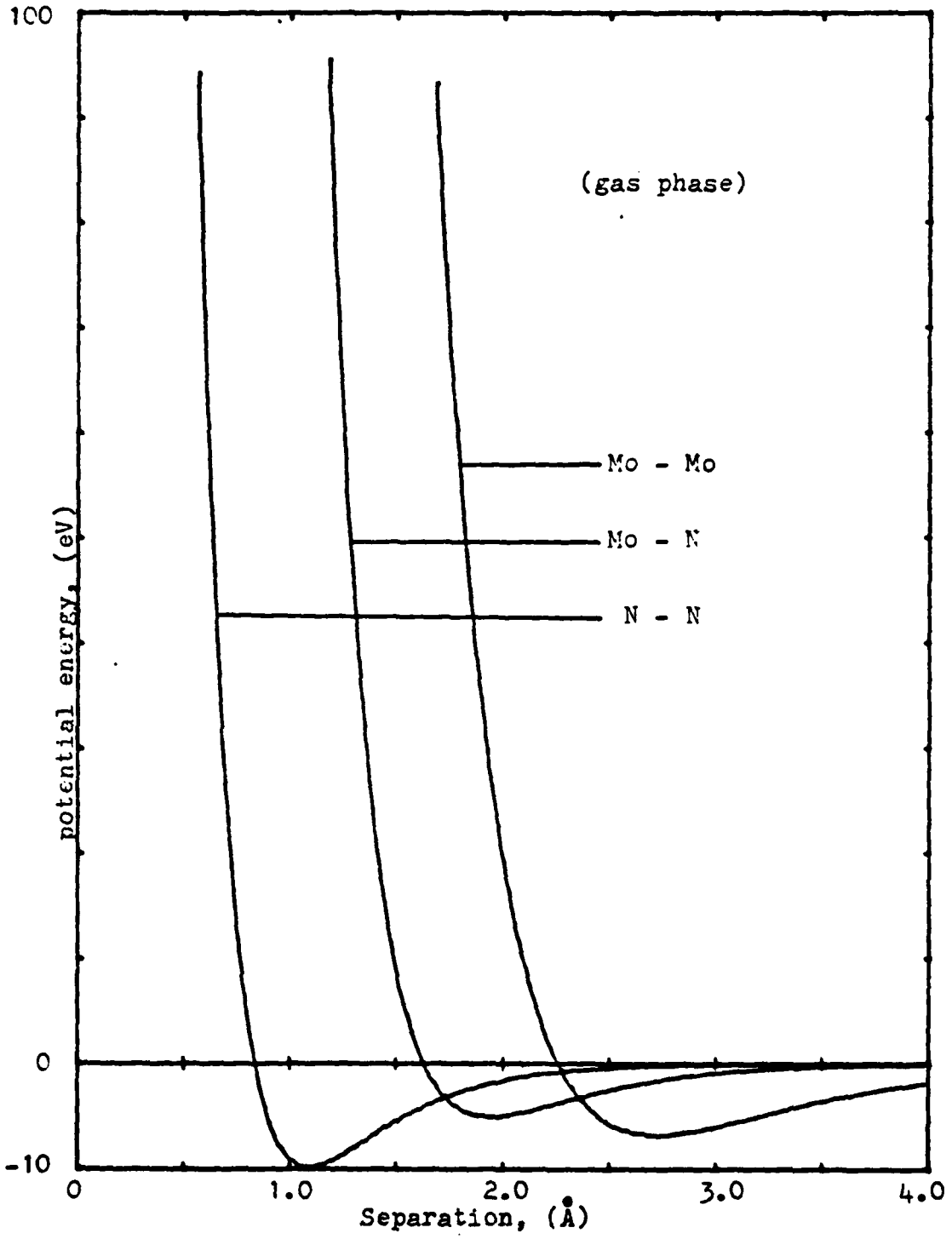


Fig. 12. Interatomic potential functions.

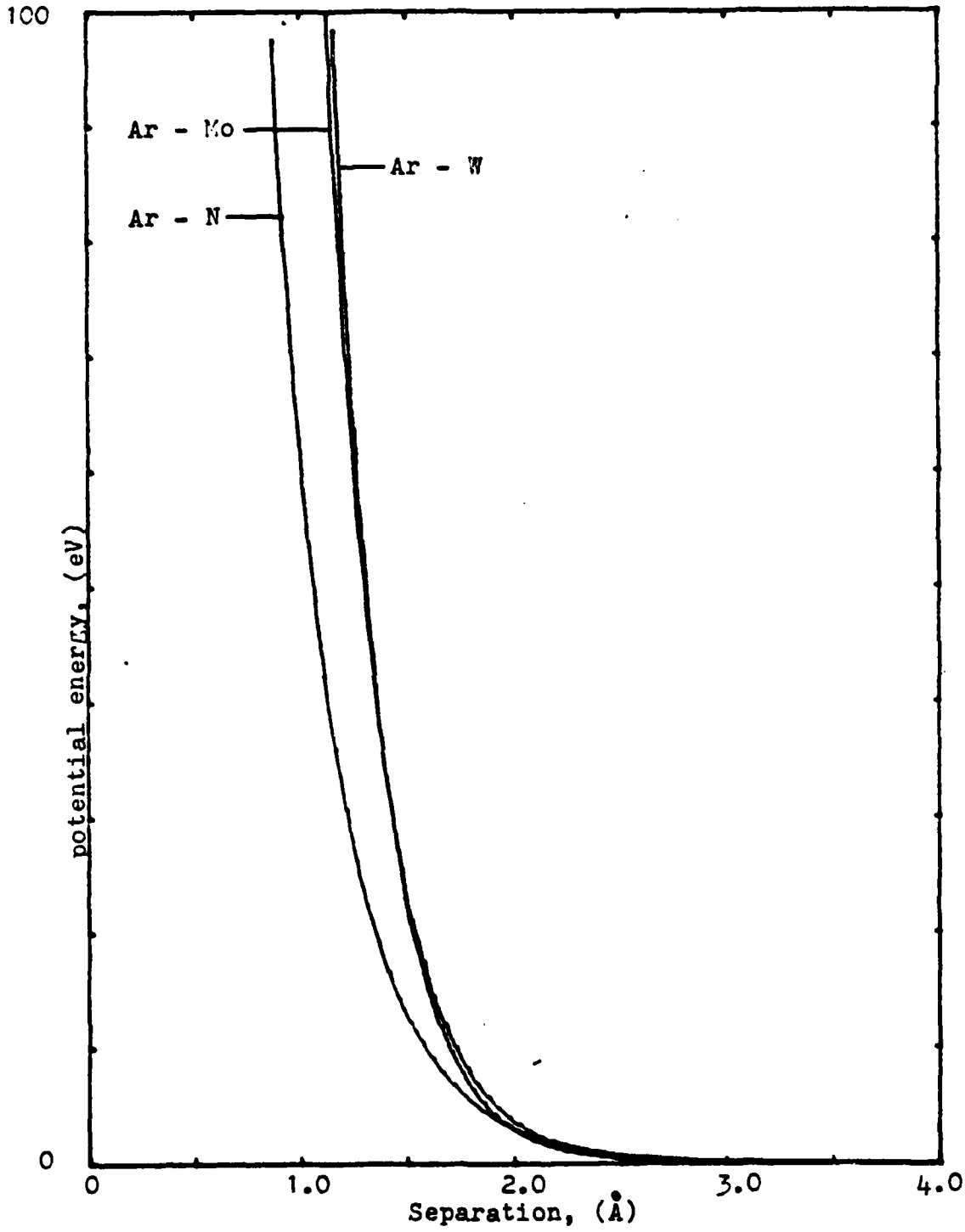


Fig. 13. Interatomic potential functions.

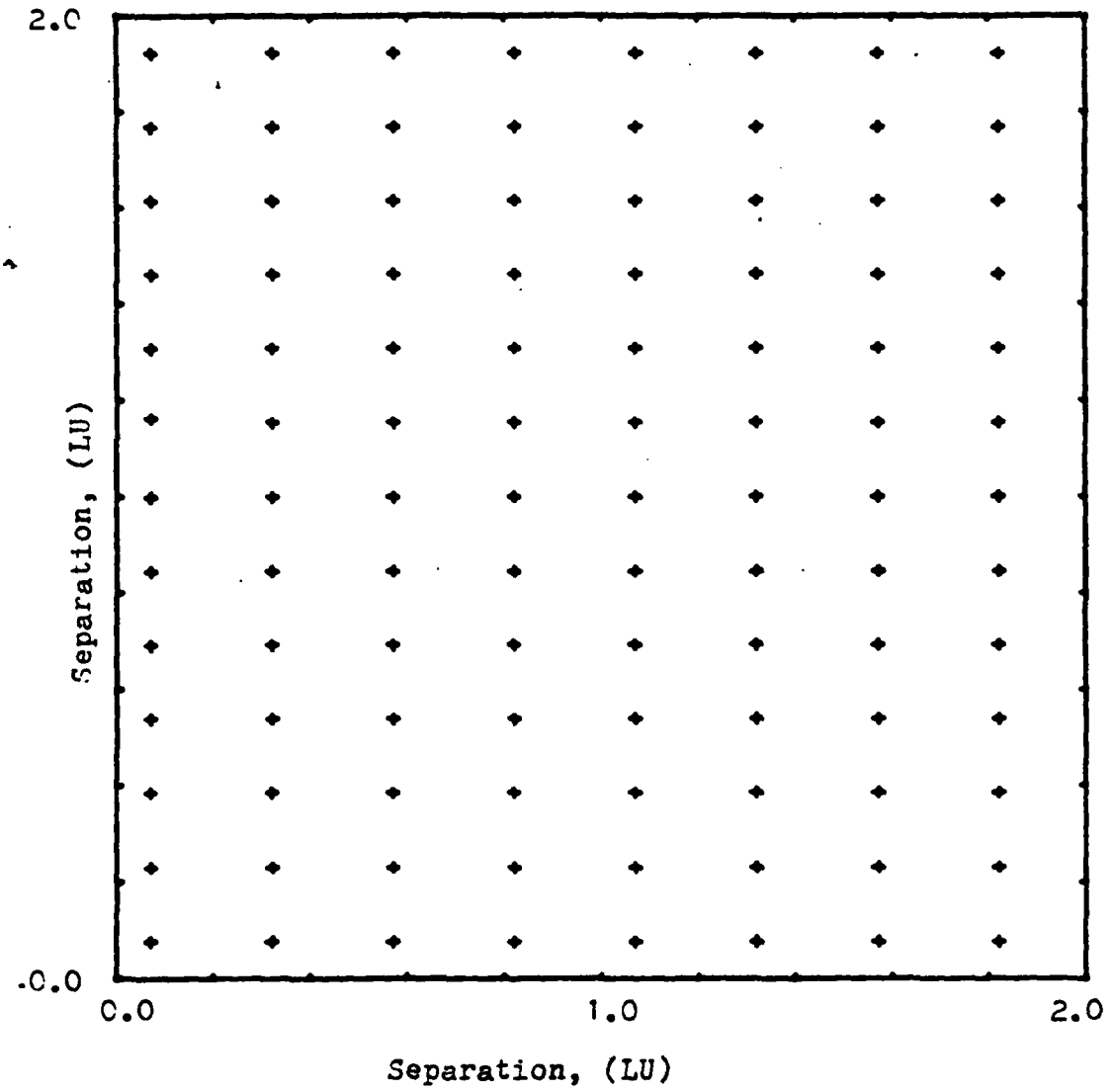


Fig. 14. Impact area.

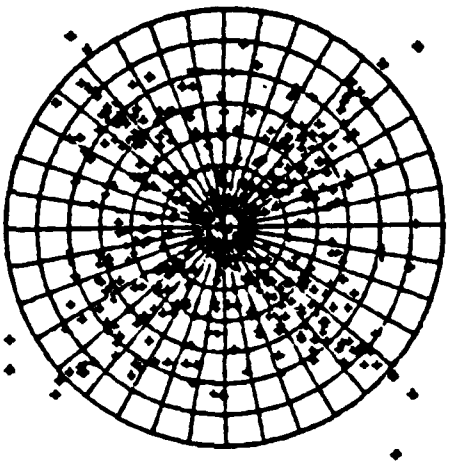

**2.0 KEV MO(001) 'MO'**

**SPOT PATTERN**

(obtained for Mo-substrate)

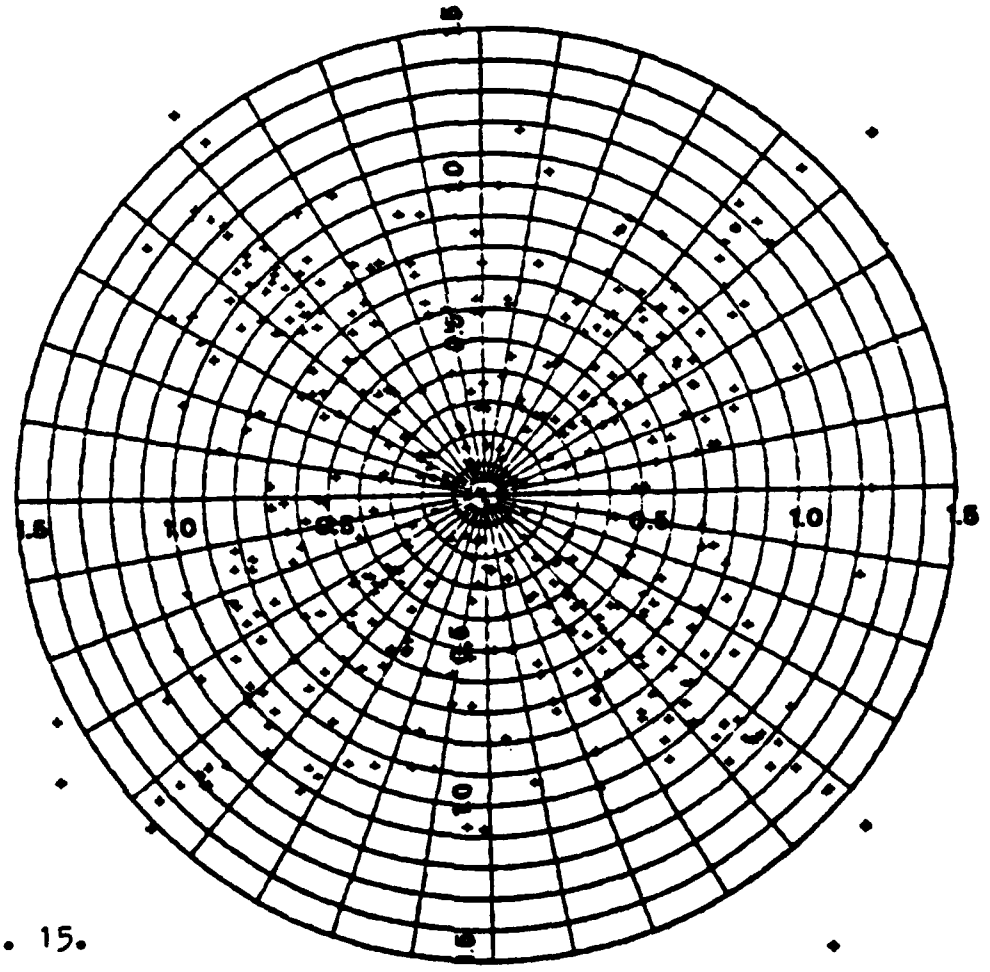


Fig. 15.

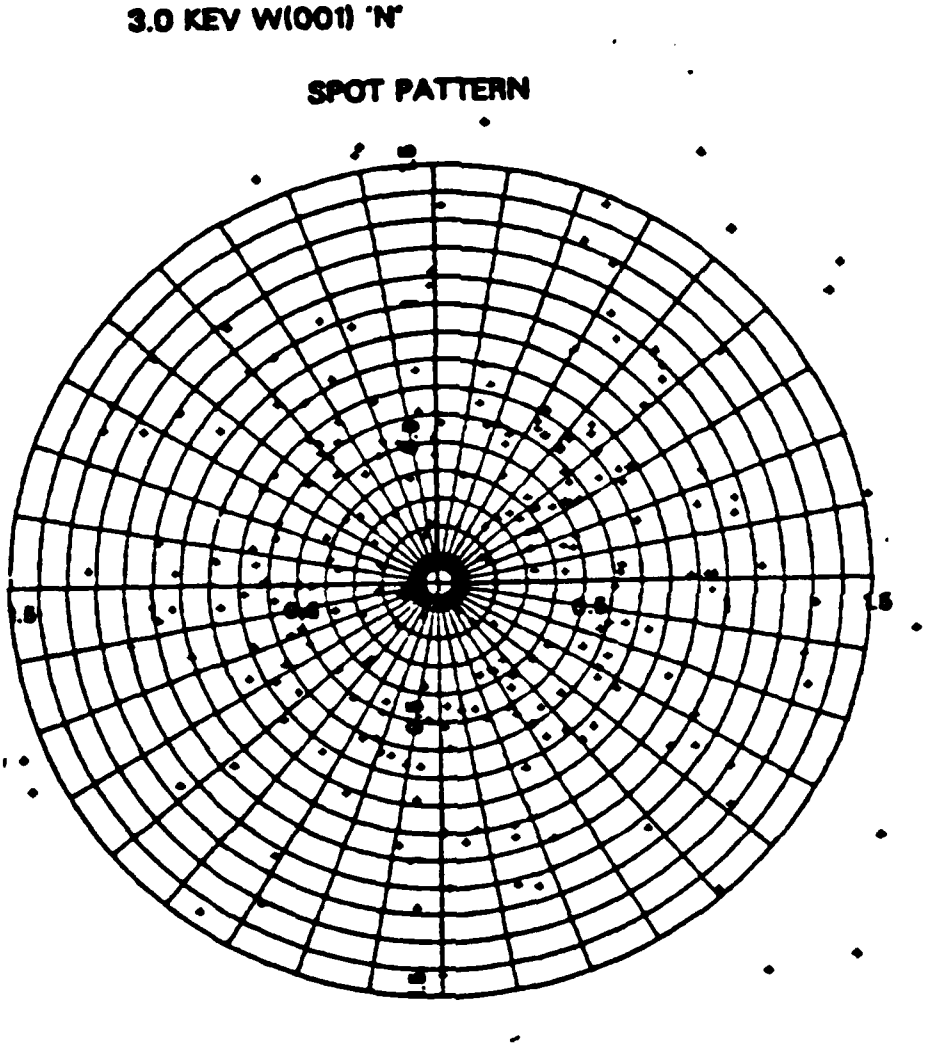


Fig. 16. Spot pattern for nitrogen atoms from a W(C01) surface.

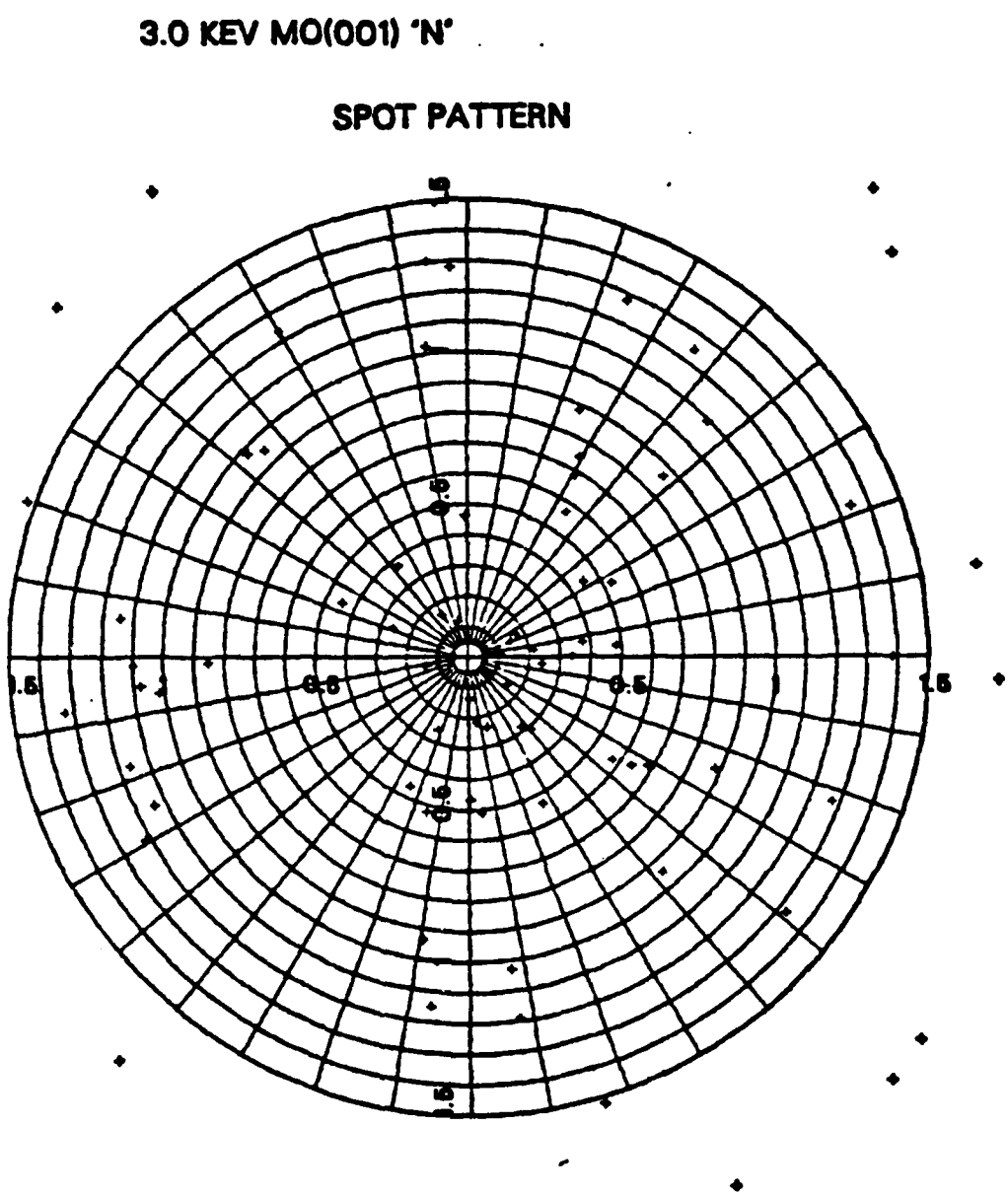


Fig. 17. Spot pattern for nitrogen atoms from a Mo(001) surface.

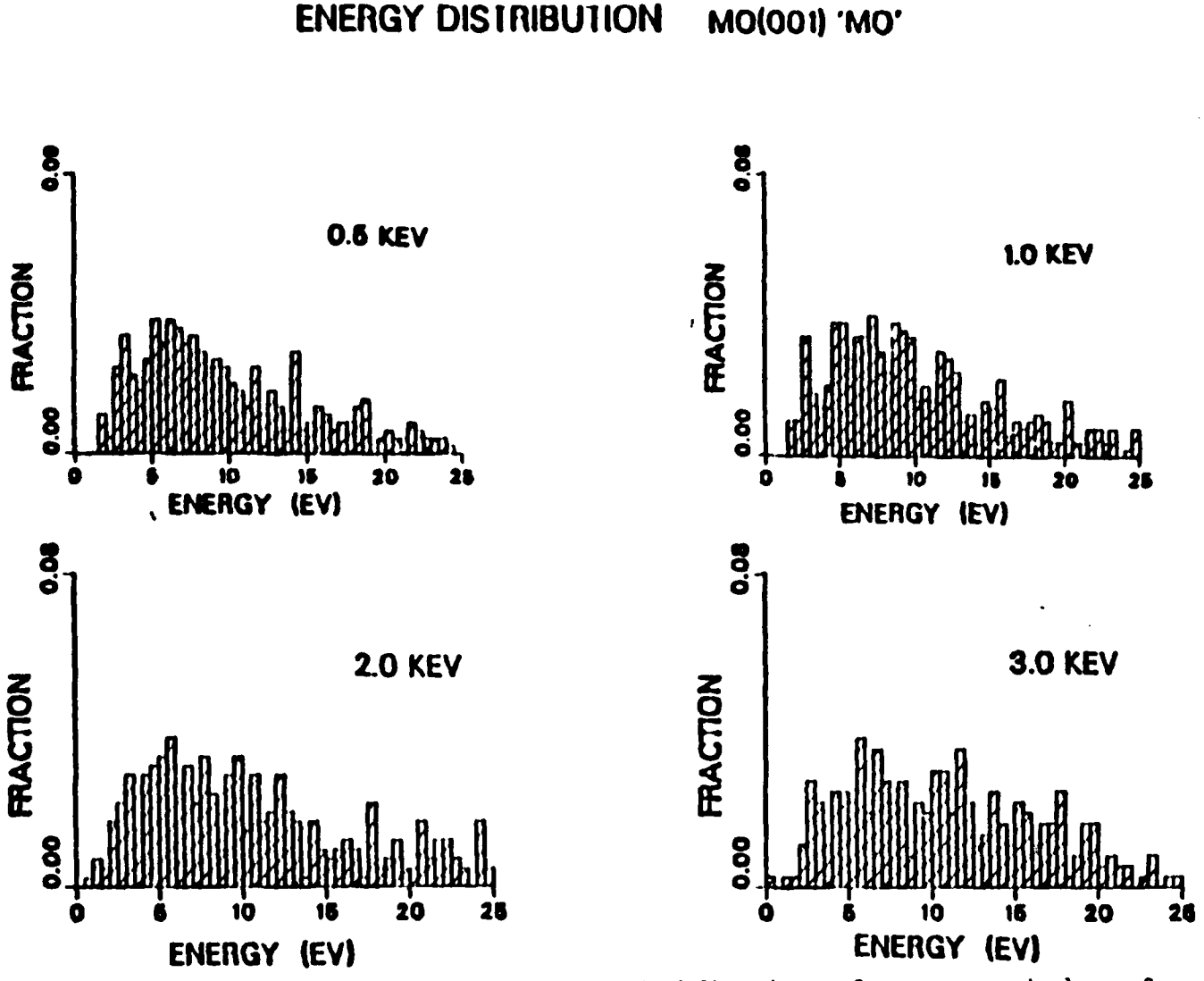


Fig. 18. Energy distribution for ejected Mo atoms from a reacted surface.

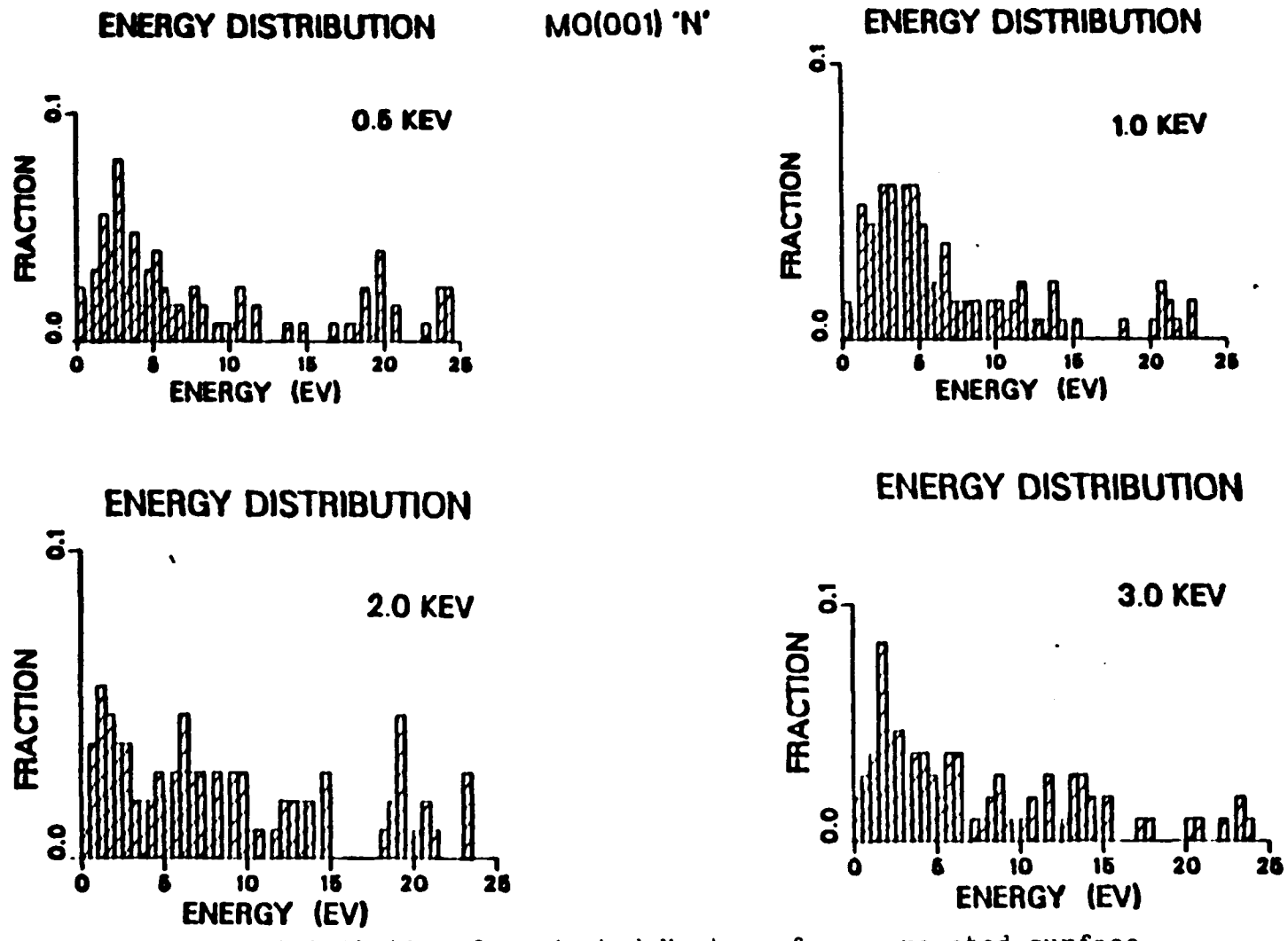


Fig. 19. Energy distribution for ejected N atoms from a reacted surface.

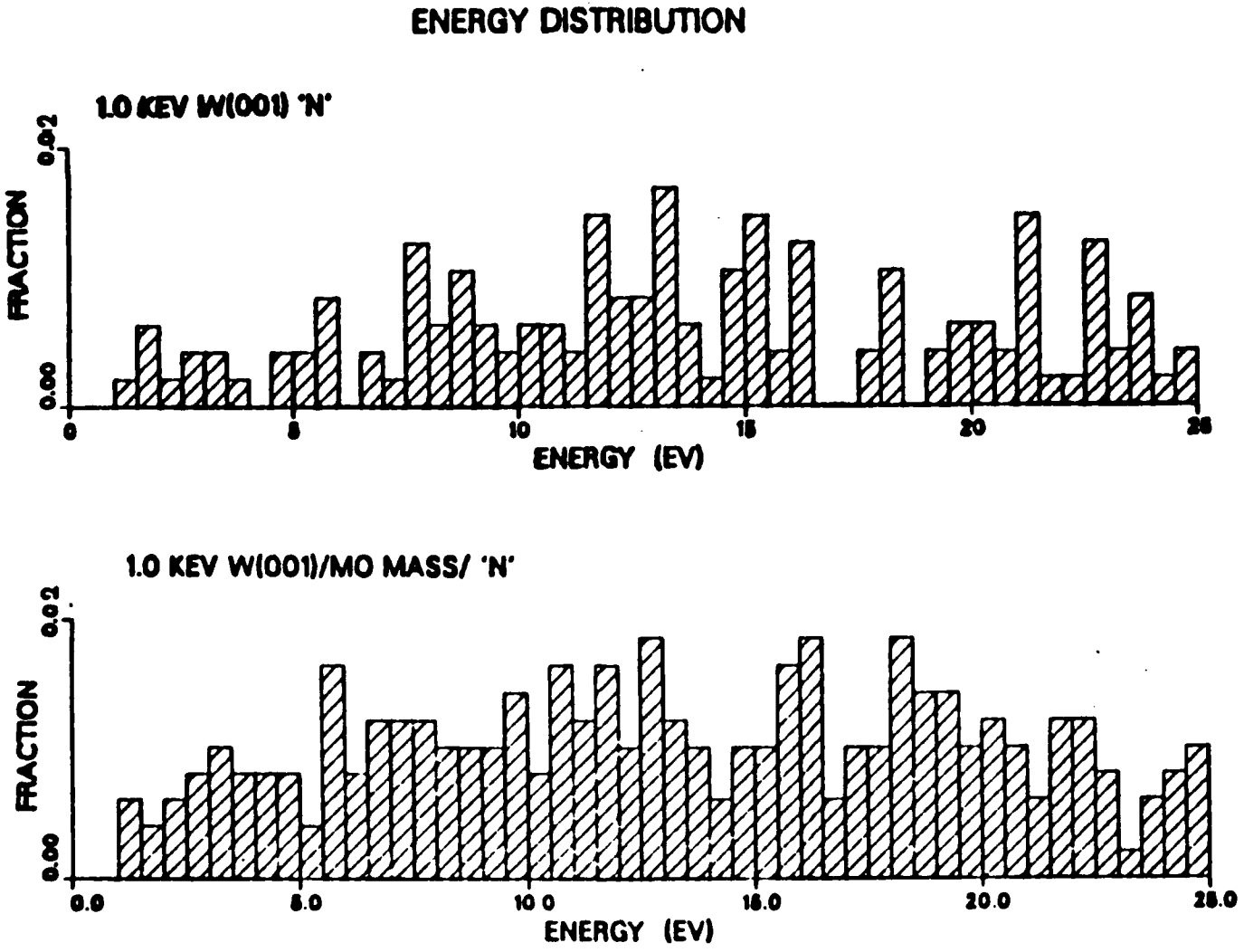


Fig. 20. Energy distribution for ejected N atoms from reacted surfaces.

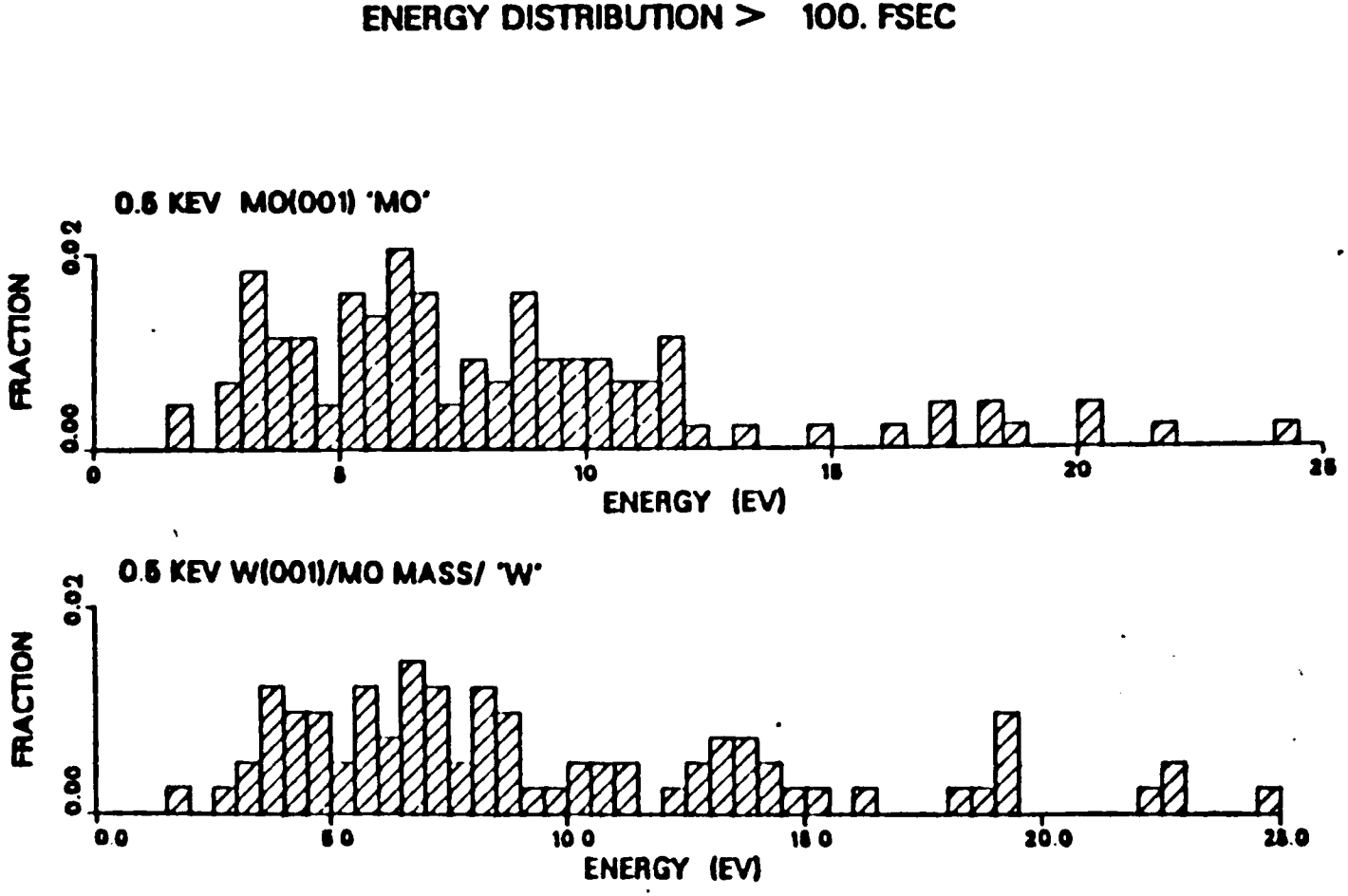


Fig. 21. Energy distribution for atoms (substrate), ejected after 100 fsec.

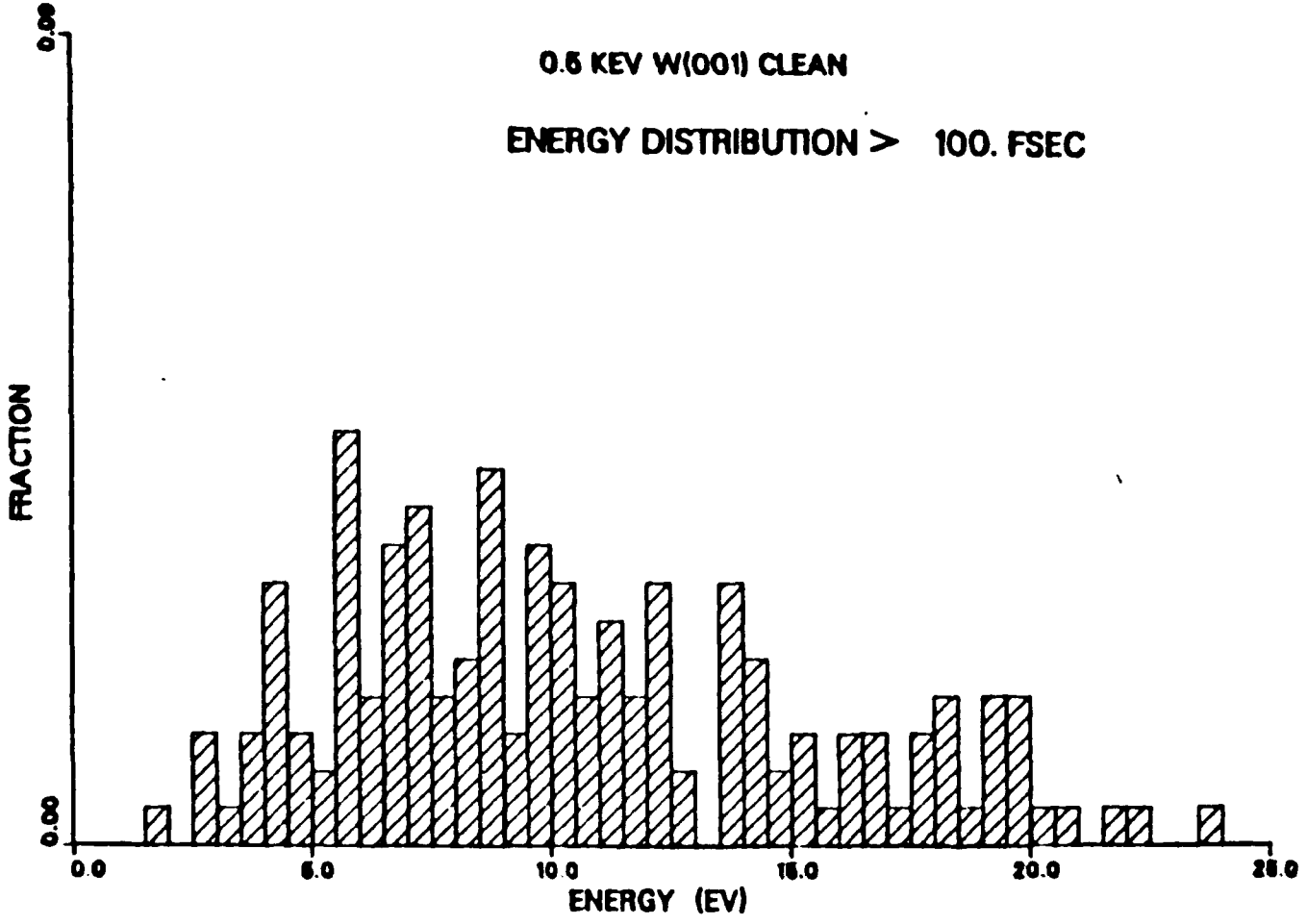


Fig. 22. Energy distribution for atoms, ejected after 100 fsec.

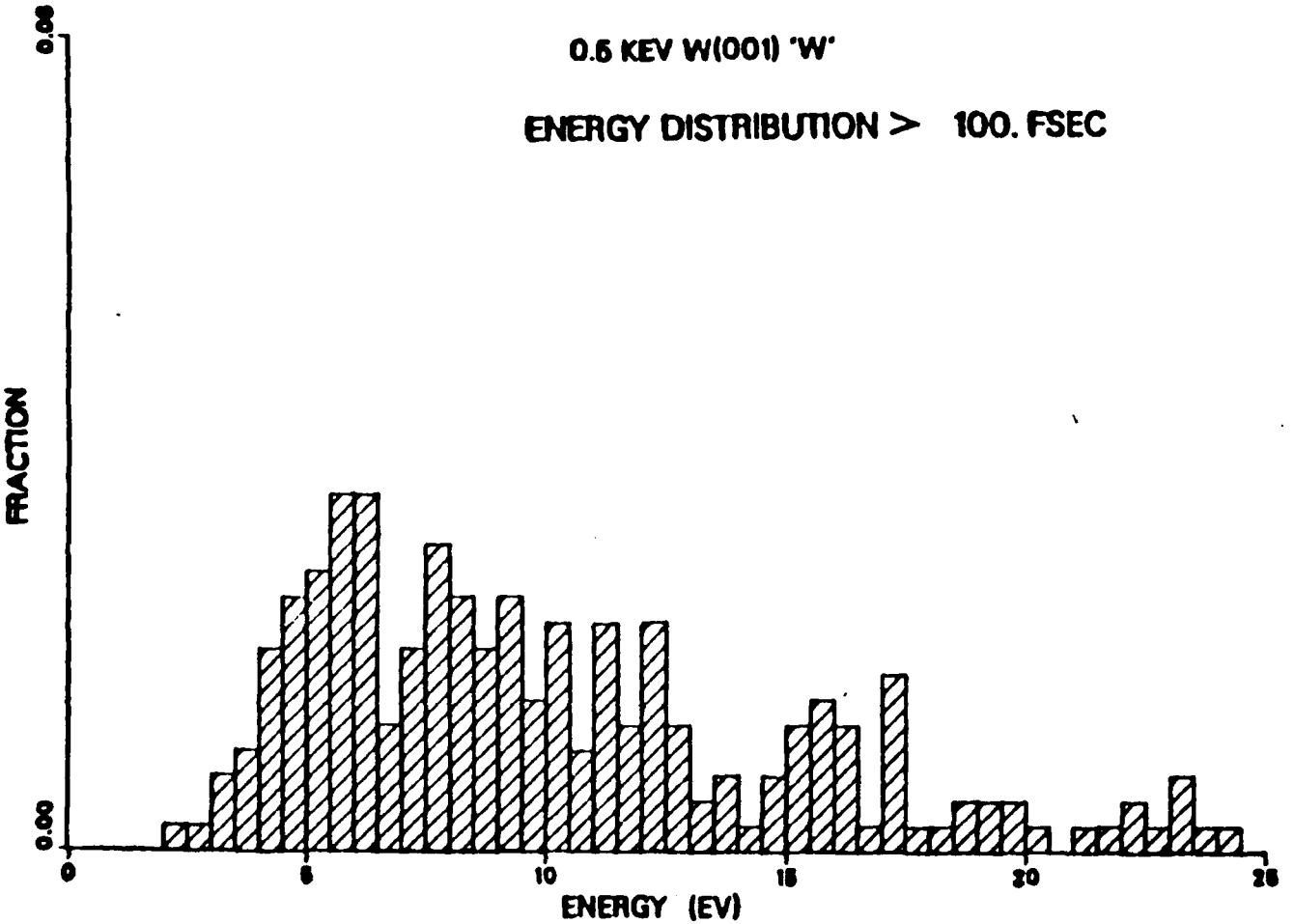


Fig. 23. Energy distribution for atoms (substrate), ejected after 100 fsec.

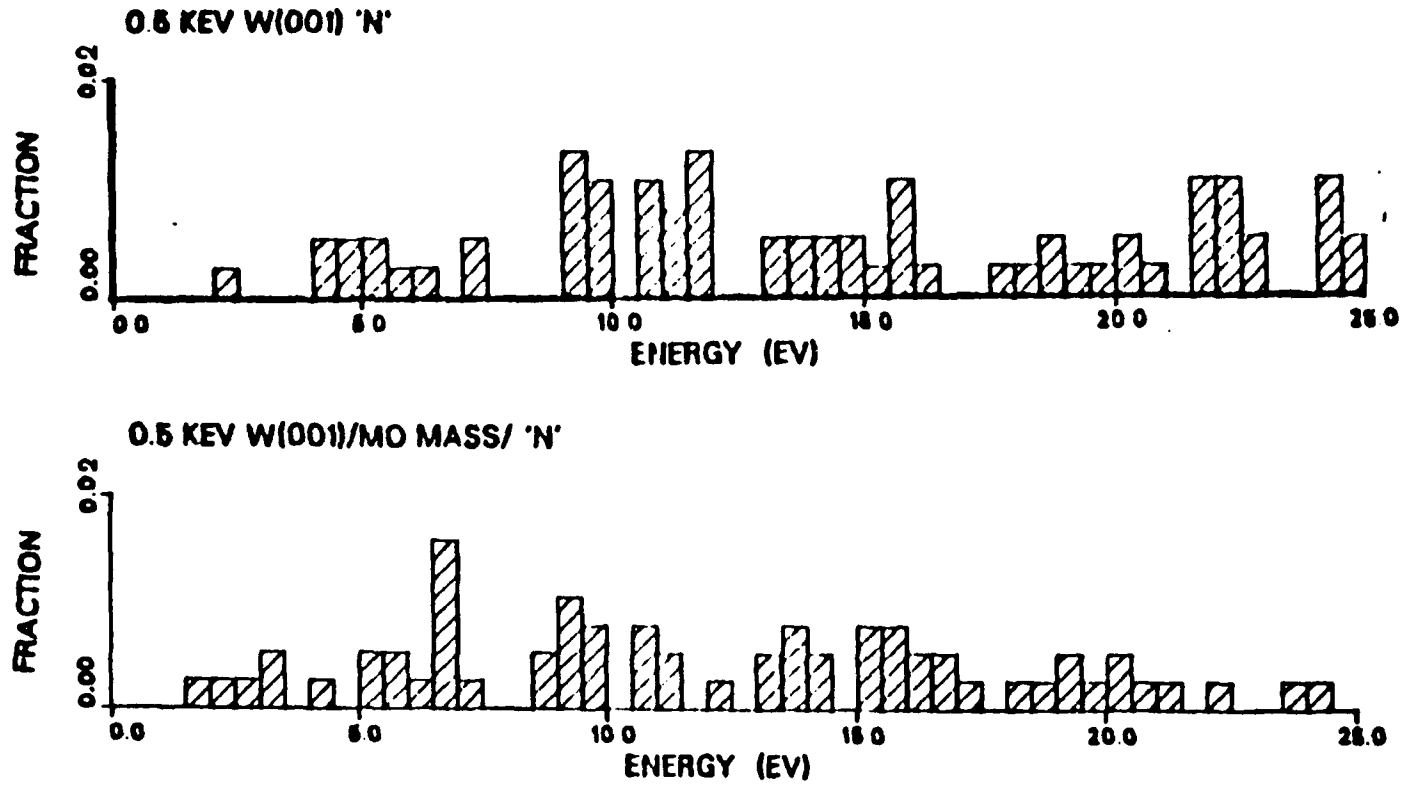


Fig. 24. Energy distribution for N atoms, ejected after 100 fsec.

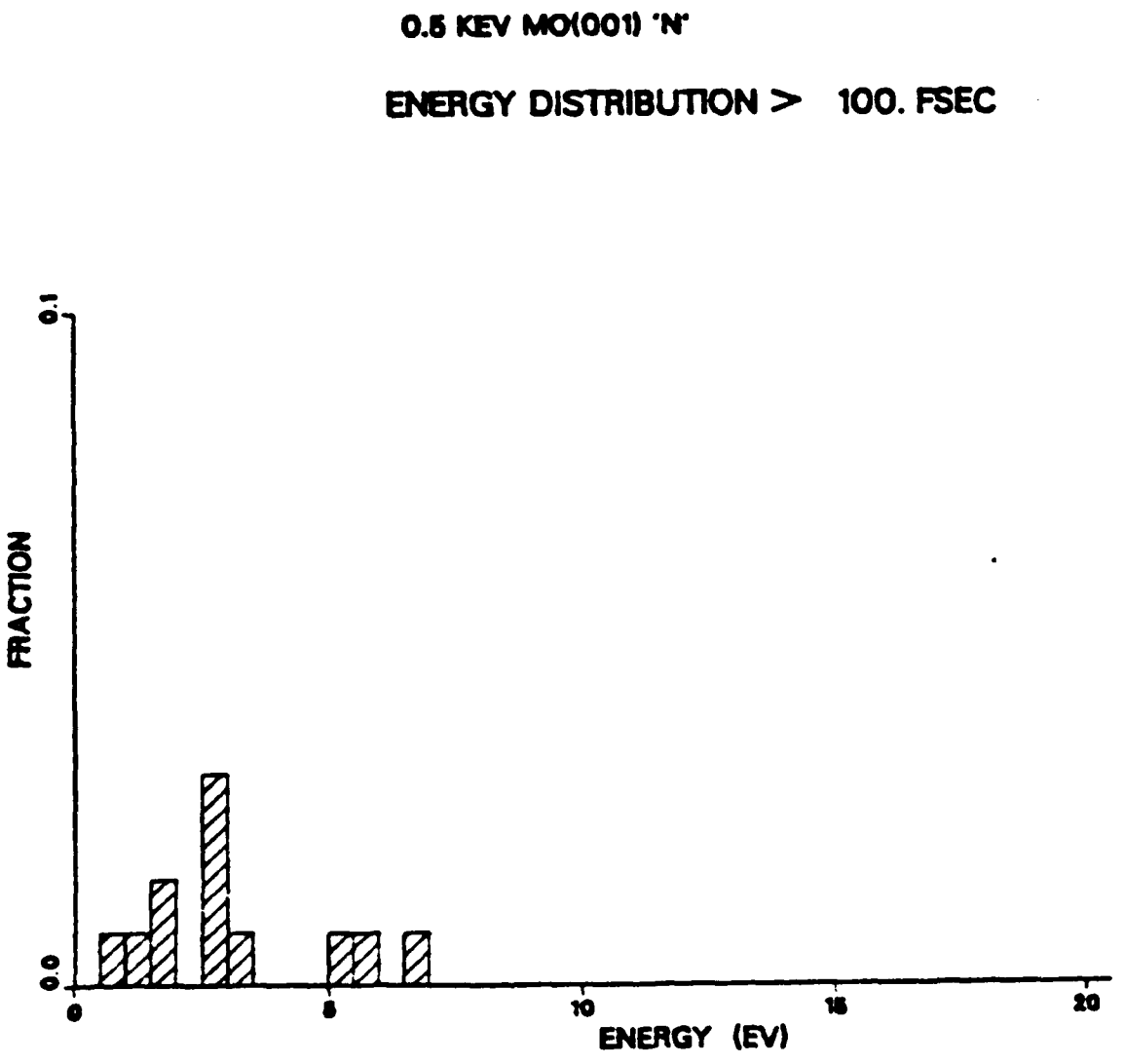


Fig. 25. Energy distribution for N atoms, ejected after 100 fsec.

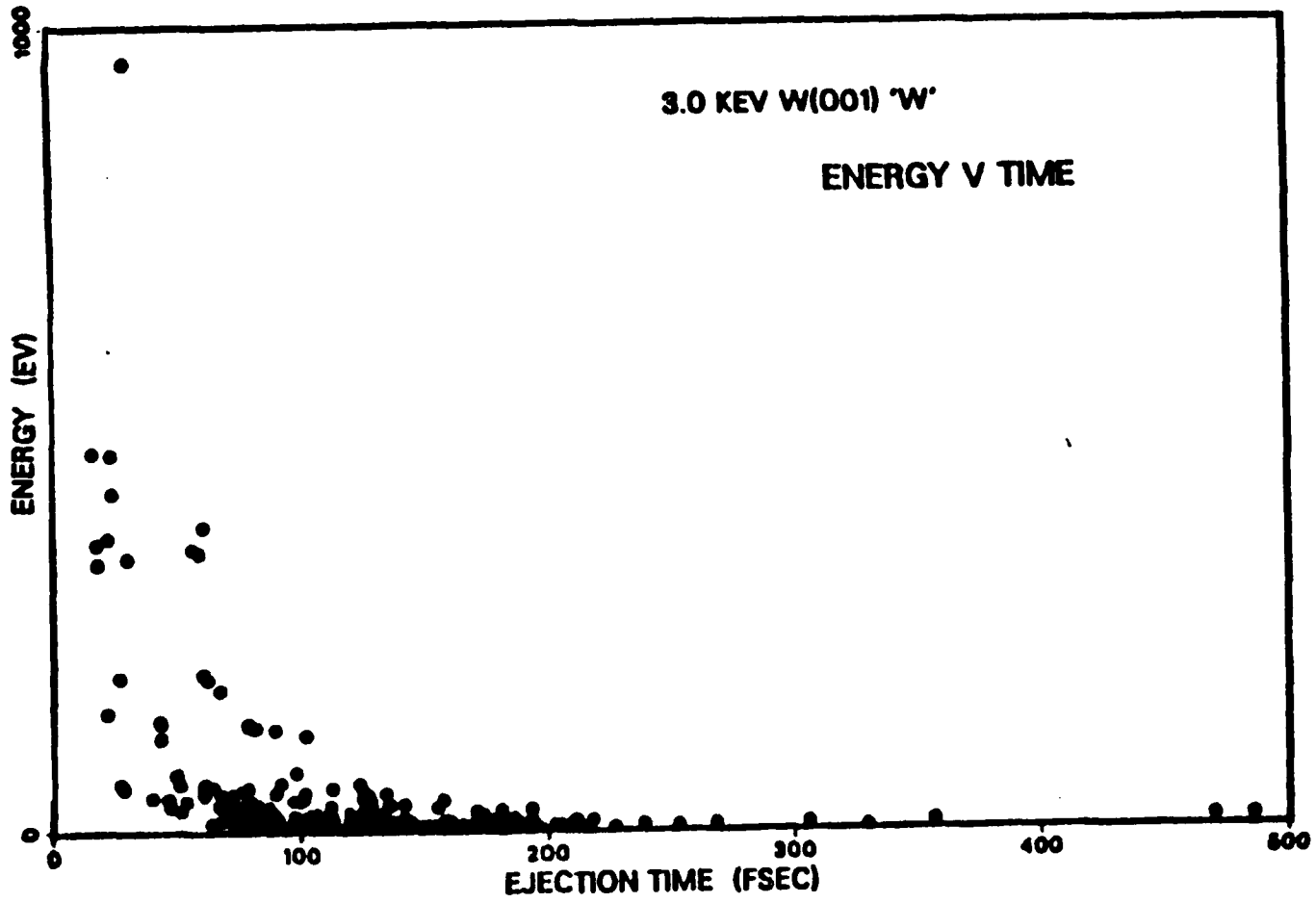


Fig. 26. Energy versus time for W atoms ejected from a reacted surface.

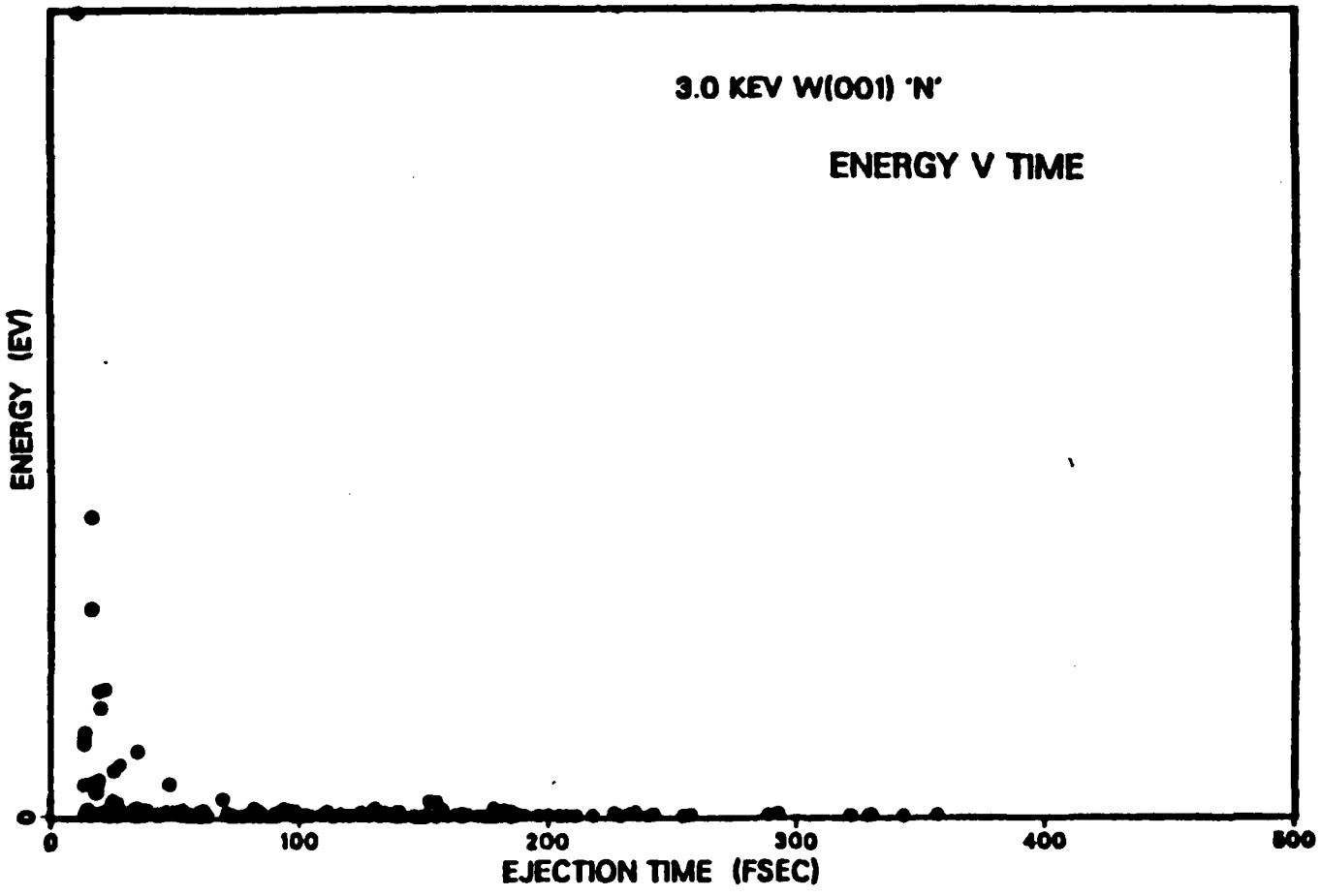


Fig. 27. Energy versus time for N atoms ejected from a reacted surface.

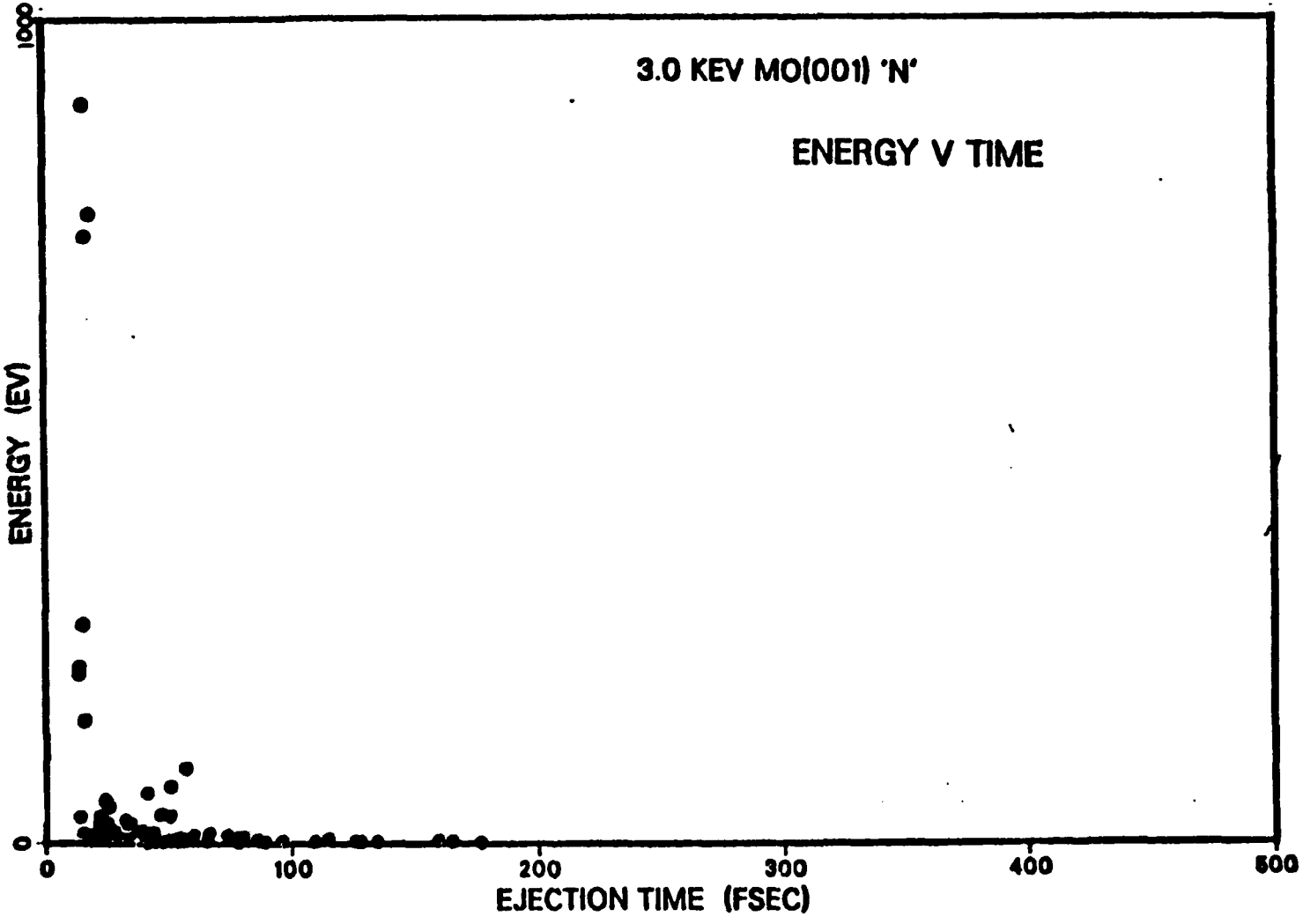


Fig. 28. Energy versus time for N atoms ejected from a reacted surface.

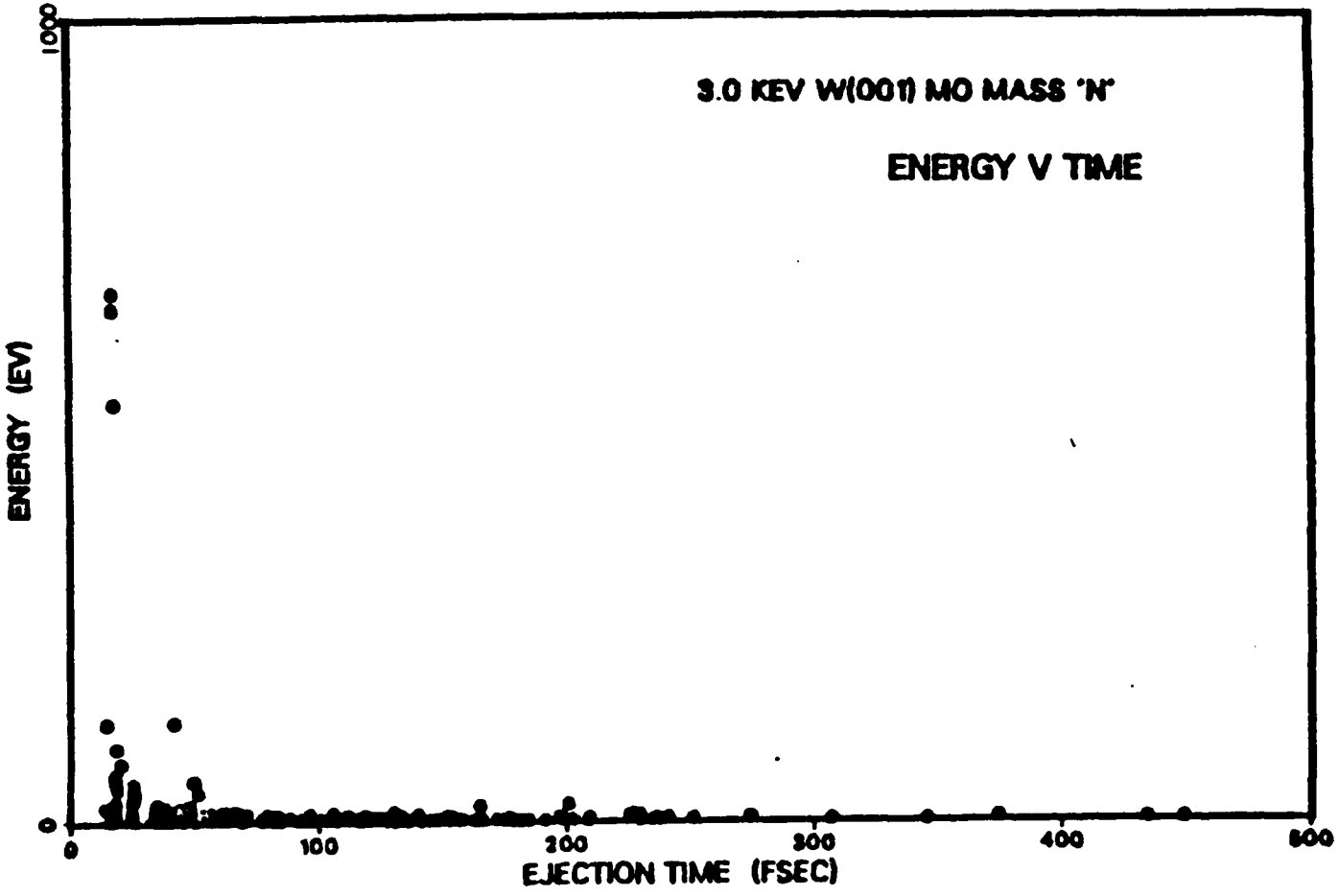


Fig. 29. Energy versus time for N atoms ejected from a reacted surface.

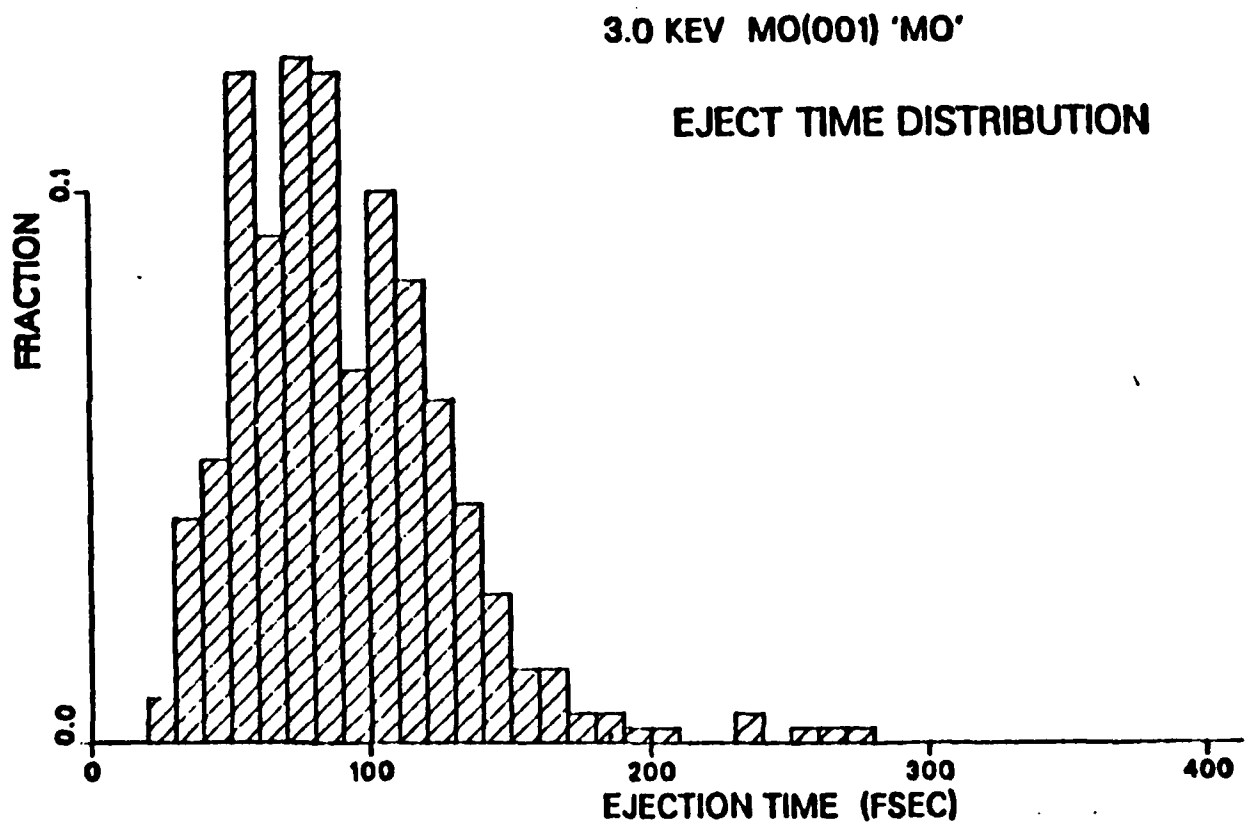


Fig. 30. Ejection time distribution for substrate atoms.

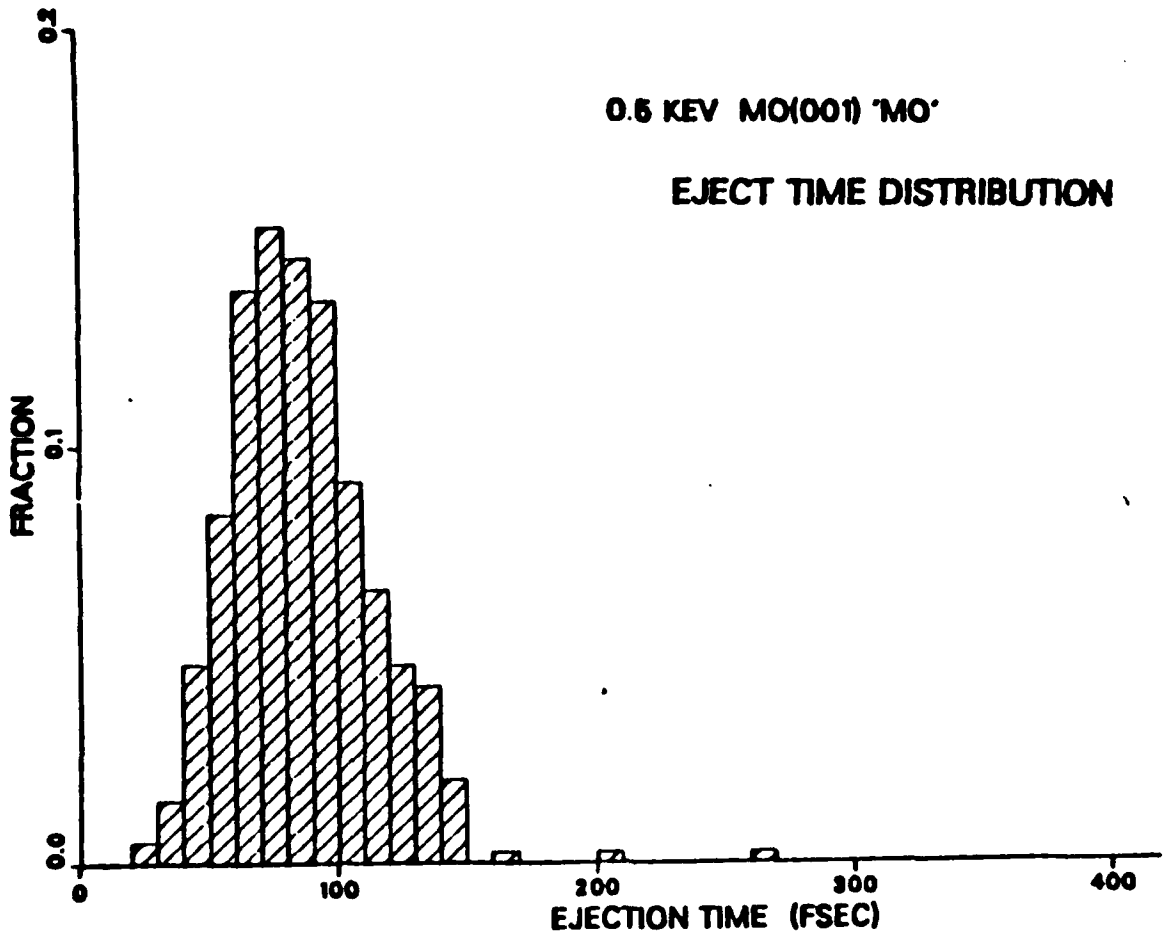


Fig. 31. Ejection time distribution for substrate atoms.

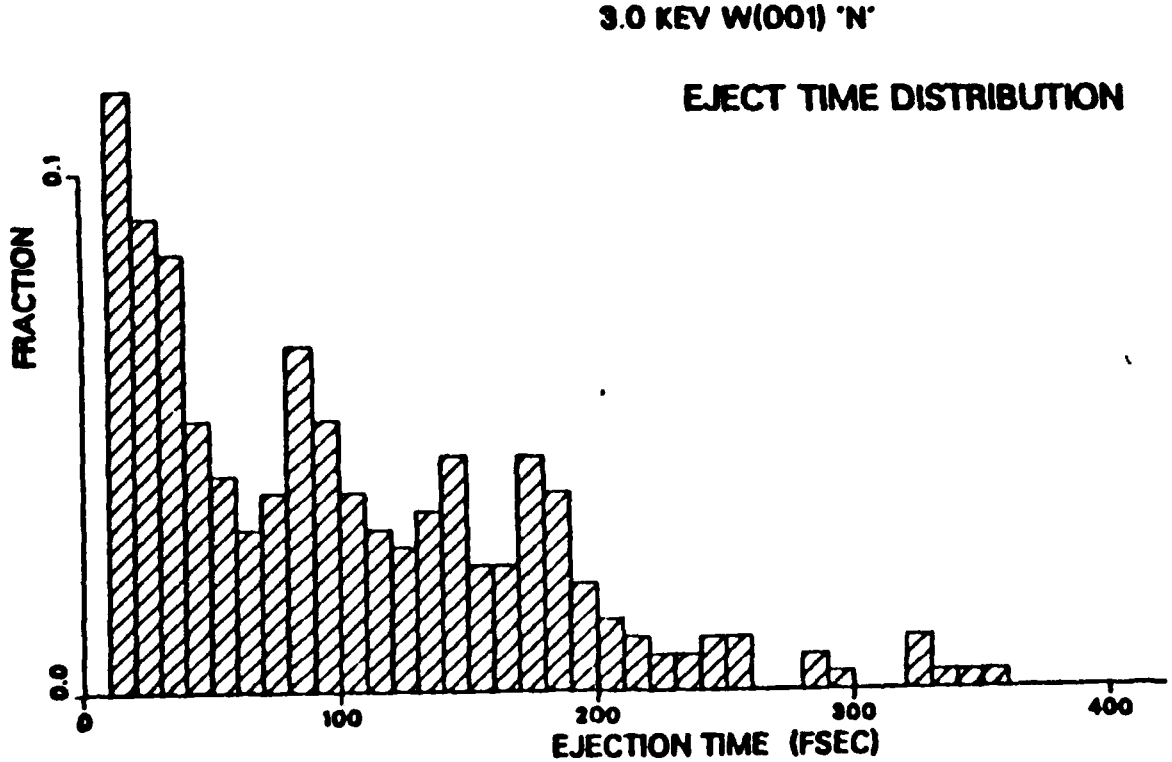


Fig. 32. Ejection time distribution for N atoms.

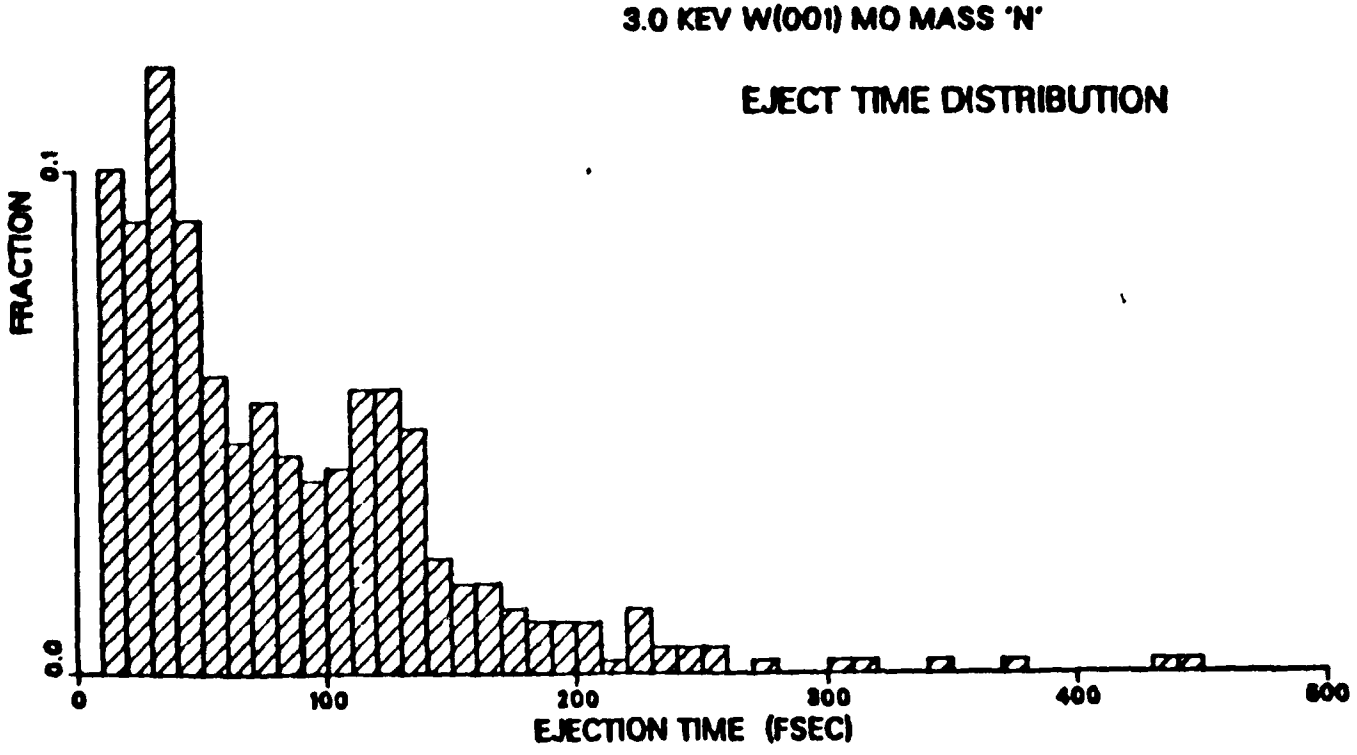


Fig. 33. Ejection time distribution for N atoms.

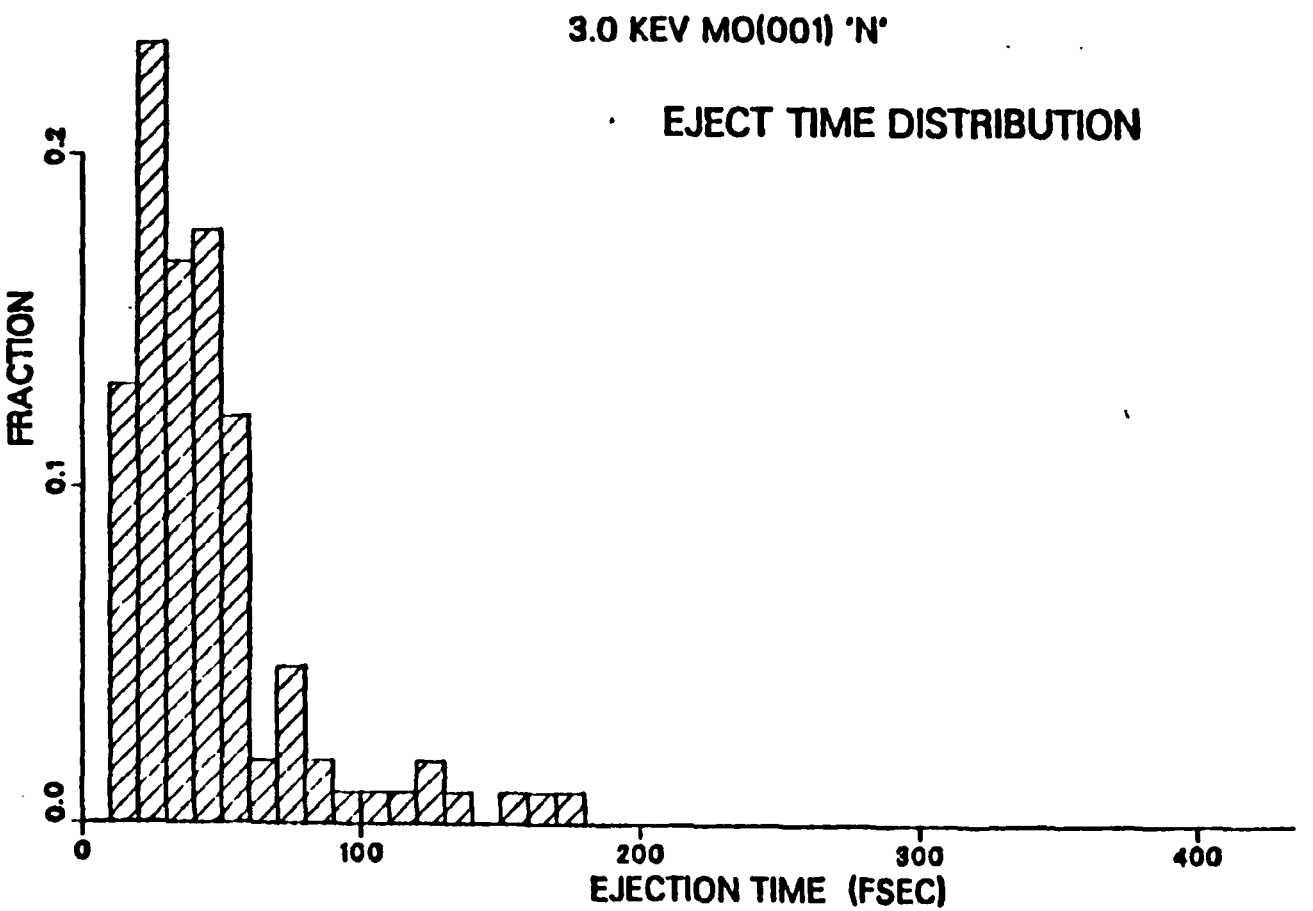


Fig. 34. Ejection time distribution for N atoms.

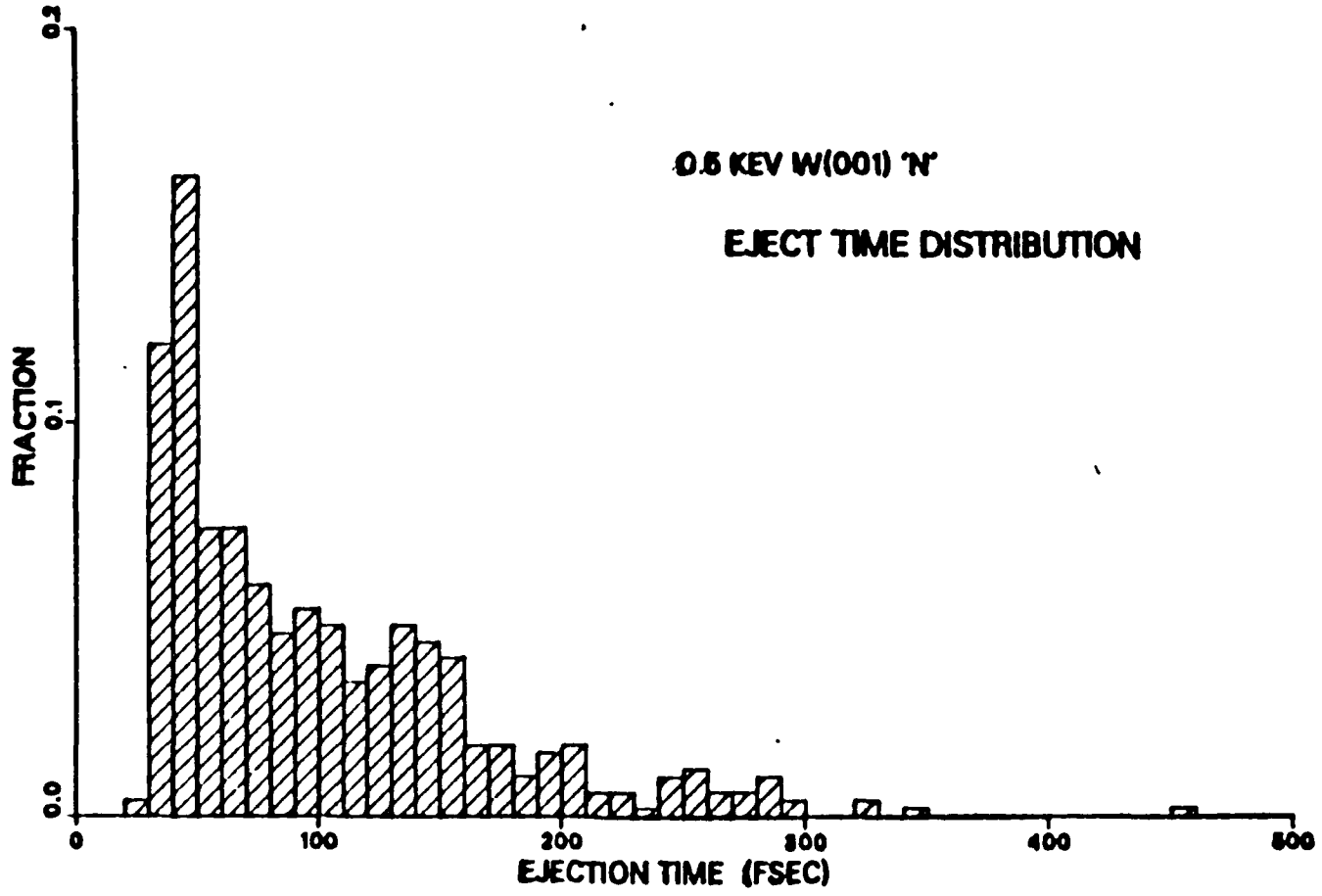


Fig. 35. Ejection time distribution for N atoms.

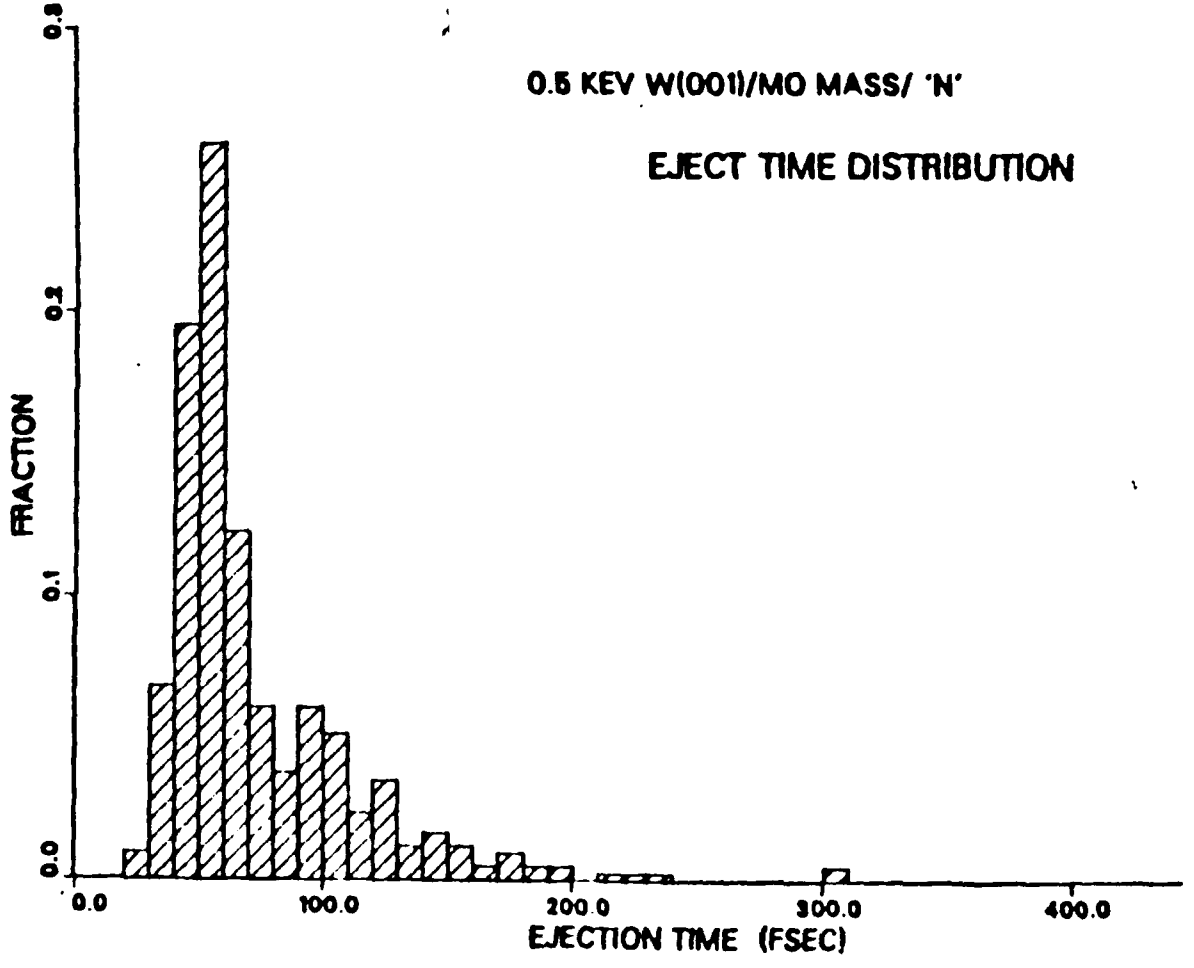


Fig. 36. Ejection time distribution for N atoms.

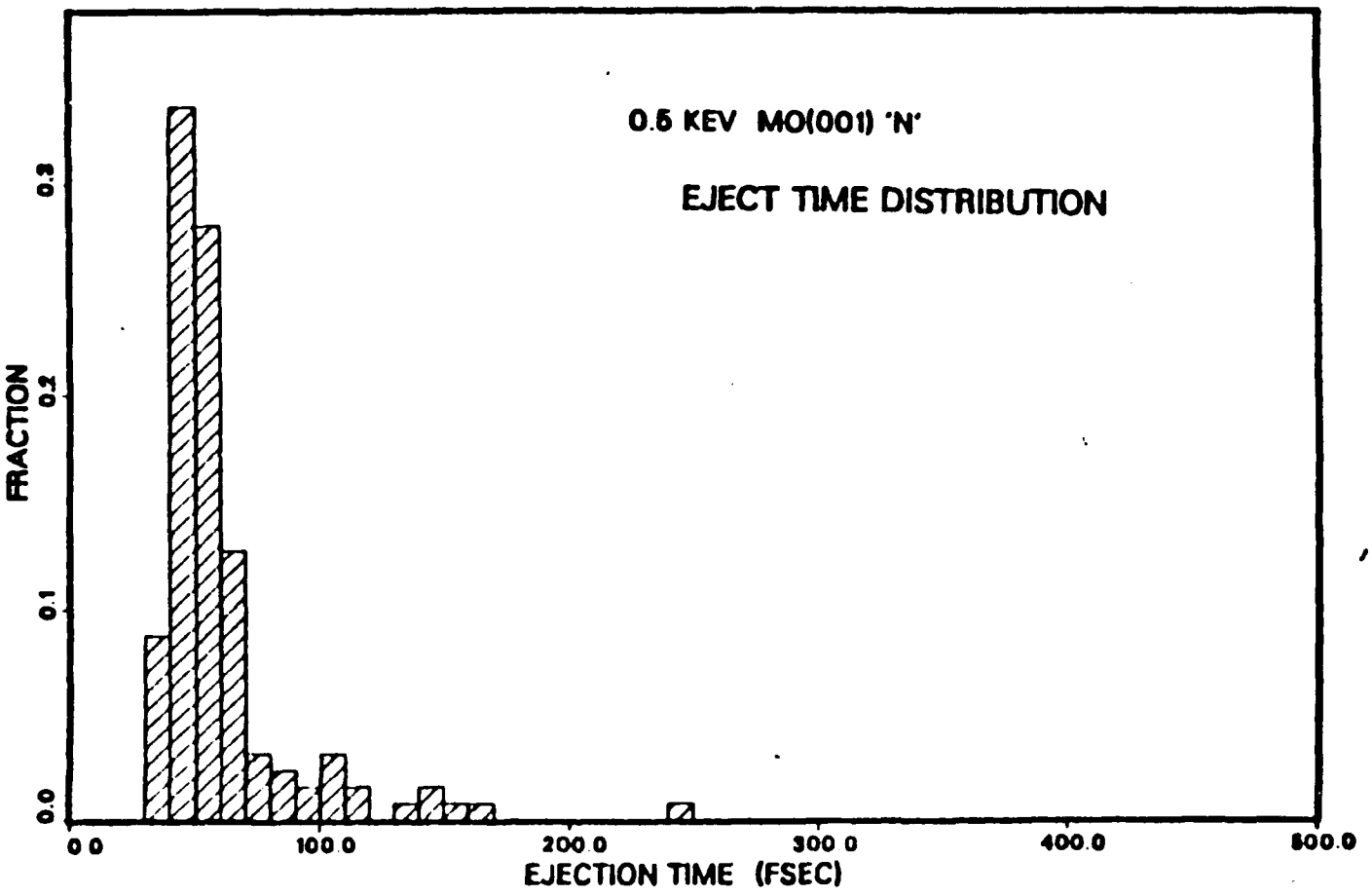


Fig. 37. Ejection time distribution for N atoms.

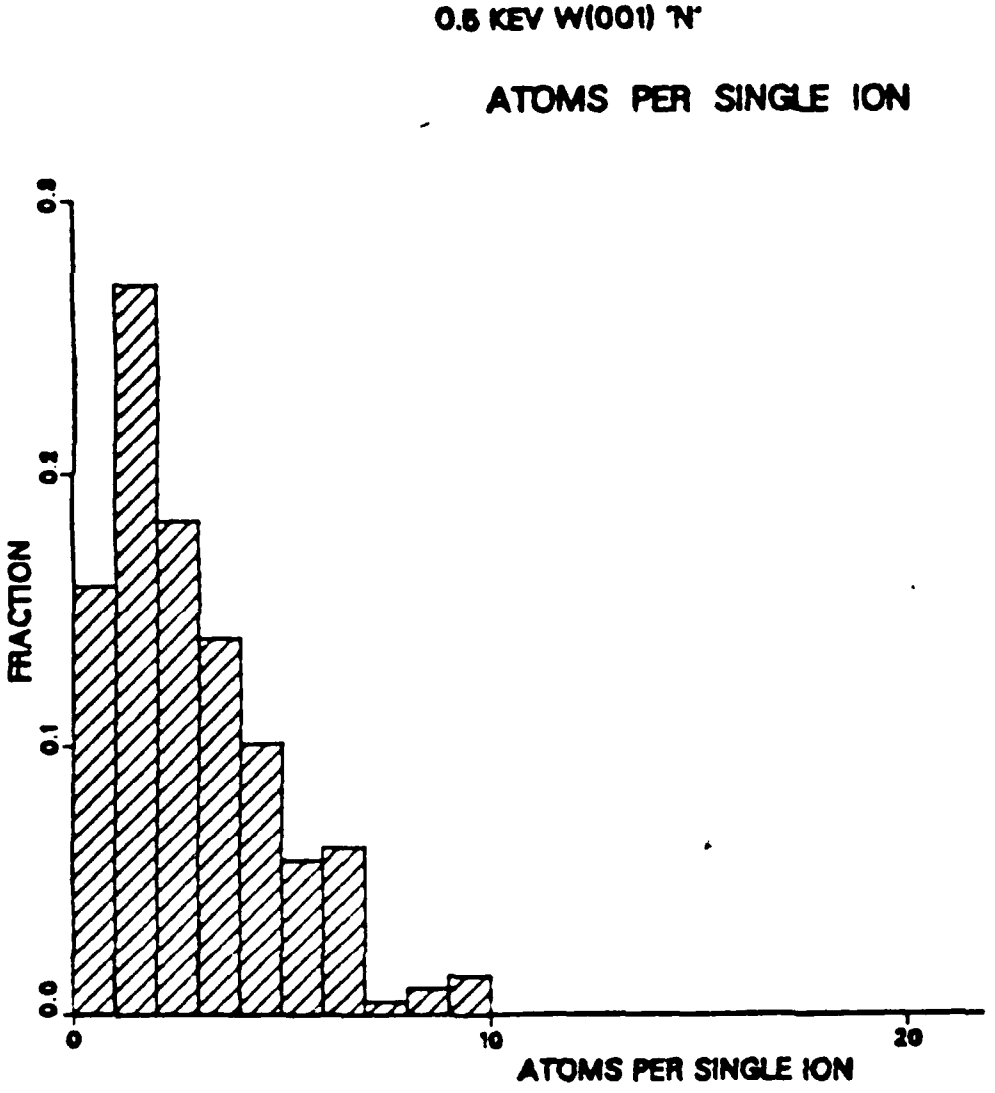


Fig. 38. ASI for ejected N atoms.

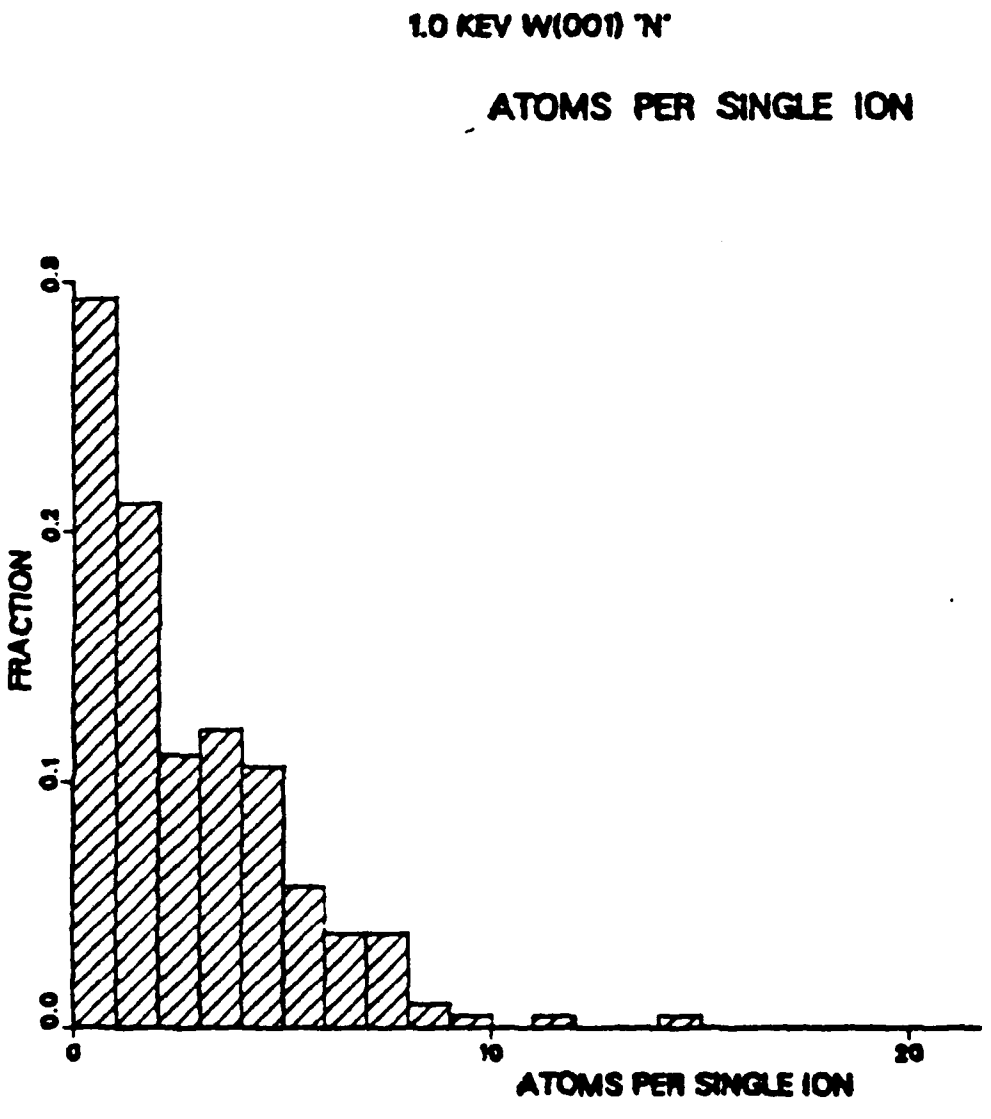


Fig. 39. ASI for ejected N atoms.

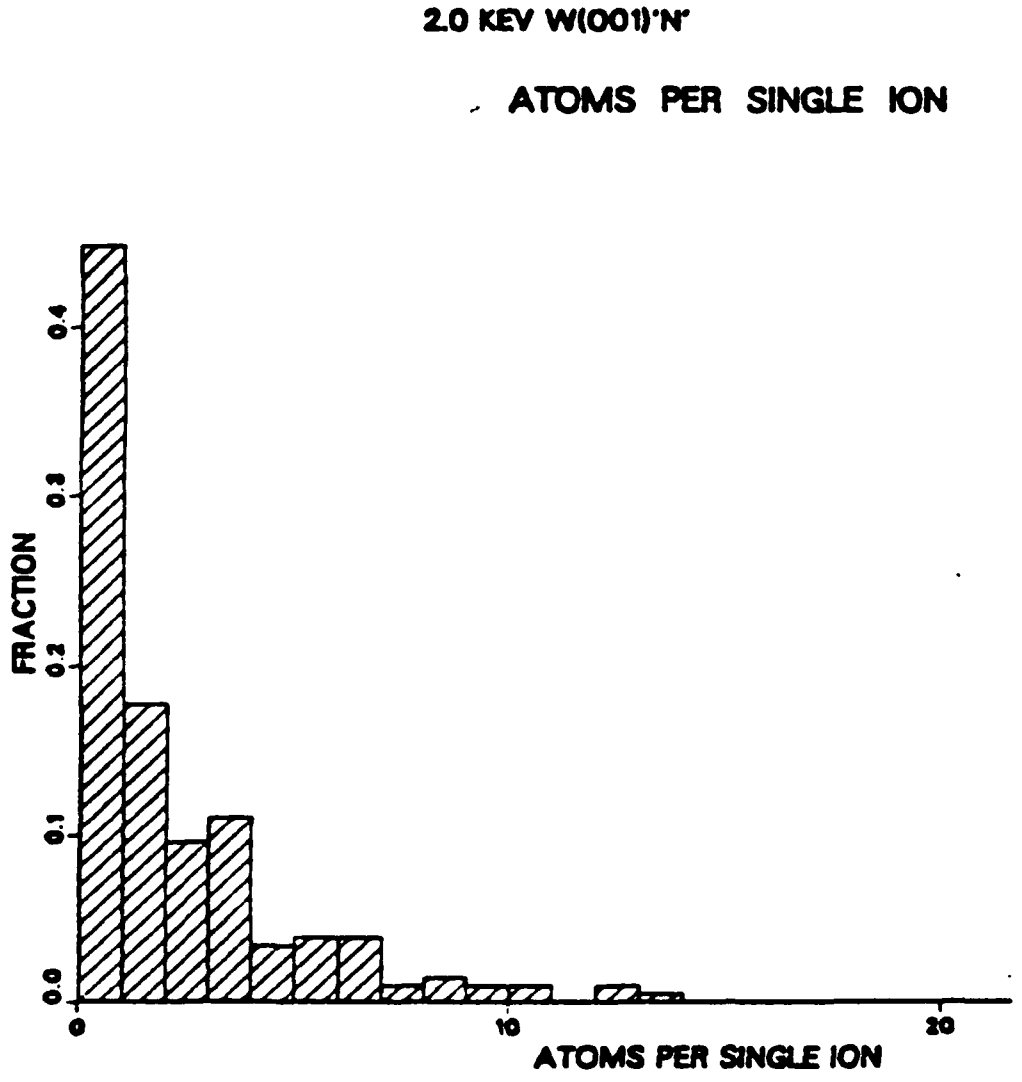


Fig. 40. ASI for ejected N atoms.

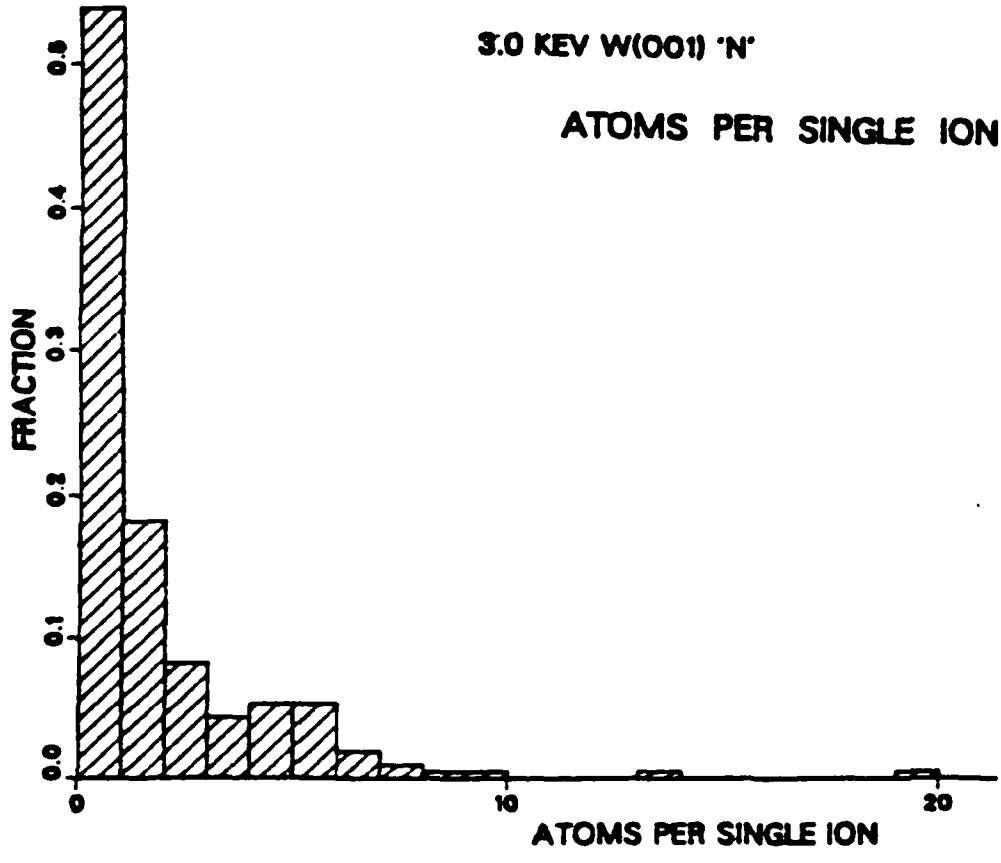


Fig. 41. ASI for ejected N atoms.

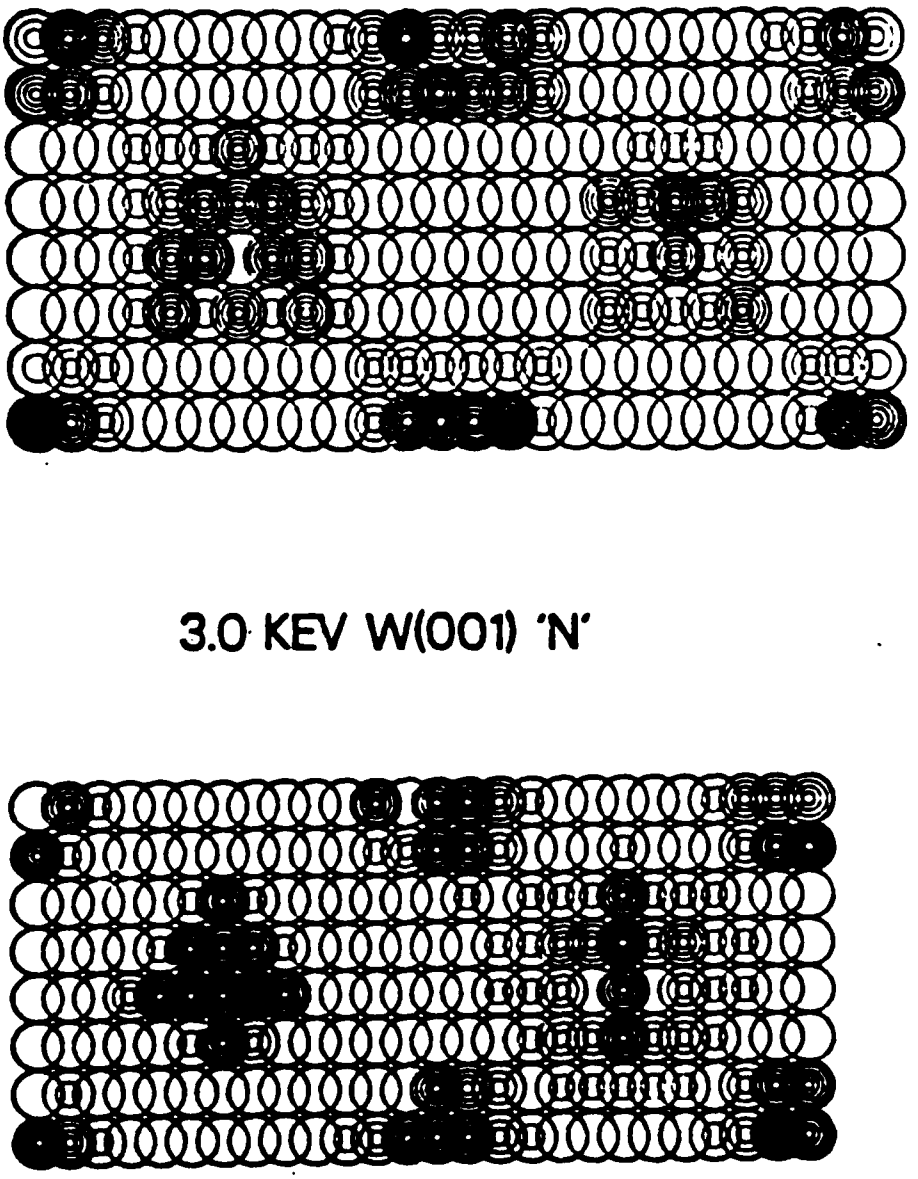


Fig. 42. Yield per single impact point.

1.0 KEV MO(001) 'MO'

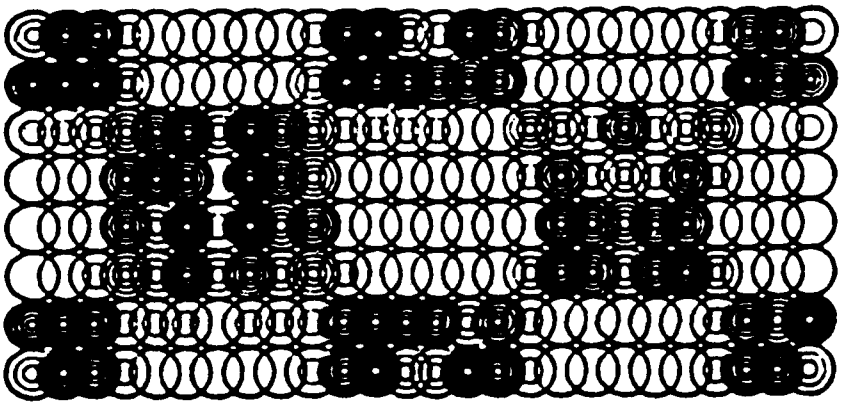

0.5 KEV MO(001) 'MO'

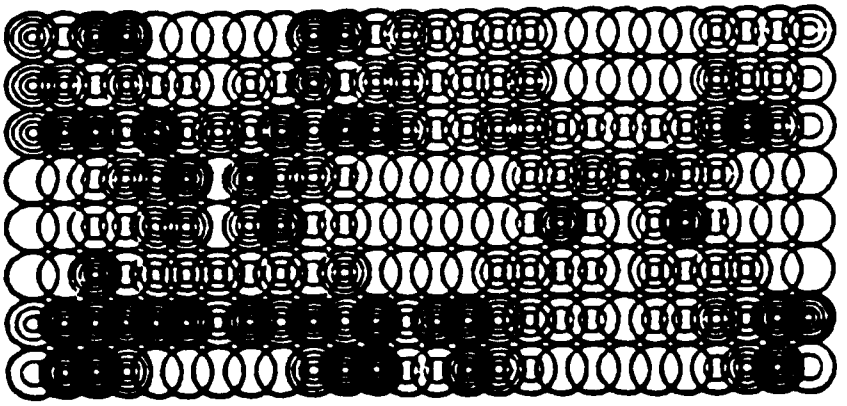

Fig. 43. Yield per single impact point.

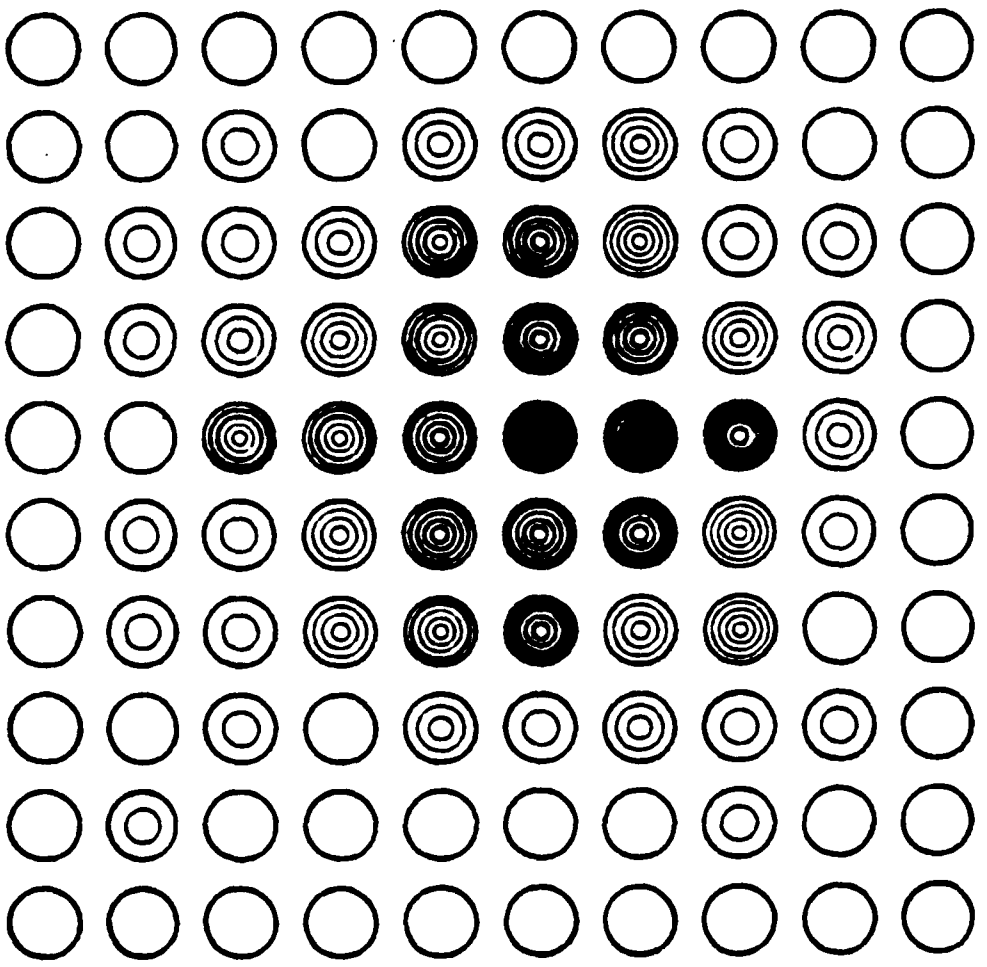


Fig. 44. Yield per surface atom.

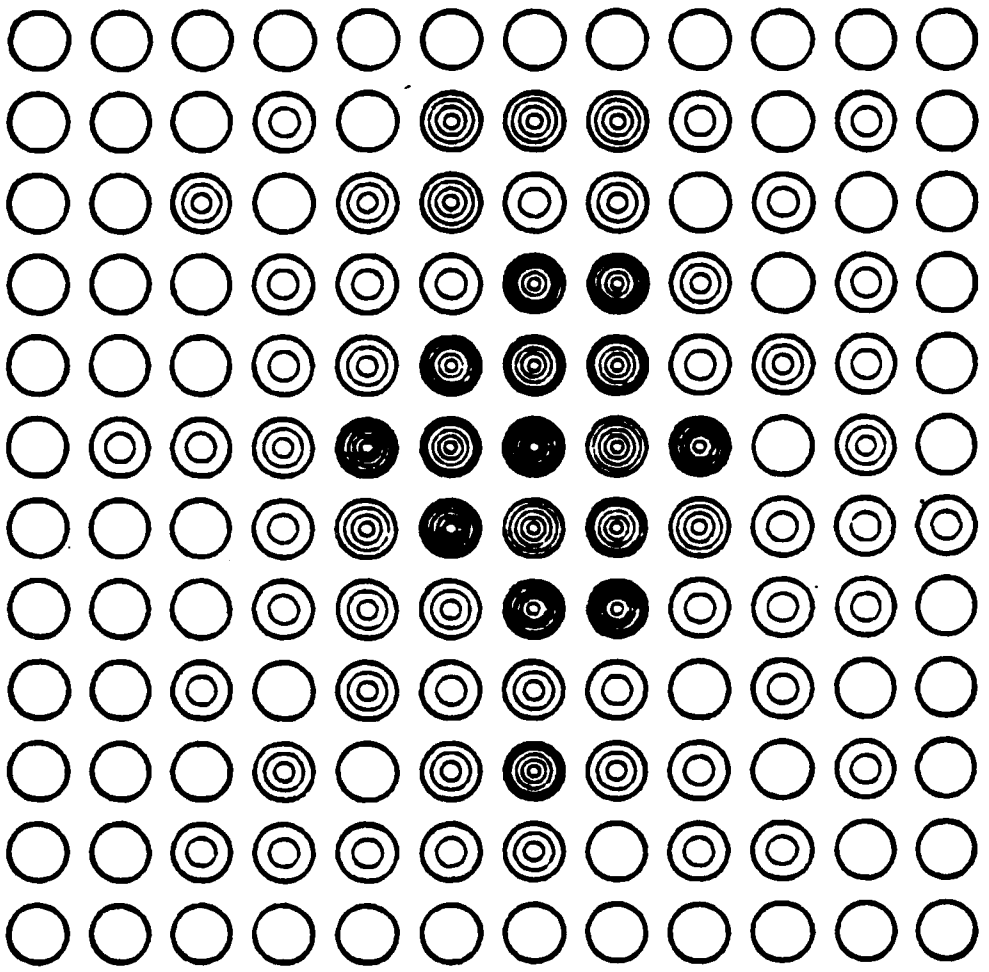


Fig. 45. Yield per surface atom.

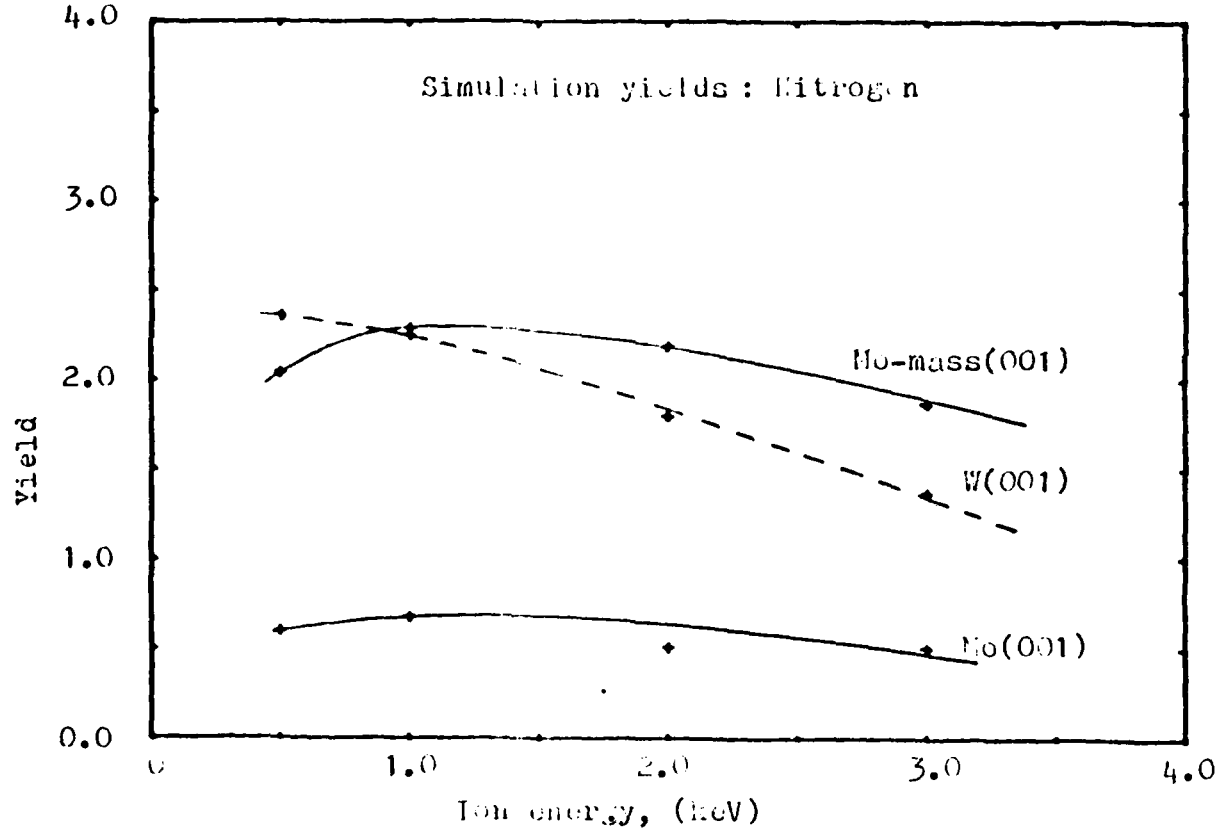


Fig. 46. Nitrogen yields from W and Mo substrates.

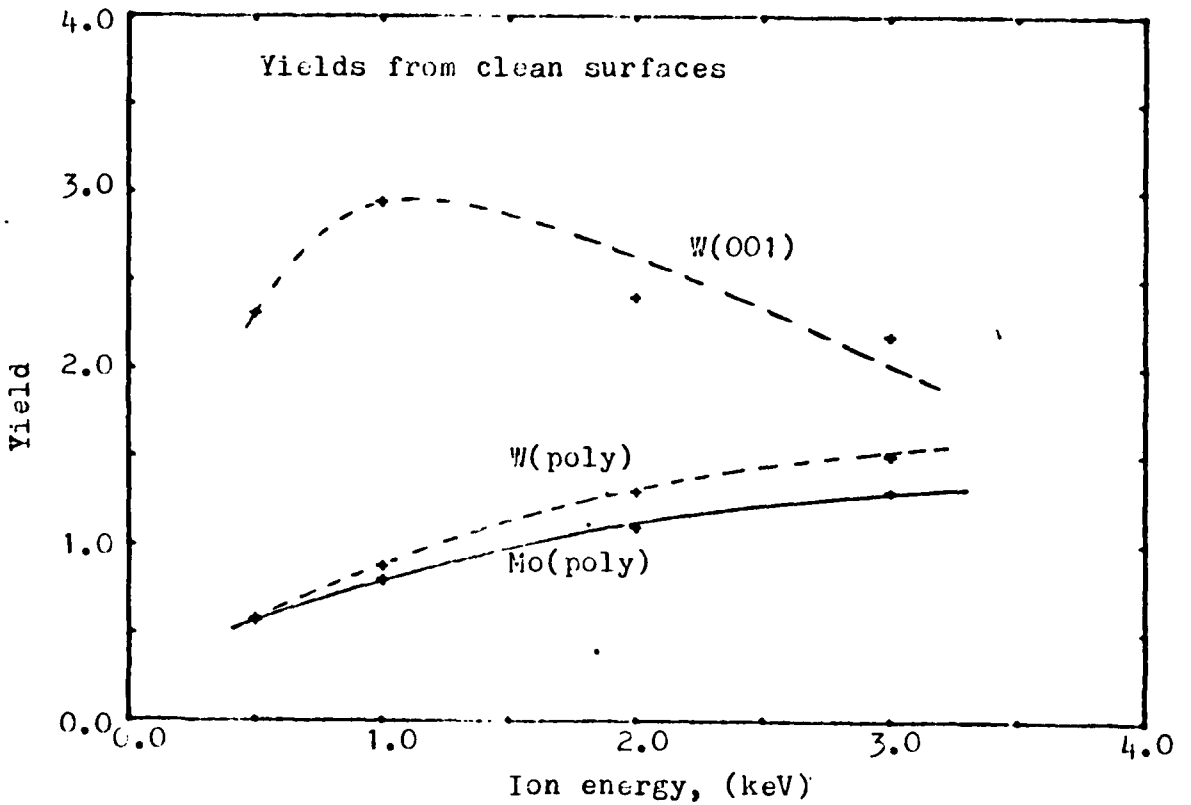


Fig. 47. Simulation yields from W(001) and experimental yields from polycrystalline W and Mo.

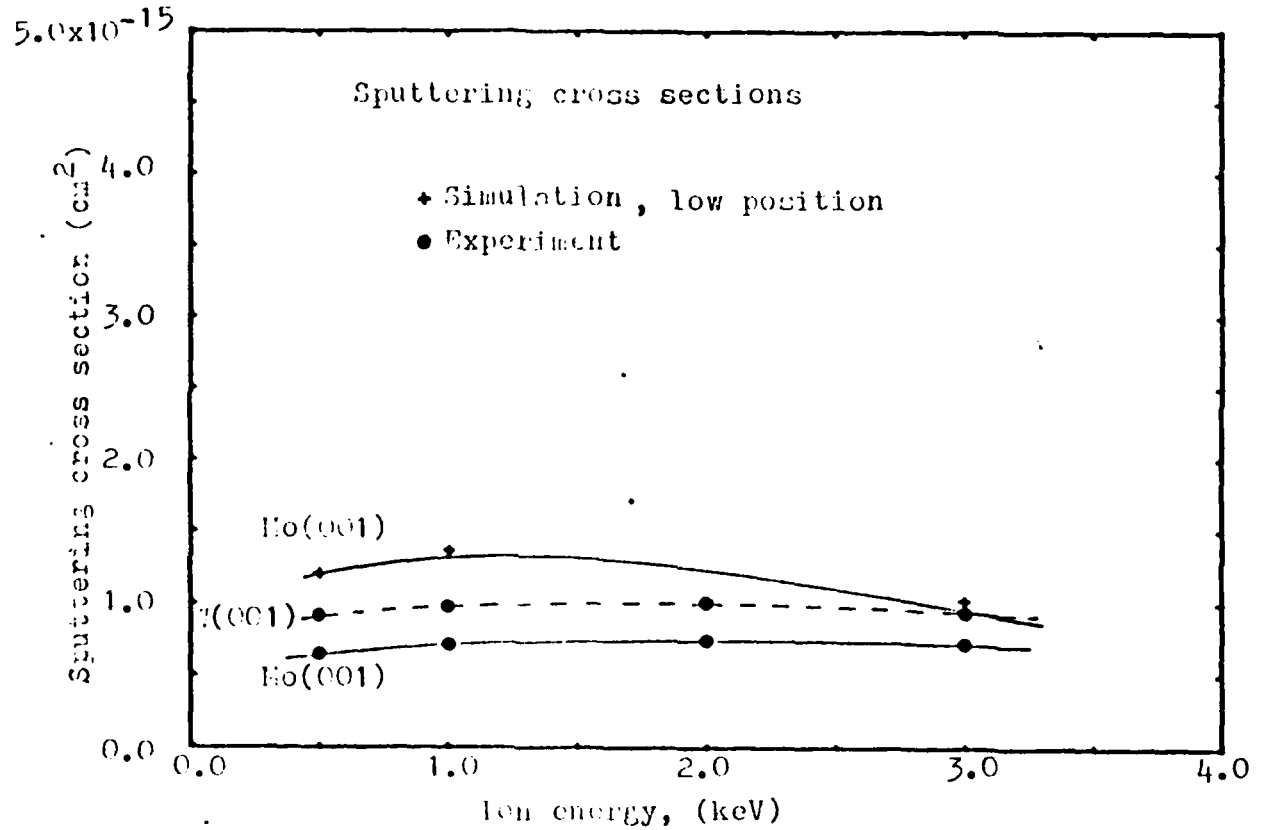


Fig. 48. Sputtering cross sections for adsorbed nitrogen.

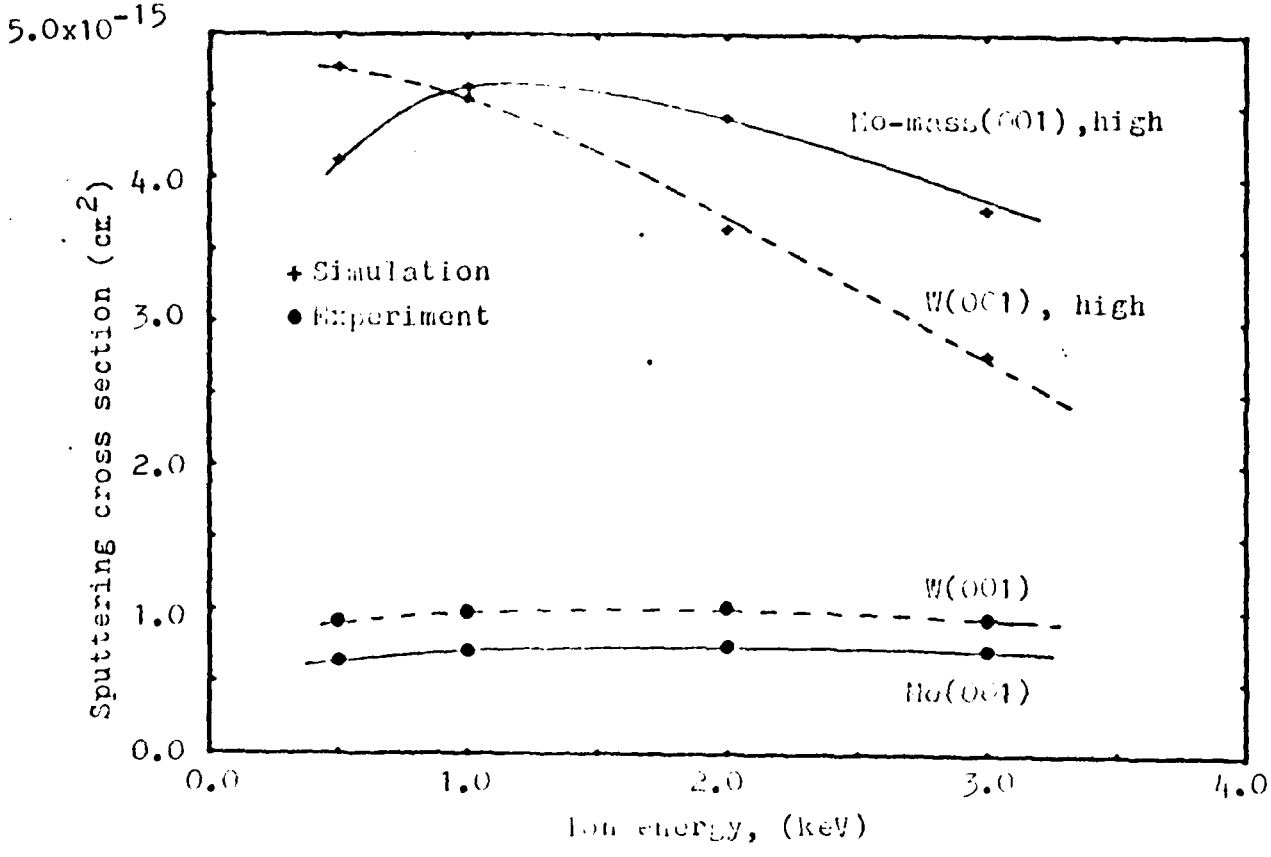


Fig. 49. Sputtering cross sections for adsorbed nitrogen.

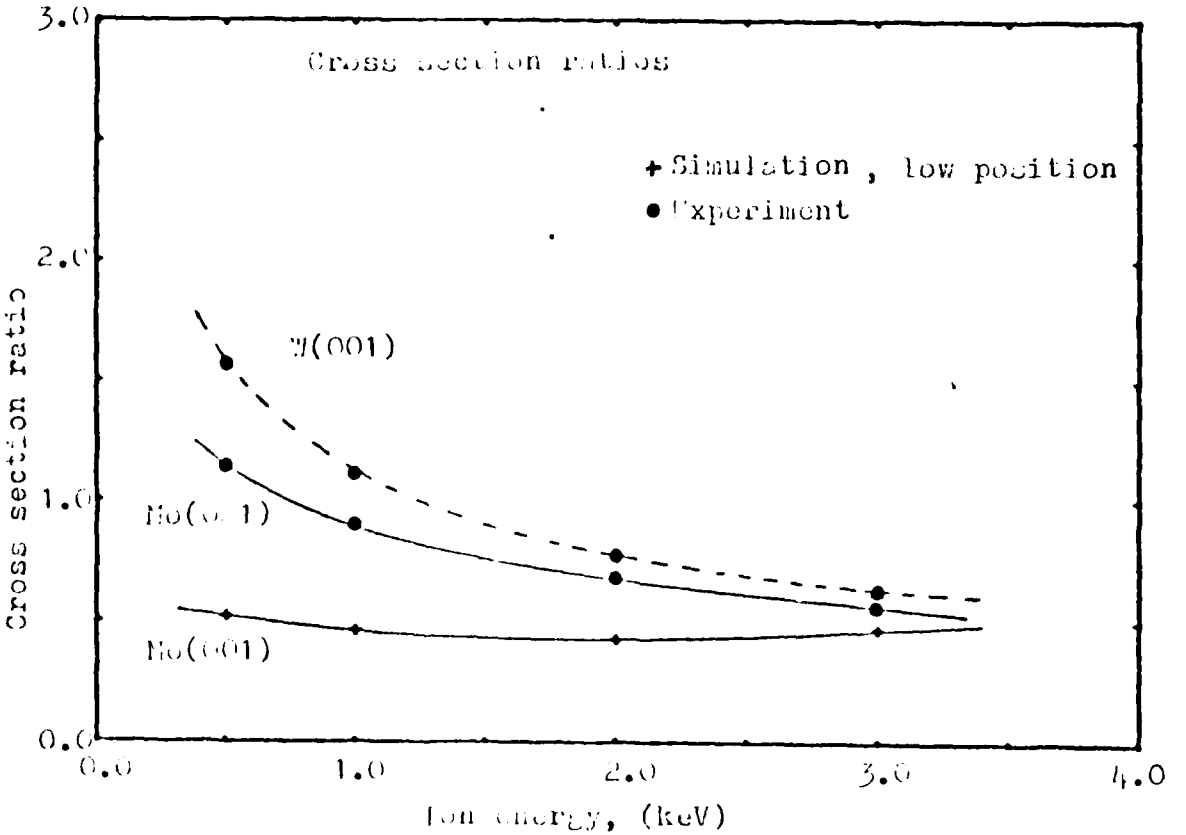


Fig. 50. Cross sections (nitrogen) / cross sections (substrate).

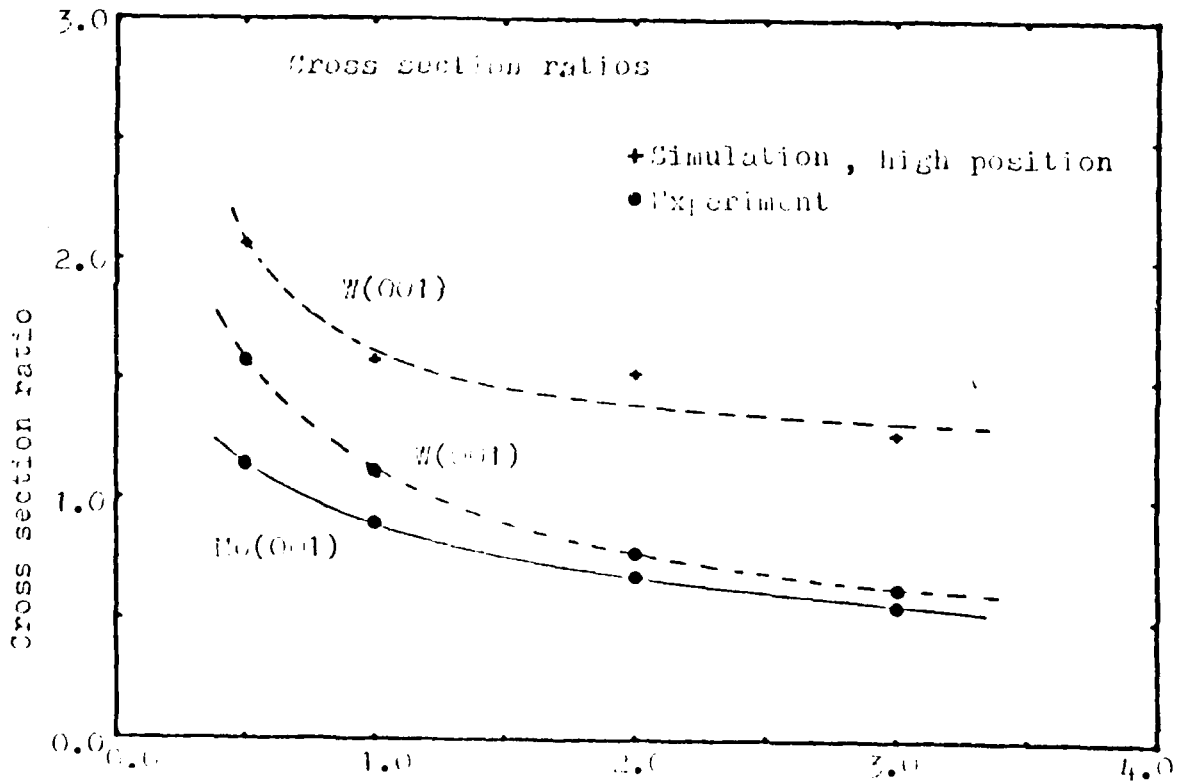
Cross section ratios
+Simulation , high position
•Experiment
W(001)
W(001)
Pt(001)
Cross section ratio
3.0
2.0
1.0
0.0
0.0
1.0
2.0
3.0
4.0

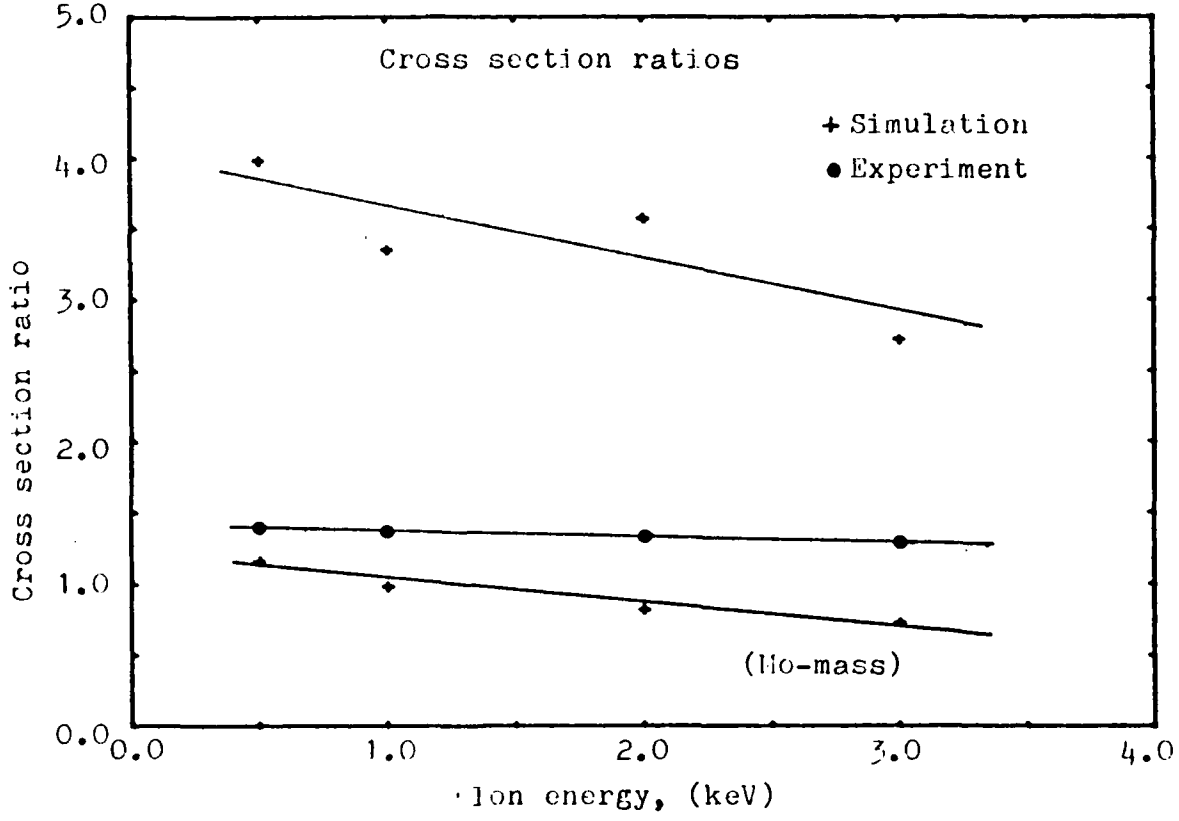


Fig. 52. Cross section ratios for N from W-substrate / N from Mo-substrate.

INITIAL DISTRIBUTION LIST

| | | No. Copies |
|---|---|---|
| 1. | Defense Technical Information Center<br>Cameron Station<br>Alexandria, Virginia 22314 | 2 |
| 2. | Library, Code 0142<br>Naval Postgraduate School<br>Monterey, California 93943 | 2 |
| 3. | Department Chairman, Code 61Sq<br>Department of Physics<br>Naval Postgraduate School<br>Monterey, California 93943 | 2 |
| 4. | Dr. Don E. Harrison, Jr., Code 61Hx<br>Department of Physics<br>Naval Postgraduate School<br>Monterey, California 93943 | 5 |
| 5. | Dirk Meyerhoff<br>Braunsberger Str. 53<br>3200 Hildesheim<br>WEST GERMANY | 1 |

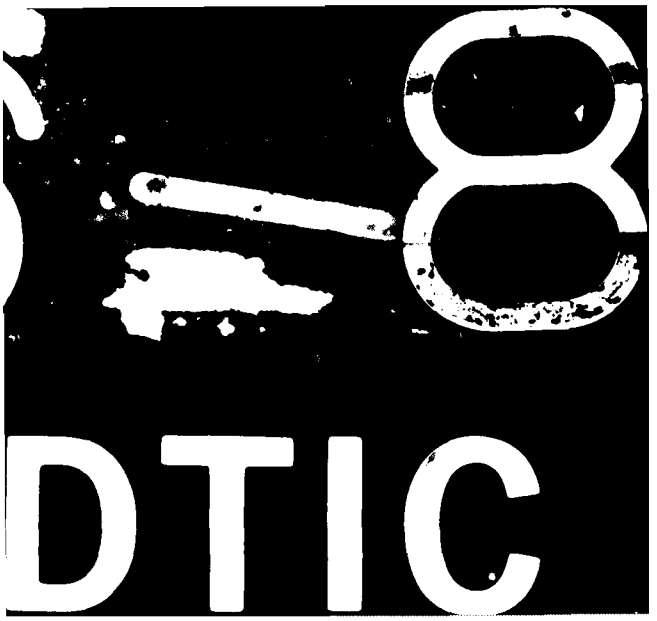
DTIC